

INVESTIGATION OF THE EFFECTIVENESS OF ELECTRICAL AND
MICROWAVE HEATING FOR OIL SHALE EXTRACTION

A THESIS SUBMITTED TO
THE GRADUATE SCHOOL OF NATURAL AND APPLIED SCIENCES
OF
MIDDLE EAST TECHNICAL UNIVERSITY

BY

SELİN GÜVEN

IN PARTIAL FULFILLMENT OF THE REQUIREMENTS
FOR
THE DEGREE OF MASTER OF SCIENCE
IN
PETROLEUM AND NATURAL GAS ENGINEERING

SEPTEMBER 2015

Approval of the Thesis:

**INVESTIGATION OF THE EFFECTIVENESS OF ELECTRICAL AND
MICROWAVE HEATING FOR OIL SHALE EXTRACTION**

submitted by **SELİN GÜVEN** in partial fulfillment of the requirements for the degree of
**Master of Science in Petroleum and Natural Gas Engineering Department, Middle
East Technical University** by,

Prof. Dr. Gülbin Dural Ünver
Dean, Graduate School of **Natural and Applied Sciences** _____

Prof. Dr. Mustafa Verşan Kök
Head of Department, **Petroleum and Natural Gas Engineering** _____

Prof. Dr. Serhat Akın
Supervisor, **Petroleum and Natural Gas Engineering Dept., METU** _____

Examining Committee Members:

Prof. Dr. Nurkan Karahanoğlu
Geological Engineering Dept., METU _____

Prof. Dr. Serhat Akın
Petroleum and Natural Gas Engineering Dept., METU _____

Assoc. Prof. Dr. N. Emre Altun
Mining Engineering Dept., METU _____

Asst. Prof. Dr. İsmail Durgut
Petroleum and Natural Gas Engineering Dept., METU _____

Asst. Prof. Dr. Emre Artun
Petroleum and Natural Gas Engineering Dept., METU NCC _____

Date: 04.09.2015

I hereby declare that all information in this document has been obtained and presented in accordance with academic rules and ethical conduct. I also declare that, as required by these rules and conduct, I have fully cited and referenced all material and results that are not original to this work.

Name, Last name: Selin Güven

Signature:

ABSTRACT

INVESTIGATION OF THE EFFECTIVENESS OF ELECTRICAL AND MICROWAVE HEATING FOR OIL SHALE EXTRACTION

Guven, Selin

M.S., Department of Petroleum and Natural Gas Engineering

Supervisor: Prof. Dr. Serhat Akin

September 2015, 130 pages

In this study, four different oil shales from Turkey (Bolu-Himmetoglu, Bolu-Hatildag, Kutahya-Seyitomer, Nigde-Ulukisla) that were subjected to retort and microwave heating w/wo three different iron powders (Fe, Fe₂O₃ and FeCl₃) with optimized doses. TGA/DSC (Thermal Gravimetric Analysis/Differential Scanning Calorimetry), FTIR (Fourier Transform Infrared Spectroscopy), X-Ray Diffraction (XRD) and SEM (Scanning Electron Microscope) were used to characterize these samples. Then, the oil shale samples before and after retort and microwave heating experiments were studied using TGA/DSC, FTIR and SEM analysis to understand the efficiencies and mechanisms of the thermal heating experiments. The effect of iron powders and the amount of them were also examined for this purpose. Moreover, TGA analyses were used to check the effect of temperature program used in retort experiments. FTIR technique was used to specify compound loss after each TGA/DSC analysis. Morphological changes were examined by using SEM analysis.

It has been seen that organic and inorganic weight loss percentages resulted from thermal analysis was proportional with oil shale content. It was understood that the clay content established via XRD did not primarily affect the mass losses. Iron powders seemed to

enhance the heating process of retort and microwave experiments; however, expected results could not be achieved in TGA/DSC analyses. Using same temperature program of retort, TGA/DSC analyses were carried out to simulate the retort experiments. The results of experiments and simulations were compared graphically and FTIR analyses. It was observed that retort experiments were successful at producing all the organic matter, except in Himmetoglu oil shale samples. By using TGA/DSC analyses, the amount of weight loss percentages during the experiments was reviewed. By doing so, we were able to confirm the production from retort analyses; however, no substantial production was seen from microwave experiments. SEM analyses helped us to recognize that retort postmortems have more char-like areas on their surface, and microwave postmortems have trace amount of increase in their surface areas.

Keywords: Fourier transform infrared spectroscopy, thermal gravimetric, differential scanning calorimetry, scanning electron microscope, x-ray diffraction, combustion, and pyrolysis

ÖZ

ELEKTRİKSEL VE MİKRODALGA ISITMA YÖNTEMLERİ VERİMLİLİĞİNİN BİTÜMLÜ ŞEYL ÇIKARIMI İÇİN İNCELENMESİ

Güven, Selin

Yüksek Lisans, Petrol ve Doğal Gaz Mühendisliği Bölümü

Tez Yöneticisi: Prof. Dr. Serhat Akın

Eylül 2015, 130 sayfa

Bu çalışmada, Türkiye’den dört ayrı bitümlü şeyl örnekleri (Bolu-Himmetoğlu, Bolu-Hatıldag, Kütahya-Seyitömer, Niğde-Ulukışla) retort ve mikrodalga ısıtma yöntemlerine tabi tutuldu. Deneysel, verimliliğini arttırmak amacı ile örnekler optimum dozlarda üç farklı demir tozu eklenerek tekrarlandı. TGA/DSC (Termal Gravimetrik Analiz/Diferansiyel Taramalı Kalorimetri), FTIR (Fourier Dönüşüm Kızılötesi Spektroskopisi), X-Ray Difraksiyonu (XRD) ve SEM (Taramalı Elektron Mikroskobu) analizleri ile karakterizasyonu yapıldı. Daha sonra termal ısıtma yöntemlerinin verimliliklerini ve mekanizmalarını anlayabilmek için bitümlü şeyl örnekleri, retort ve mikrodalga ısıtma yöntemlerinden önce ve sonra TGA/DSC (Termogravimetrik Analiz/Diferansiyel Taramalı Kalorimetri), FTIR (Fourier Dönüşüm Kızılötesi Spektroskopisi) ve SEM (Taramalı Elektron Mikroskobu) analizlerine tabi tutuldu. Bu amaçla demir tozunun deneysel olan etkisi ve miktarları da ele alındı. Aynı zamanda, TGA analizleri, retort deneylerinde kullanılan sıcaklık programının etkisini araştırmak amacıyla kullanıldı. FTIR tekniği ile TGA/DSC analizlerinden sonra yok olan maddeler belirlendi. Yüzeydeki biçimsel değişiklikler ise SEM analizleri kullanılarak incelendi.

Termal analizlerde gerçekleşen organik ve inorganik dekompozisyon yüzdelerinin bitümlü şeyl içeriğine göre doğru orantılı olarak değiştiği gözlemlendi. XRD ile saptanan kil içeriğinin, kütle kayıplarında birincil bir etkisine rastlanılmadı. Demir tozlarının retort ve

mikrodalga deneyleri sırasında ısıtma sürecini iyileştirdiği gözlemlenirken, TGA/DSC analizlerinde beklenen sonuçlara ulaşılamadı. Retort deneylerinin sıcaklık programı kullanılarak, TGA/DSC ile retort deneylerinin benzetimi gerçekleştirildi. Deney ve benzetim sonuçları, grafik yorumlamaları ve FTIR analizi ile karşılaştırıldı. Bunun sonucunda, retort deney programlarının Himmetoğlu bitümlü şeyli dışındaki örnekler için, tüm organik maddeyi üretmekte başarılı olduğu görüldü. Retort ve mikrodalga deneyleri sonrası örnekleri üzerinde yapılan TGA/DSC analizlerinde ise, deneyler esnasında ne kadar yüzde kütle kaybı gerçekleştiği gözden geçirildi. Bu sayede, retort deneyleri sırasındaki üretim bir kez daha doğrulanırken, mikrodalga deneyleri sırasında dikkate eğer bir üretim olmadığı görüldü. SEM analizleri ile retort sonrası örneklerin yüzey yapılarında daha çok kömürleşmiş yüzeye rastlanırken, mikrodalga sonrası örneklerde yüzey alanının eser miktarda da olsa artmış olduğu gözlemlendi.

Anahtar Kelimeler: Fourier dönüşüm kızılötesi spektroskopisi, termal gravimetrik, diferansiyel taramalı kalorimetri, taramalı elektron mikroskobu, x-ray difraksiyon, yanma, piroliz.

to my family...

ACKNOWLEDGMENTS

I wish to express my deepest appreciation to my supervisor Prof. Dr. Serhat Akin for his guidance, advice, criticism, encouragements, support, and patience throughout the research. Also, I would like to thank for the openings he provided that help broad my vision,

I am indebted to my co-advisor Asst Prof. Dr. Berna Haşçakır for the opportunities she provided, her endless guidance and encouragements during the experiments, and advices about work discipline which I implemented my life,

Also, I acknowledge the financial support and the opportunity provided by the Texas A&M University to conduct experiments in the Ramey Thermal Recovery Laboratory, and the member of Heavy Oil, Oil shales, Oil sands, & Carbonate Analysis and Recovery Methods (HOCAM) Research Team at Texas A&M University, Petroleum Engineering Department, for their help,

I would like to express my appreciations to my beloved family, Nevin, Rifat and Öner, for their endless patience and moral support. I am glad to have you,

I am grateful to end such a hard period with the support, patience and friendship of my precious workmates Tuğçe, Berk, Aslı, Javid, Ashkan, Shirin, Tunç and Betül; and my cherished friends Ecem, Emre, Elif, Çağdaş, Nilay, and Emel. Thank you for your endless friendship. I would like to thank Günseli, Şükran, Emine, Mercan, and Seden for helping me to get used to my new life, also for their friendship, favour and patience,

Finally, I would like to thank Öney, Yasin, and Taniya for their help and support during my working period in College Station, Texas.

NOMENCLATURE

Abbreviations

AMSO	American Shale Oil LLC
CCR	Conduction, Convection, Reflux
DSC	Differential Scanning Calorimetry
HRS	Hot Recycled Solid
ICP	In-situ Combustion
NER	Net Energy Recovery
NTU	Navada-Texas-Utah Retort
SEM	Scanning Electron Microscope
TGA	Thermal Gravimetric Analysis
TOSCO	The Oil Shale Corporation
XRD	X-Ray Diffraction

Roman Symbols

E_a	Activation energy
A	Arrhenius constant
w	Weight of the sample
t	Time
n	Reaction order
R	Universal gas constant
T	Temperature

TABLE OF CONTENTS

ABSTRACT	v
ÖZ.....	vii
ACKNOWLEDGMENTS.....	x
NOMENCLATURE.....	xi
TABLE OF CONTENTS	xii
LIST OF FIGURES.....	xiv
LIST OF TABLES	xix
CHAPTERS	1
1 INTRODUCTION.....	1
2 LITERATURE REVIEW	3
2.1 Oil Shale	3
2.1.1 Oil Shale Resources	5
2.2 Oil Shale Extraction Methods.....	7
2.2.1 Surface Retorting.....	8
2.2.2 In-situ Retorting	9
2.3 Oil Shale Heating Methods.....	9
3 STATEMENT OF THE PROBLEM	15
4 MATERIALS AND METHODS	17
4.1 Oil Shale Samples and Locations	17
4.2 Retort and Microwave Postmortems	18
4.3 Iron Powders.....	18
4.4 Experimental Procedure	19
4.4.1 Sample Preparation	19
4.4.2 Experimental Period and Temperature Measurement.....	19
4.5 Material Analyses	19
4.5.1 X-Ray Diffraction (XRD)	20
4.5.2 Scanning Electron Microscope/Energy Dispersive X-Ray Spectroscopy (SEM/EDS)	21
4.5.3 Fourier Transform Infrared Spectroscopy (FTIR)	21
4.5.4 Thermal Gravimetric Analysis/Differential Scanning Calorimetry (TGA/DSC).....	21
5 RESULTS AND DISCUSSIONS	25

5.1	Original Samples	25
5.1.1	X-Ray Diffraction (XRD) Analysis Results of Original Samples	25
5.1.2	Scanning Electron Microscope/Energy Dispersive X-Ray Spectroscopy (SEM/EDS) Analysis Results of Original Samples	29
5.1.3	Fourier Transform Infrared Spectroscopy (FTIR) Analysis Results of Original Samples	31
5.1.4	Thermal Gravimetric Analysis/Differential Scanning Calorimetry (TGA/DSC) Analysis Results of Original Samples	33
5.2	Postmortems	50
5.2.1	X-Ray Diffraction (XRD) Analysis Results of Postmortems	51
5.2.2	Scanning Electron Microscope Analysis Results of Postmortems	51
5.2.3	Fourier Transform Infrared Spectroscopy (FTIR) Analysis Results of Postmortems	54
5.2.4	Thermal Gravimetric Analysis/Differential Scanning Calorimetry (TGA/DSC) Analysis Results of Postmortems	57
6	CONCLUSIONS	59
	REFERENCES	63
	APPENDICES	69
A.	THERMAL GRAVIMETRIC ANALYSIS	69
A.1	Identical Heating of Retort Postmortem with Air	69
A.2	Identical Heating of Microwave Postmortem with Air	71
A.3	Differential Thermal Gravimetric Analysis (DTG)	73
A.4	Arrhenius Model Plots	81
B.	FOURIER TRANSFORM INFRARED SPECTROSCOPY	95
B.1	Retort Postmortems	95
B.2	Microwave Postmortems	98
B.3	Combustion Postmortems	101
B.4	Pyrolysis Postmortems	103
B.5	Retort Simulation Postmortems	106
C.	SCANNING ELECTRON MICROSCOPE/ ENERGY DISPERSIVE X-RAY SPECTROSCOPY	109
C.1	Original Samples	109
C.2	Retort Postmortems	115
C.3	Microwave Postmortems	123

LIST OF FIGURES

FIGURES

Figure 2-1. The van Krevelen Diagram for depositional history of oil shales.....	4
Figure 2-2 Classification of organic sediments.....	6
Figure 4-1 Locations of the oil shale samples.....	17
Figure 4-2 Analyses Methods Workflow	20
Figure 4-3 Optimum temperature program of retort experiments.....	22
Figure 4-4 Analysis instruments	23
Figure 5-1 XRD spectra of original oil shale samples	28
Figure 5-2 Inorganic content of Himmetoglu oil shale from SEM.....	29
Figure 5-3 Organic content of Himmetoglu and Seyitomer oil shale from SEM	30
Figure 5-4 FTIR spectra of original oil shale samples	32
Figure 5-5 Retort simulation of original oil shale samples	35
Figure 5-6 Weight loss comparison of retort experiment and retort simulation	36
Figure 5-7. Retort simulation of original oil shale samples (with iron powder).....	38
Figure 5-8 Weight loss comparison of retort experiment and retort simulation (with iron powder).....	39
Figure 5-9 TGA/DSC results of identical heating under air injection	41
Figure 5-10 TGA/DSC results of identical heating under air injection (with iron powder)	43
Figure 5-11 TGA/DSC results of identical heating under nitrogen injection	45
Figure 5-12 TGA/DSC results of identical heating under nitrogen injection (with iron powder).....	46
Figure 5-13 Retort and microwave postmortems of Himmetoglu oil shale	52
Figure A-1 TGA/DSC results of identical heating of retort postmortems	69
Figure A-2 TGA/DSC results of identical heating of retort postmortems (with iron powder).....	70
Figure A-3 TGA/DSC results of identical heating of microwave postmortems	71
Figure A-4 TGA/DSC results of identical heating of microwave postmortems (with iron powder).....	72

Figure A-5 TG vs. DTG curves of Himmetoglu under air injection.....	73
Figure A-6 TG vs. DTG curves of Himmetoglu under air injection (with iron powder)	73
Figure A-7 TG vs. DTG curves of Himmetoglu under nitrogen injection.....	74
Figure A-8 TG vs. DTG curves of Himmetoglu under nitrogen injection (with iron powder)	74
Figure A-9 TG vs. DTG curves of Hatildag under air injection	75
Figure A-10 TG vs. DTG curves of Hatildag under air injection (with iron powder).....	75
Figure A-11 TG vs. DTG curves of Hatildag under nitrogen injection	76
Figure A-12 TG vs. DTG curves of Hatildag under nitrogen injection (with iron powder)	76
Figure A-13 TG vs. DTG curves of Seyitomer under air injection	77
Figure A-14 TG vs. DTG curves of Seyitomer under air injection (with iron powder) ..	77
Figure A-15 TG vs. DTG curves of Seyitomer under nitrogen injection	78
Figure A-16 TG vs. DTG curves of Seyitomer under nitrogen injection (with iron powder)	78
Figure A-17 TG vs. DTG curves of Ulukisla under air injection	79
Figure A-18 TG vs. DTG curves of Ulukisla under air injection (with iron powder)	79
Figure A-19 TG vs. DTG curves of Ulukisla under nitrogen injection	80
Figure A-20 TG vs. DTG curves of Ulukisla under nitrogen injection (with iron powder)	80
Figure A-21 Arrhenius plot of Himmetoglu for LTO at 10 °C/min	81
Figure A-22 Arrhenius plot of Himmetoglu for HTO at 10 °C/min.....	81
Figure A-23 Arrhenius plot of Himmetoglu (with iron powder) for LTO at 10 °C/min .	82
Figure A-24 Arrhenius plot of Himmetoglu (with iron powder) for HTO at 10 °C/min.	82
Figure A-25 Arrhenius plot of Hatildag for LTO at 10 °C/min.....	83
Figure A-26 Arrhenius plot of Hatildag for HTO at 10 °C/min	83
Figure A-27 Arrhenius plot of Hatildag (with iron powder) for LTO at 10 °C/min.....	84
Figure A-28 Arrhenius plot of Hatildag (with iron powder) for HTO at 10 °C/min	84
Figure A-29 Arrhenius plot of Seyitomer for LTO at 10 °C/min	85
Figure A-30 Arrhenius plot of Seyitomer for HTO at 10 °C/min.....	85
Figure A-31 Arrhenius plot of Seyitomer (with iron powder) for LTO at 10 °C/min.....	86

Figure A-32 Arrhenius plot of Ulukisla for LTO at 10 °C/min87

Figure A-33 Arrhenius plot of Ulukisla for HTO at 10 °C/min.....87

Figure A-34 Arrhenius plot of Ulukisla (with iron powder) for LTO at 10 °C/min88

Figure A-35 Arrhenius plot of Ulukisla (with iron powder) for HTO at 10 °C/min.....88

Figure A-36 Arrhenius plot of Himmetoglu for pyrolysis at 10 °C/min.....89

Figure A-37 Arrhenius plot of Himmetoglu (with iron powder) for pyrolysis at 10 °C/min89

Figure A-38 Arrhenius plot of Hatildag for pyrolysis at 10 °C/min90

Figure A-39 Arrhenius plot of Hatildag (with iron powder) for pyrolysis at 10 °C/min.90

Figure A-40 Arrhenius plot of Seyitomer for pyrolysis (I. region) at 10 °C/min91

Figure A-41 Arrhenius plot of Seyitomer for pyrolysis (II. region) at 10 °C/min91

Figure A-42 Arrhenius plot of Seyitomer (with iron powder) for pyrolysis (I. region) at 10 °C/min92

Figure A-43 Arrhenius plot of Seyitomer (with iron powder) for pyrolysis (II. region) at 10 °C/min92

Figure A-44 Arrhenius plot of Ulukisla for pyrolysis at 10 °C/min93

Figure A-45 Arrhenius plot of Ulukisla (with iron powder) for pyrolysis at 10 °C/min.93

Figure B-1 FTIR spectra of Himmetoglu retort postmortem95

Figure B-2 FTIR spectra of Himmetoglu retort postmortem (with iron powder).....95

Figure B-3 FTIR spectra of Hatildag retort postmortem.....96

Figure B-4 FTIR spectra of Hatildag retort postmortem (with iron powder)96

Figure B-5 FTIR spectra of Seyitomer retort postmortem96

Figure B-6 FTIR spectra of Seyitomer retort postmortem (with iron powder).....97

Figure B-7 FTIR spectra of Ulukisla retort postmortem.....97

Figure B-8 FTIR spectra of Ulukisla retort postmortem (with iron powder).....97

Figure B-9 FTIR spectra of Himmetoglu microwave postmortem98

Figure B-10 FTIR spectra of Himmetoglu microwave postmortem (with iron powder).98

Figure B-11 FTIR spectra of Himmetoglu Shale Oil98

Figure B-12 FTIR spectra of Hatildag microwave postmortem99

Figure B-13 FTIR spectra of Hatildag microwave postmortem (with iron powder)99

Figure B-14 FTIR spectra of Seyitomer microwave postmortem.....99

Figure B-15 FTIR spectra of Seyitomer microwave postmortem (with iron powder) ..	100
Figure B-16 FTIR spectra of Ulukisla microwave postmortem	100
Figure B-17 FTIR spectra of Ulukisla microwave postmortem (with iron powder)	100
Figure B-18 FTIR spectra of Himmetoglu combustion postmortem	101
Figure B-19 FTIR spectra of Himmetoglu combustion postmortem (with iron powder)	101
Figure B-20 FTIR spectra of Hatildag combustion postmortem	101
Figure B-21 FTIR spectra of Hatildag combustion postmortem (with iron powder)	102
Figure B-22 FTIR spectra of Seyitomer combustion postmortem.....	102
Figure B-23 FTIR spectra of Seyitomer combustion postmortem (with iron powder)..	102
Figure B-24 FTIR spectra of Ulukisla combustion postmortem.....	103
Figure B-25 FTIR spectra of Ulukisla combustion postmortem (with iron powder)	103
Figure B-26 FTIR spectra of Himmetoglu pyrolysis postmortem	103
Figure B-27 FTIR spectra of Himmetoglu pyrolysis postmortem (with iron powder)..	104
Figure B-28 FTIR spectra of Hatildag pyrolysis postmortem	104
Figure B-29 FTIR spectra of Hatildag pyrolysis postmortem (with iron powder)	104
Figure B-30 FTIR spectra of Seyitomer pyrolysis postmortem.....	105
Figure B-31 FTIR spectra of Seyitomer pyrolysis postmortem (with iron powder).....	105
Figure B-32 FTIR spectra of Ulukisla pyrolysis postmortem.....	105
Figure B-33 FTIR spectra of Ulukisla pyrolysis postmortem (with iron powder)	106
Figure B-34 FTIR spectra of Himmetoglu retort simulation postmortem	106
Figure B-35 FTIR spectra of Himmetoglu retort simulation postmortem (with iron powder)	106
Figure B-36 FTIR spectra of Hatildag retort simulation postmortem	107
Figure B-37 FTIR spectra of Hatildag retort simulation postmortem (with iron powder)	107
Figure B-38 FTIR spectra of Seyitomer retort simulation postmortem.....	107
Figure B-39 FTIR spectra of Seyitomer retort simulation postmortem (with iron powder)	108
Figure B-40 FTIR spectra of Ulukisla retort simulation postmortem.....	108

Figure B-41 FTIR spectra of Ulukisla retort simulation postmortem (with iron powder)	108
.....	
Figure C-1 EDS of albite mineral (from Himmetoglu oil shale)	109
Figure C-2 EDS of (diatom) organic content (from Himmetoglu oil shale)	110
Figure C-3 EDS of pyrite mineral (from Himmetoglu oil shale)	110
Figure C-4 SEM images of Himmetoglu oil shale	111
Figure C-5 SEM images of Hatildag oil shale	112
Figure C-6 SEM images of Seyitomer oil shale	113
Figure C-7 SEM images of Ulukisla oil shale	114
Figure C-8 SEM images of Himmetoglu retort postmortem	115
Figure C-9 SEM images of Himmetoglu retort postmortem (with iron powder)	116
Figure C-10 SEM images of Hatildag retort postmortem	117
Figure C-11 SEM images of Hatildag retort postmortem (with iron powder)	118
Figure C-12 SEM images of Seyitomer retort postmortem	119
Figure C-13 SEM images of Seyitomer retort postmortem (with iron powder)	120
Figure C-14 SEM images of Ulukisla retort postmortem	121
Figure C-15 SEM images of Ulukisla retort postmortem (with iron powder)	122
Figure C-16 SEM images of Himmetoglu microwave postmortem	123
Figure C-17 SEM images of Himmetoglu microwave postmortem (with iron powder)	124
.....	
Figure C-18 SEM images of Hatildag microwave postmortem	125
Figure C-19 SEM images of Hatildag microwave postmortem (with iron powder)	126
Figure C-20 SEM images of Seyitomer microwave postmortem	127
Figure C-21 SEM images of Seyitomer postmortem (with iron powder)	128
Figure C-22 SEM images of Ulukisla microwave postmortem	129
Figure C-23 SEM images of Ulukisla microwave postmortem (with iron powder)	130

LIST OF TABLES

TABLES

Table 2-1 Oil shale resources by country (billion barrels).....	7
Table 4-1 Characteristics of oil shale samples	18
Table 5-1 Crystalline minerals from XRD analysis of original samples	26
Table 5-2 Temperature program of retort experiments.....	33
Table 5-3 Temperature program of retort experiments (with iron powder).....	37
Table 5-4 Weight loss percentages	47
Table 5-5 Activation energies of combustion calculated from Arrhenius Method at a heating rate of 10 °C min ⁻¹	48
Table 5-6 Activation energies of pyrolysis calculated from Arrhenius Method at a heating rate of 10 °C min ⁻¹	49
Table 5-7 Effect of temperature program.....	50
Table 5-8 Minerals from XRD analysis of postmortems	53

CHAPTER 1

INTRODUCTION

The depletion of conventional oil reserves make the world being in quest of alternative sources. Thus, unconventional oil reserves became popular and economic. As unconventional source, shale oil is a major substitute for conventional petroleum. The total oil shale reserves of the world are predicted to be 3,500 billion barrels (World Energy Council, 2010). In Turkey, oil shale is the second fossil fuel potential with 2.2 billion tons of explored reserves (Altun, Hiçyılmaz, Hwang, Bağcı, & Kök, 2006). Oil shales can be recovered by using thermal heating methods, which decreases the viscosity of the oil. As the most effective thermal heating method, retorting is used to produce shale oil. Besides, microwave is regarded as alternative heating method for oil recovery from oil shales with the advantage of low processing times.

In the background of this study, four different oil shales from Turkey were tested experimentally by using retort and microwave heating techniques with and without the iron powder additives. After the experiments, the electrical heating option of a reservoir simulator (CMG, STARS 2007) was used to simulate the retort experiment; while microwave experiment results were modeled by analytical models (Hascakir, 2008). Earlier experiments give information about the recovery characteristics and viscosities of shale oils, and feasibility of heating processes. By taking the conducted experiments a step further, this thesis proposes a literature review of qualitative and quantitative analysis of four oil shale before and after the heating experiments. This thesis will discuss the organic compounds and the amount of organic matters of the oil shale samples by considering the effects of additives to understand the mechanisms behind the thermal heating experiments.

CHAPTER 2

LITERATURE REVIEW

2.1 Oil Shale

Oil shale is generally defined as a sedimentary rock containing organic matter. The oil shale is the source rock for most of the conventional oils; therefore, the oil shale rock does not originally contain mature oil, but it can be upgraded into hydrocarbons by releasing the organic matter inside with sufficient heat. The hydrocarbons in oil shale can be used as an alternative to conventional petroleum and natural gas.

Oil shales consist of both organic and inorganic components; they are kerogen, bitumen and inorganic matrix. The insoluble part, kerogen includes the major part of the organic matter; while; the soluble part, bitumen constitutes insignificant portion (Yen & Chilingarian, 1976).

The net calorific value of a typical oil shale is 5.60 MJ/kg. Moreover, the specific heat capacity of oil shale is larger than other minerals; while, the permeability, porosity and the thermal conductivity is very low (Abbasov, Mamedov, & Ismailov, 2008; Pan, Zhang, Wang, & Yang, 2012).

Oil shale is commonly classified by their depositional environments and mineral contents. Depositional history of the sedimentary rock is the indicator for the type of the environment of the rock. According to their depositional environments kerogen in the sedimentary rocks can be classified into three types: Type I, Type II and Type III.

Type I kerogen is generally from lacustrine origin. The initial atomic H/C ratio of Type I is 1.5 or higher; while, O/C is 0.1 and lower. Type II kerogen is associated with marine environments and their oil generating potential is less than Type I. The H/C ratio of Type II is lower and O/C ratio is higher than Type I. Type III kerogen represents the terrestrial environments. Coals and coaly shale belong to Type III. The initial atomic H/C ratio is generally less than 1.0 and O/C ratio is higher than 0.2 (Speight, 1999). The van Krevelen Diagram can be used to classify the depositional environments of the oil shales by using H/C ratio (Figure 2-1).

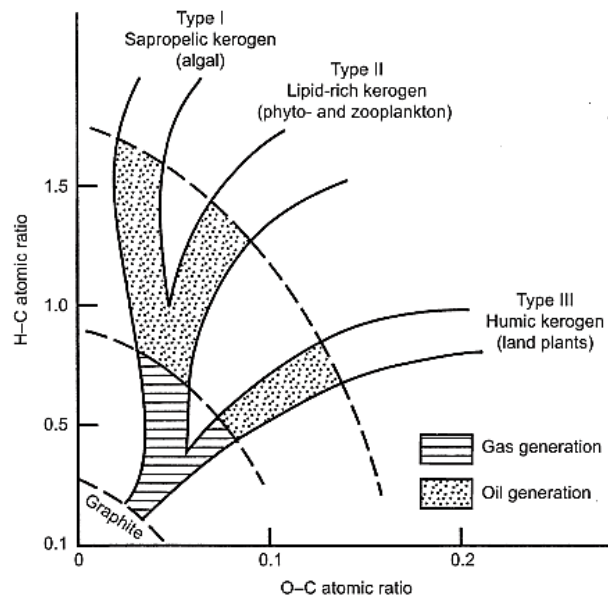


Figure 2-1. The van Krevelen Diagram for depositional history of oil shales (Speight, 1999)

According to their mineral contents, oil shale can be classified into three main types: carbonate rich shale, siliceous shale, and coaly shale (cannel shale). Carbonate rich shale comprises carbonate in high quantity. Calcite and dolomite are the most common carbonate minerals seen in carbonate rich shale. The carbonate rich shale is generally from lacustrine origin. Among others, the carbonate rich shale is the most precious ones. However, for combustion retorting this kind of shale is not favorable due to the hard rubblization (Lee, 1990). Siliceous shale is dark brown or black and rich in silica minerals

such as chert or opal and generally from marine environments. The deposits from tertiary period and Mesozoic Era show precious oil product; while, Paleozoic Era deposits shows poor oil yield. Generally, siliceous oil shale is appropriate for mining operations. Coaly shales (cannel shale) are from terrestrial origin, contain inertine and vitrinite minerals, and seen in dark brown and black colors. Moreover, via conventional distillation most of the organic matter can be converted to oil, with char remaining.

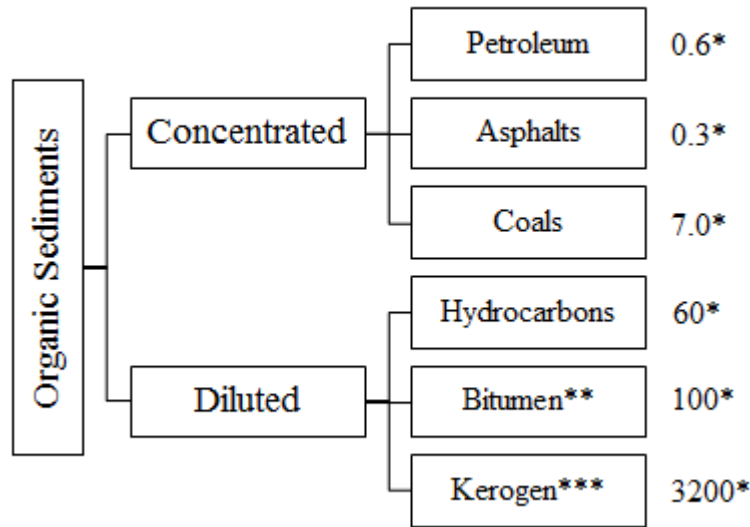
2.1.1 Oil Shale Resources

Oil shale is considered as unconventional oil resource. As alternative for conventional oil, the unconventional resources are so huge that it is several times larger than the conventional oil resources (World Energy Council, 2010). Moreover, the abundance of the components of oil shale is immense as alternative sources to concentrated fossil fuels (Figure 2-2) (Yen, 1976).

The total oil shale reserves of the world are predicted to be more than 3,500 billion barrels; 1,000 billion barrels of which are thought to be technically recoverable (World Energy Council, 2010). In Turkey, oil shale is the second fossil fuel potential with 2.2 billion tons of explored reserves (Altun et al., 2006).

Since the oil shale is the source rocks of the conventional oils, their distributions are generally close to the oil fields in the world and seen in 100 major deposits (Biglarbigi, Mohan, & Killen, 2009). The United States, Russia, Democratic Republic of the Congo, Brazil, Italy, Morocco, Jordan, Australia, China, Canada and Estonia are the top known countries having the major oil shale deposits.

The United States is the most known oil shale host in the world. The United States is followed by Russia and Democratic Republic of the Congo; with 290 and 100 barrels of original oil in place, respectively. Table 2-1 shows the oil shale resources of the top known countries with technically recoverable oil shale resources.



* The abundance of various fossil fuels in the ecosystem present in trillion tons.

** Non-hydrocarbon; extractable.

*** Non-extractable.

Figure 2-2 Classification of organic sediments
(Yen, 1976)

The United States is having more than 3,000 billion barrels which constitutes approximately 77% of the world's known recoverable oil shale potential. The major oil shale deposits in the United States are the Eocene Green River Deposits and Devonian-Mississippian Black Shale. 83% of the United States' oil shale resources are supplied from the Green River; while 5% is from Black Shale (Biglarbigi et al., 2009).

Turkey also has a remarkable amount of oil shale capacity such that it is the second fossil fuel potential in Turkey. The total oil shale reserves in Turkey are predicted to be more than 3-5 billion tons; 2.2 billion tons of which are thought to be technically recoverable. Oil shale deposits in Turkey are mostly located in near Ankara, near Manisa and near Ereğli coal field in the North West of Turkey. The four main deposits of Turkey are Himmetoğlu in Bolu, Seyitömer in Kütahya, Hatildağ in Bolu and Beypazari in Ankara. The host rocks are marlstone and claystone from Paleocene to Eocene age (Güleç & Önen, 1992).

Table 2-1 Oil shale resources by country (billion barrels)

(International Energy Agency, 2010)

Countries	Oil Originally in Place	Technically Recoverable
United States	$\geq 3,000$	$\geq 1,000$
Russia	290	n.a.
Dem. Rep. of Congo	100	n.a.
Brazil	85	3
Italy	75	n.a.
Morocco	55	n.a.
Jordan	35	30
Australia	30	12
China	20*	4
Canada	15	n.a.
Estonia	15	4
Other (30 Countries)	60	20
World	$\geq 3,500$	n.a.

2.2 Oil Shale Extraction Methods

Extraction of the shale oil from oil shale can be accomplished by several methods (Yen & Chilingarian, 1976). One of them is breaking the chemical bonds of the organics for upgrading the solid hydrocarbons. This is achieved by releasing the kerogen inside with sufficient heat. This heating process is called retorting.

During the retorting process, the kerogen inside the oil shale is converted to shale oil through pyrolysis. The term “pyrolysis” is identified as a thermochemical decomposition of oil shale. Unlike combustion, the pyrolysis does not require oxygen for reactions, and mostly occurs in the anoxic atmosphere. In this process, the oil shale is decomposed into solid (char), liquid (heavy molecules), and gaseous products (light molecules) (Fernandez,

Arenillas, & Menendez, 2011). The process is achieved by heating the kerogen to the temperature of about 500°C. The oil shale extraction can be performed either by surface retorting or in-situ retorting; according to the location of the process.

2.2.1 Surface Retorting

During the surface retorting process, oil shale is mined by either surface (open pit mining) or underground mining, then crushed and finally be conducted to the retorting process at the surface in an oil shale retort facilities.

In order to heat the oil shale to yield oils both pyrolysis and combustion methods are used in the surface retorting (Speight, 2012).

First known modern industrial oil shale production began with mining of the oil shale in the 19th century in Autun mines, France (Laherrere, 2005). The first major experimental retort was tested in 1951 by the United States Bureau of Mines, in Rifle, Colorado; which had the capacity of processing six tons of oil shale per day. This progress of the state has been aroused the interest of the many private company to this issue and established different methods (Smith, Shadle, & Hill, 2007; Yen & Chilingarian, 1976).

Union A and B retorts of Union Oil, Cameron and Jones, TOSCO II of the Oil Shale Corporation, Nevada-Texas-Utah (NTU), Lurgi-Rohrgas processes are the most known surface retorting projects after this progress (Speight, 2012; Yen, 1976).

Today, most of the projects comprise the surface retorting technology; since, it is easy to control the process variables. Moreover, it provides relatively high recovery efficiency with 80-90% (Yen, 1976). However, due to the environmental (spent shale disposal) and economic problems, and mining application limits; it is expected to increase the number of in-situ retorting projects in the near future.

2.2.2 In-situ Retorting

In-situ retorting is used to remove hydrocarbon materials from underground formation but does not require mining of shale. In order to recover the hydrocarbon material from underground formation, chemical and physical properties of them should be changed (Vinegar, Bass, & Hunsucker, 2005). There are two in-situ methods in the literature: True in-situ and modified in-situ. During in-situ retorting, the oil shale formation is first fractured then directly heated; afterwards, the recovered hydrocarbons are produced directly from reservoir as conventional production of crude oil. Apart from true in-situ method, modified in-situ process starts with surface mining, and continues with same heating step. In order to heat the oil shale during in-situ retorting, combustion, introducing heated gas or liquids, and electric rods are used (Speight, 2012; Zheng, Li, Ma, & Wang, 2012).

American Shale Oil LLC (AMSO), Chevron CRUSH, ExxonMobil Electrofrac, Shell in-Situ Conversion (ICP), Dow, and Occidental Modified In Situ processes are current in-situ retorting projects, currently (Speight, 2012). In-situ retorting technology generally does not require the mining, transportation and crushing processes; therefore, there is no spent shale disposal problems with this process and seems more economic. Besides, since process is similar to the conventional oil production, it is suitable for deep burial depths of oil shale formation (Yen, 1976). Minimizing the environmental and expenditure problems arouse interest on in-situ retorting method. However, due to the low permeability of oil shale, the process control for in-situ retorting is limited and recovery is very low; therefore, there is no commercial production of in-situ retorting at the present time.

2.3 Oil Shale Heating Methods

To heat the oil shale for endothermic kerogen decomposition, the energy need is supplied by several heating techniques.

Heating methods for oil shale retorting can be divided into two as; direct and indirect heating methods. Direct heating method can be defined basically as the internal combustion of oil shale. However, indirect heating methods should be defined and classified by the ways of conveying the heat to the oil shale formation.

Combustion is highly exothermic process; the heat generated is used as a combustion front during the heating procedure. In this method, some interior igniting materials are added to burn the organics to supply hot gases for the retorting. The heat is then directly used for pyrolysis of the oil shale (Das, 2009).

As heating method, combustion can be used in both surface and in-situ retorting. In surface retorting, the direct heating process is achieved by a mixture of combustion gases and reheated recycled gases. Union A, NTU and Paraho Direct processes are performed with surface retorting by direct heating method. During in-situ retorting, the combustion process are carried out by creating the zones underground: Combustion zone and pyrolysis zone (the heat for pyrolysis supplied from combustion zone). First, a portion of the formation is ignited; subsequently, as from the well the combustion is maintained by burning the carbons in the oil shale.

During this heating process, combustion and pyrolysis take place simultaneously. Therefore, the combustion gases mixed with the pyrolysis products; which results the reduction of the value of the gaseous products (J. E. Bridges, Taflove, & Snow, 1978).

Through the indirect heating methods, the heat is generally supplied by heating external material to heat the oil shale. The known methods are conduction through a wall, externally generated hot gas, hot recycled solid (HRS), and reactive fluids (Burnham & Mcconaghy, 2006). Among the surface retorting projects; Fischer Assay, Union B, TOSCO II, and Hytort Process of Institute of Gas Technology projects are using the conduction through a wall, externally generated hot gas, HRS and reactive fluid heating methods, respectively. In-situ projects American Shale oil CCR, Chevron CRUSH, and Shell ICP are using conduction through a wall, externally generated hot gas, and reactive fluids as heating methods (Burnham & Mcconaghy, 2006; Yen, 1976).

2.3.1.1 Unconventional Heating

Above-mentioned methods are regarded as conventional methods; where the heat transfer is achieved through conduction and convection. However, studies show that oil shale is a poor heat conductor and it takes long time when heating large treated area (Chen, Wang, Sun, Guo, & Yan, 2013; Meredith, 1998). Therefore, it is time and money consuming to transfer the heat by conventional heating methods.

Apart from other methods, electrical volumetric heating provides heating for the treated formation in a molecular level. Therefore, the heating process offers an ideal heating to almost all the volume of the work piece.

The techniques for electrical volumetric heating are electrical currents (ohmic heating), radiofrequency and microwave methods. Parker, (1964) proclaimed the usage of electric currents for oil shale heating after the invention of Sarapuu, (1957). Using this method the well is heated via electric currents between two electrodes creating ohmic (resistance) heating. The adjacent formation is then heated by this power, up to expected temperature for pyrolysis.

Another technique, in the high frequency band of electromagnetic spectrum, radiofrequency is examined by J. E Bridges, Stresty, Taflove, & Snow (1979) with Utah tar sands. In this method, the shale body is heated uniformly unlike conventional methods, which transfers the heat as from outside the shale body by conduction. The main purpose of this method is reducing the viscosity of the hydrocarbons in order to be pumped easily by decreasing the number of the required wells and producing a more uniformly distributed temperature distribution (Savage, 1985). This is achieved by placing the antennas into the oil shale formation (Mallon, 1980). Latter studies of radiofrequency experiments conducted by Mallon (1980) and Carlson, Blase, & Mclendon (1981) shows that this heating technique is also suitable and economic for oil shale.

Microwave heating is another way in the high frequency range (frequencies between 300 and 0.3 GHz); which provides dielectric heating like radiofrequency. The heating process can be achieved by the movement and collisions of the molecules subjected to the microwave energy. Microwave heating, similar to the radiofrequency, directly heats the oil shale body in a molecular level rather than convection or conduction. Microwave heating is also mentioned as dielectric heating due to the fact that dielectric substances absorb the microwave radiation rather than reflecting or letting to pass through.

Early studies were conducted by Abernethy (2013) lays the foundations of the microwave heating. Latter studies of Wilson (1987) and Pringle, Everleigh, & Forthe, (2010) about microwave heating for oil shale give favorable results and were secured by patents.

To see whether the this technique is favorable or not, Bridges et al. (1978) calculated the net energy recovery (NER) of this method and stated that in-situ microwave heating method can offer more energy than consumed during the heating process. In 1983, Butts, Lewis, & Steward examined the microwave heating of New Brunswick oil shale; the results were compared with the previous work of Bridges et al. (1978) and obtained similar results.

During microwave pyrolysis, oil and gas yield depends on the dielectric properties of oil shale. Oil shale is a poor microwave absorbing material for obtaining valuable results. Therefore, the effect, amount and variety of dielectric properties of oil shale during microwave heating were examined with several studies conducted by Briggs, Lewis, & Tranquilla (1983), Al-Harashsheh et al. (2009) and Hakala, Stanchina, Soong, & Hedges (2011) in terms of applied frequency, mineral phases present, water content, organic content and temperature. During the microwave pyrolysis, there is a decrease in amount of volatiles; this reduction results in the production of the char. The pyrolysis process is prolonged due to dielectric characteristics of the char.

One of the advantages of the microwave heating is that the quality of the produced oil is high. Bradhurst & Worner (1996) and El harfi, Mokhlisse, Chanaa, & Outzourhit (1999)

applied the microwave heating to the Australian and Moroccan oil shale. It is found that the produced oil is maltenic, less polar and contains light hydrocarbons, less sulfur and nitrogen unlike the oil produced via conventional retorting.

Another significant advantage of the microwave heating over other methods is that the processing time of microwave pyrolysis is shorter than the conventional pyrolysis. However, as Hascakir & Akin (2010) stated, in order to obtain high recovery the rapid heating of microwave radiation should be upheld later on reaching the pyrolysis temperature.

Recently, in order to compare the unconventional methods, Alomair, Alarouj, Althenayyan, Alsaleh, & Mohammad (2012) studied the effects of the three unconventional heating methods on heavy oils. In this study, it was seen that the highest recovery percent did not belong to microwave heating. However, by comparing both power consumption and recoveries of the three methods, it was observed that microwave heating is the most economic one amongst others.

CHAPTER 3

STATEMENT OF THE PROBLEM

Electrical and microwave heating techniques are relatively new methods for oil shale extraction. The development of this technology is limited and there is lack of knowledge about electrical and microwave heating mechanisms of oil shale. Therefore, the aim of this study is to analyze the oil shale samples before and after the heating experiments qualitatively and quantitatively, to understand mechanisms of retort and microwave heating.

For these purposes, TGA/DSC, XRD, FTIR, and SEM instruments were used;

1. To analyze the reactivity and extraction potential of oil shale samples under retort and microwave heating,
2. To understand mechanisms of retort and microwave heating experiments, and
3. To extend our knowledge by analyzing different types of oil shale samples with variety of mineralogical changes and which have different kerogen content.

CHAPTER 4

MATERIALS AND METHODS

4.1 Oil Shale Samples and Locations

Original oil shale samples were collected from Hatildag, Himmetoglu, Seyitomer, and Ulukisla. All oil shale samples are from Tertiary Period and located near Bolu (Hatildag and Himmetoglu), Kutahya (Seyitomer) and Nigde (Ulukisla) (See Fig. 4-1). For all original oil shale samples, analyses have been conducted on crushed samples that have 3-5 mm particle sizes.

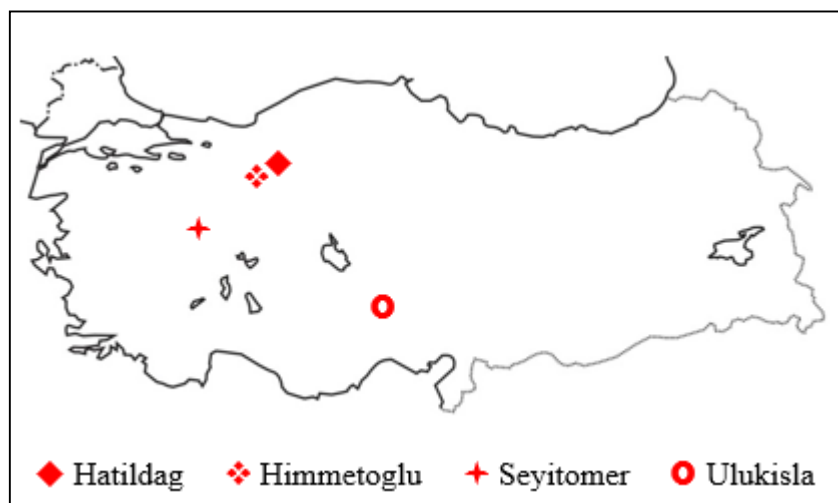


Figure 4-1 Locations of the oil shale samples

Below summarizes the characteristics of four oil shale sample

Table 4-1 Characteristics of oil shale samples

Deposit	Calorific Value (MJ/kg)	Reserves (million ton)	Total Organic Content (wt. %)
Himmetoglu	3.25	150	21.5
Hatıldag	3.24	150	3.32
Seyitomer	3.55	110	12.47
Ulukisla	2.63	130	~1

4.2 Retort and Microwave Postmortems

Earlier in this study, retort and microwave experiments were conducted by (Hascakir, 2008). Retorted samples of Hascakir (2008) are preserved well until now; therefore, we used these samples during the analyses. Particle size of retort postmortems are larger than original samples due to accretion after the heating experiments and they are 3-10 mm in size.

Microwave heated samples, however, were not stored well and we could not find sufficient amount of sample to be analyzed. Therefore, the microwave experiments were conducted once more to be able to conduct analyses. Postmortems have original sample size after the microwave experiments.

4.3 Iron Powders

Iron powders (Iron and Iron (III) Oxide) were added to samples to enhance to efficiencies of the heating experiments. Aim of using iron powder in retort experiments was to increase thermal conductivity of the samples; while, in microwave experiments they were used as a microwave absorber to achieve rapid temperature increase. Particle sizes of iron powders were measured by using Brookhaven Instruments Corp. NanoBrook 90Plus Particle Size

Analyzer and varies as follows: Iron (Fe) has 2.74 μm , and Iron (III) Oxide (Fe_2O_3) has 400.7 nm effective diameters. For microwave experiments and analysis, the optimum percentages defined by Hascakir (2008) were used. 0.1% wt. Fe_2O_3 was used for Hatildag oil shale, 0.1% wt. Fe was used for Himmetoglu oil shale, 0.5% wt. Fe was used for Seyitomer oil shale, and 0.1% wt. Fe_2O_3 was used for Ulukisla oil shale.

4.4 Experimental Procedure

Microwave experiments were conducted by using Hamilton Beach conventional kitchen microwave oven. Power specification of the microwave oven is 120V~60Hz, with 1000W input and 900W output power, and its operation frequency is 2450 MHz. 50 ml beaker was used as a sample holder.

4.4.1 Sample Preparation

Original size of oil shale samples was maintained during microwave experiments. Each experiment was conducted for each oil shale sample, separately. Weight of the samples placed in a 50 ml beaker varied from 30-40 g. In order to enhance the microwave heating, different iron powders were added to each oil shale sample with different percentages.

4.4.2 Experimental Period and Temperature Measurement

Hascakir (2008) conducted microwave heating experiments for 3 minutes. To get best results from the analyses, we planned to hold each microwave experiment for 10 minutes. Typical type K thermocouples were used to measure final temperature at the end of the microwave heating experiments. Final temperatures were measured outside the microwave oven, individually.

4.5 Material Analyses

First, characterization studies were achieved with Fourier Transform Infrared Spectroscopy (FTIR) to determine the molecular structure, X-Ray Diffraction (XRD) to

define mineralogy, and Scanning Electron Microscope (SEM) to visualize the surface stratigraphy before and after the heating experiments. Thermal Gravimetric Analyses (TGA/DSC) were conducted under nitrogen and air atmosphere to determine the reactivity of rock samples at varying temperature ranges, understand the effectiveness of retort, and microwave experiments.

Second, after retort and microwave heating experiments each postmortem were further analyzed by four analyses methods again to understand the change in mineralogical and organic content of the samples. Below workflow summaries the analyses methods:

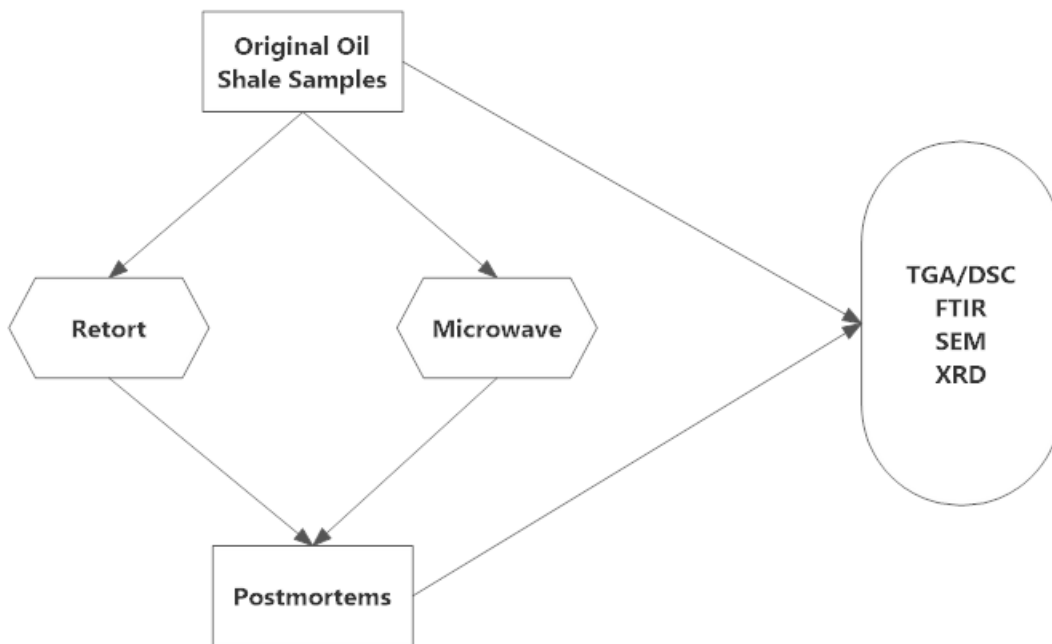


Figure 4-2 Analyses Methods Workflow

4.5.1 X-Ray Diffraction (XRD)

XRD analyses were performed with Bruker D8 Advanced XRD instrument (See Fig. 4-4 (c)) on original oil shale samples. The samples were powdered and placed in the sample holder of a two-circle goniometer. The X-ray source was a 2.2 kW Cu X-ray tube and maintained at an operating current of 40 kV and 40 mA. The two-circle 250 mm diameter

goniometer was computer controlled with independent stepper motors and optical encoders for the θ and 2θ circles with the smallest angular step size of $0.0001^\circ 2\theta$.

4.5.2 Scanning Electron Microscope/Energy Dispersive X-Ray Spectroscopy (SEM/EDS)

High magnification JEOL/JSM-7500F Field Emission Scanning Electron Microscope (See Fig. 4-4 (d)) was used to check the surface morphology of original samples and retort-microwave postmortems. All samples were uncoated (except for microwave postmortem of Himmetoglu oil shale) and placed on a brass sample mounts. Microwave postmortem of Himmetoglu oil shale sample was coated by platinum/palladium alloy. Original sample size was maintained for SEM analyses.

4.5.3 Fourier Transform Infrared Spectroscopy (FTIR)

FTIR analyses were performed using Agilent Cary 630 FTIR Spectrometer (See Fig. 4-4 (b)). The range of the spectra is $4000\text{-}650\text{ cm}^{-1}$ at a spectral resolution of 8 cm^{-1} for 32 background and sample scans with Happ-Genzel apodization. Analyses have been repeated three times for each sample. Measurements were conducted on original and four postmortem sets of TGA/DSC analysis to observe the mineralogical changes with absorbance finger prints. Before each FTIR measurement, all original samples were brought to 60 mesh size.

4.5.4 Thermal Gravimetric Analysis/Differential Scanning Calorimetry (TGA/DSC)

TGA/DSC analyses were performed with Netzsch STA 449 F3 Jupiter instrument (See Fig. 4-4 (a)) at heating rate of $10\text{ }^\circ\text{C}/\text{min}$ with aluminum oxide (Al_2O_3) crucibles. Samples were grinded to size of <60 mesh and 30-40 mg of each was used in the experiments. Four sets of experiments were conducted with TGA/DSC on original oil shale samples and postmortems.

In the first set, original samples with and without iron powders were subjected to the same temperature program of the original retort experiments conducted by Hascakir (2008) in order to mimic the retort experiments. During retort experiments, below temperature program was found as optimum:

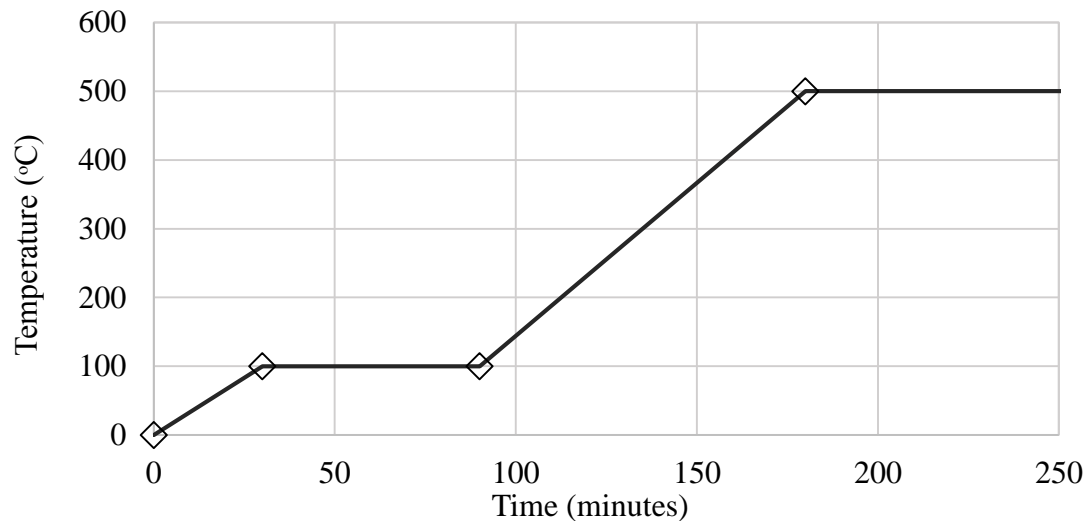


Figure 4-3 Optimum temperature program of retort experiments

In the second set, original samples with and without iron powders were subjected to identical heating (from 24 °C to 900 °C) under 50 ml/min air (purge) and 20 ml/min nitrogen protective gas flow to check the organic and inorganic decomposition periods during combustion.

In the third set, original samples with and without iron powders were heated under 50 ml/min nitrogen (purge) and 20 ml/min nitrogen protective gas flow (24 and 900 °C) in order to understand the pyrolysis behaviors of each oil shale sample under identical heating.

In the fourth set, all postmortems of retort and microwave heating experiments were heated from 24 °C to 900 °C under 50 ml/min air (purge) and 20 ml/min nitrogen protective

gas flow to check the efficiency of the retort and microwave experiments. The samples at the end of the four tests were kept for further analysis.

	
(a) TGA/DSC Instrument	(b) FTIR Instrument
	
(c) XRD Instrument	(d) SEM/EDS Instrument

Figure 4-4 Analysis instruments

CHAPTER 5

RESULTS AND DISCUSSIONS

5.1 Original Samples

In this section, X-Ray Diffraction (XRD), Thermal Gravimetric Analysis/Differential Scanning Calorimetry (TGA/DSC), Fourier Transform Infrared Spectroscopy (FTIR), and Scanning Electron Microscope/Energy Dispersive X-Ray Spectroscopy (SEM/EDS) analysis results of original oil shale samples are mentioned and discussed. In this section, the analyses results were discussed for characterization purposes, mainly.

5.1.1 X-Ray Diffraction (XRD) Analysis Results of Original Samples

The minerals of the oil shale samples obtained from XRD analysis show that quartz and dolomite/calcite are the leading minerals (See Table 5-1). Other minerals commonly seen in samples are gypsum, aragonite, muscovite, albite and pyrite minerals.

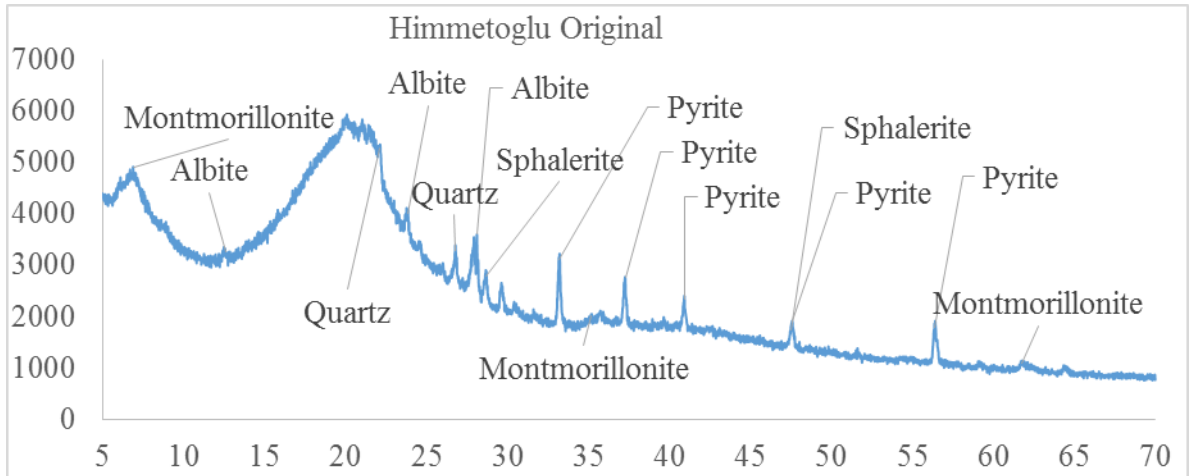
Note that, although all oil shale sample have clay minerals, the XRD results show a few. The reason is that with the used XRD technique we were able to identify crystalline minerals. Since the clay minerals are fine grained, it is difficult to identify all of them by common XRD technique. Further examinations are needed to define clay minerals.

Figure 5-1 shows XRD spectra of the four original oil shale samples. Big hump, seen at low theta values in XRD spectrum of Himmetoglu oil shale indicates low degree of crystallinity; showing that the sample is mostly amorphous (See Fig. 5-1 a). Amorphous content in the oil shale represents Type I kerogen.

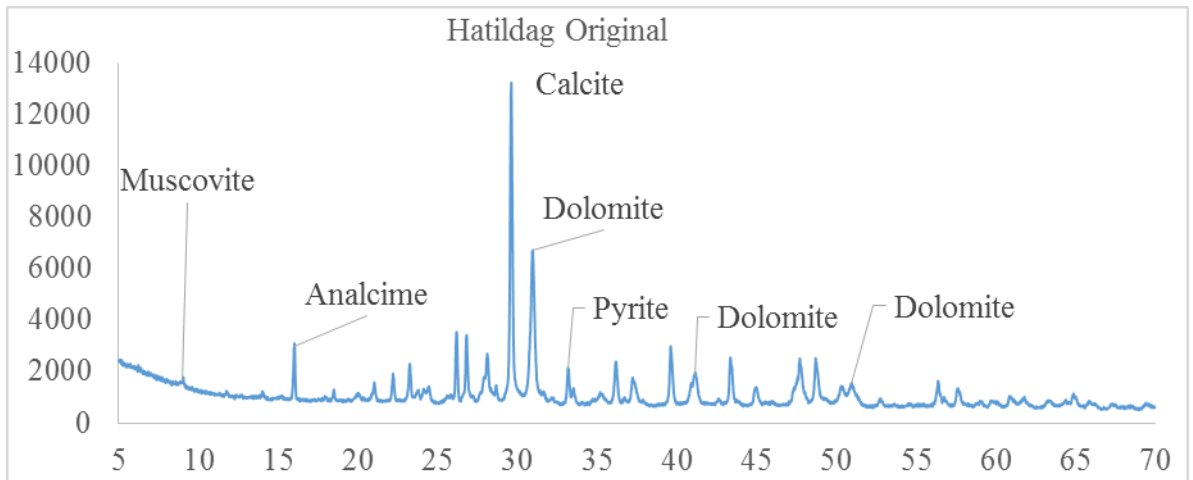
Table 5-1 Crystalline minerals from XRD analysis of original samples

<i>Oil shales</i>	<i>Crystalline minerals with chemical formula</i>
Ulukisla	Gypsum [CaSO ₄ ·2H ₂ O], Aragonite [CaCO ₃], Quartz [SiO ₂], Dolomite [CaMg(CO ₃) ₂], Illite [K _{0.65} Al ₂ (Al _{0.65} Si _{3.35} O ₁₀)(OH) ₂]
Himmetoglu	Sphalerite [ZnS], Pyrite [FeS ₂], Albite [NaAlSi ₃ O ₈], Quartz [SiO ₂], Montmorillonite [(Na,Ca) _{0.33} (Al,Mg) ₂ (Si ₄ O ₁₀)(OH) ₂ ·nH ₂ O]
Hatildag	Pyrite [FeS ₂], Dolomite [CaMg(CO ₃) ₂], Albite [NaAlSi ₃ O ₈], Analcime [Na ₂ (Al ₂ Si ₄ O ₁₂)·2H ₂ O], Gypsum [CaSO ₄ ·2H ₂ O], Illite [K _{0.65} Al ₂ (Al _{0.65} Si _{3.35} O ₁₀)(OH) ₂]
Seyitomer	Gypsum [CaSO ₄ ·2H ₂ O], Aragonite [CaCO ₃], Quartz [SiO ₂], Pyrite [FeS ₂], Dolomite [CaMg(CO ₃) ₂], Albite [NaAlSi ₃ O ₈], Illite [K _{0.65} Al ₂ (Al _{0.65} Si _{3.35} O ₁₀)(OH) ₂], Lithiophorite [(Al,Li)MnO ₂ (OH) ₂], Clinocllore [(Mg,Fe ²⁺) ₅ Al(AlSi ₃ O ₁₀)(OH) ₈], Montmorillonite [(Na,Ca) _{0.33} (Al,Mg) ₂ (Si ₄ O ₁₀)(OH) ₂ ·nH ₂ O]

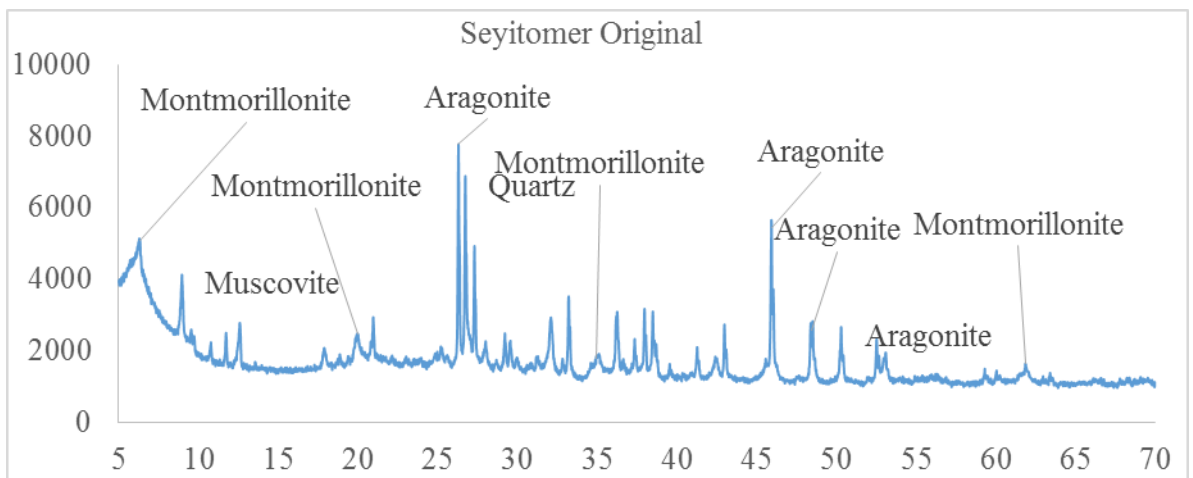
Moreover, Largeau et al. (1990) stated that kerogen in oil shale appear to be composed of homogeneous and amorphous organic matter; therefore, we can say that Himmetoglu oil shale has significant amount of kerogen when compared to others.



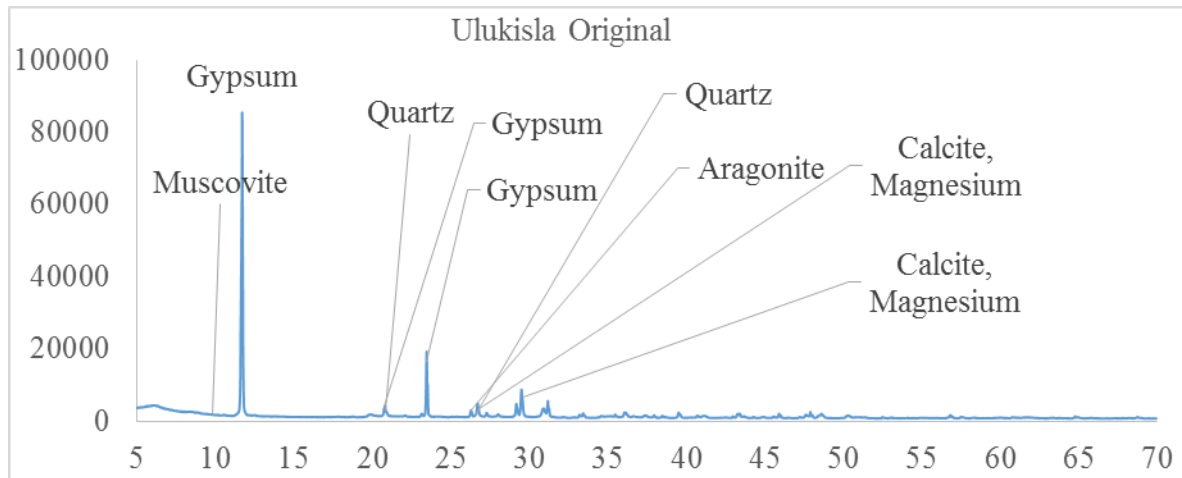
(a)



(b)



(c)

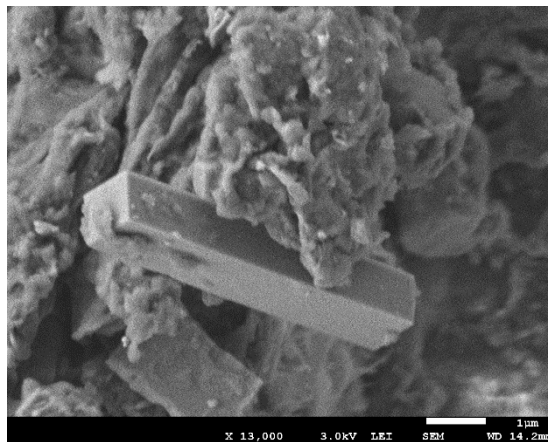


(d)

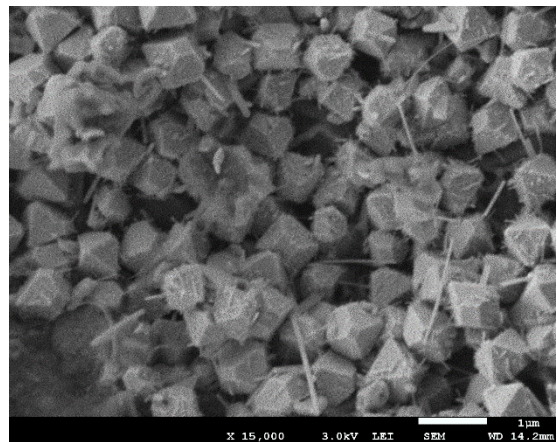
Figure 5-1 XRD spectra of original oil shale samples

5.1.2 Scanning Electron Microscope/Energy Dispersive X-Ray Spectroscopy (SEM/EDS) Analysis Results of Original Samples

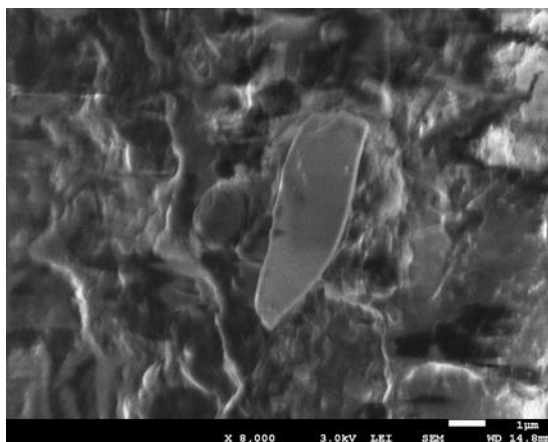
On the analyses of original oil shale samples, SEM was used to confirm some inorganic content the samples. When needed, EDS analyses were also taken for further evidence of the existence of those minerals (See Appendix C.1). The images confirm the presence of pyrite, quartz, albite and kaolinite.



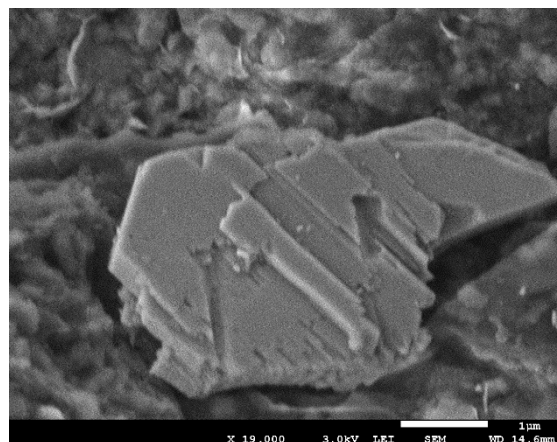
Pyrite



Quartz



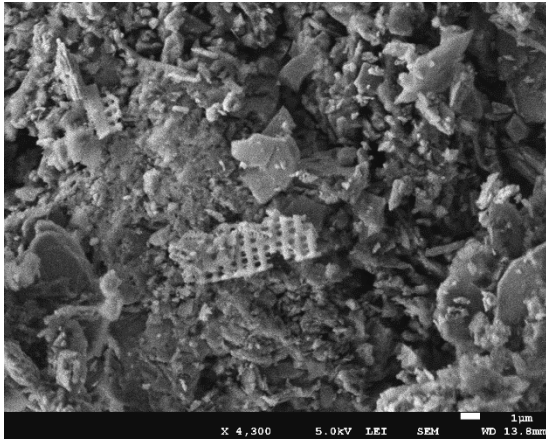
Albite



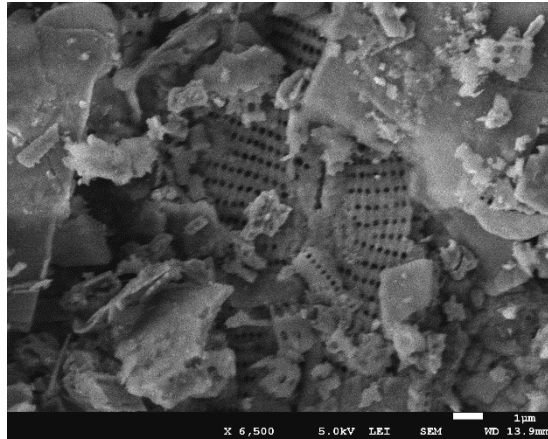
Kaolinite

Figure 5-2 Inorganic content of Himmetoglu oil shale from SEM

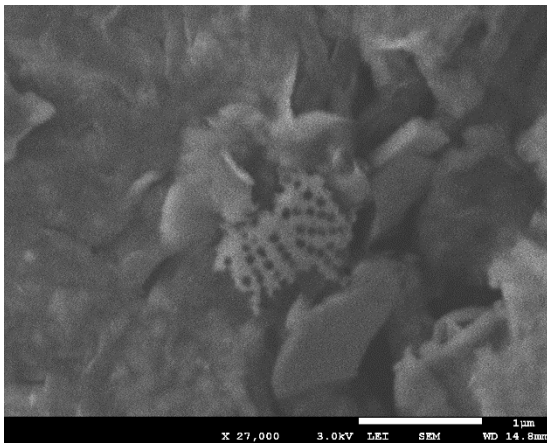
Algae and some diatoms are indicative of marine environments. During the SEM analysis, fossils of algae, and diatoms were recognized in Himmetoglu and Seyitomer samples (See Fig. 5-3). The simultaneous EDS analysis with SEM confirms the organic content of these fossils with high oxygen counts and silica content (See Appendix C.1).



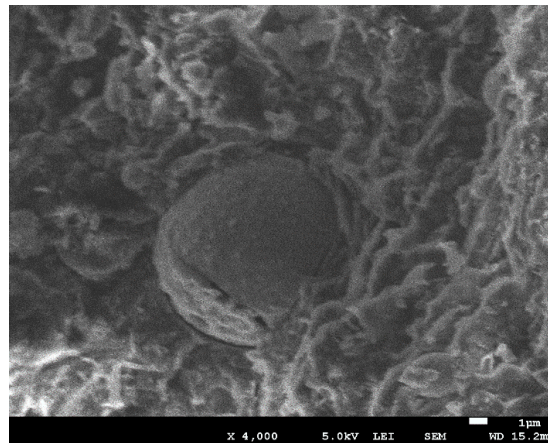
Diatom Fossil (Seyitomer)



Diatom Fossil (Seyitomer)



Diatom Fossil (Himmetoglu)



Tasmanite Alga (Himmetoglu)

Figure 5-3 Organic content of Himmetoglu and Seyitomer oil shale from SEM

5.1.3 Fourier Transform Infrared Spectroscopy (FTIR) Analysis Results of Original Samples

FTIR uses the interaction of infrared radiation with the vibrating dipole moments of molecules. FTIR spectra represent the molecular absorption of the different chemical bonds and certain bonds of the original oil shale samples (Fig. 5-4). It is seen that almost all of the samples have similar kerogen bands from FTIR spectra as stated in other studies (Alstadt, Katti, & Katti, 2012; Levy & Stuart, 1984; Rouxhet, Robin, & Nicaise, 1980). Between 3570 and 3200 cm^{-1} a hydroxyl group, H-bonded OH stretch can be seen as a broad band in some of the samples (Coates & Ed, 2000).

The FTIR spectra show that almost all the original oil shale samples have asymmetric and symmetric CH_2 bridge bands of kerogen at around 2920 and 2850 cm^{-1} , respectively. Moreover, from near 1700 cm^{-1} carbonyl $\text{C}=\text{O}$ stretch bands and from 1600 cm^{-1} $\text{C}=\text{C}$ aromatic structures can be noticed. The band around 1440 cm^{-1} shows C-H bending vibrations of CH_2 and CH_3 , and the peak at around 1375 cm^{-1} represents the C-H bending of CH_3 . Right hand side of the FTIR spectra shows the mineral bands of shale samples. The distinct broad peak at around 1436 cm^{-1} represents the CO_3^{2-} ion from dolomite and calcite. Other two sharp peaks at 876 and 727 cm^{-1} represent carbonate ion from dolomite and calcite (Alstadt et al., 2012; Downs, 2006). Other broad peak around 1050 cm^{-1} with small peaks around 770 and 700 cm^{-1} represents Si-O stretch of quartz and silica.

Based on the intensity of the peaks around 2920, 2850, 1440, and 1375 cm^{-1} , we can say that the kerogen of Himmetoglu oil shale has high aliphatic content. Hatildag and Seyitomer oil shale also have relatively high aliphatic content with high asymmetric and symmetric stretch of methyl groups. The kerogen of Ulukisla oil shale sample is more aromatic because of the relatively high $\text{C}=\text{C}$ aromatic structures around 1600 cm^{-1} .

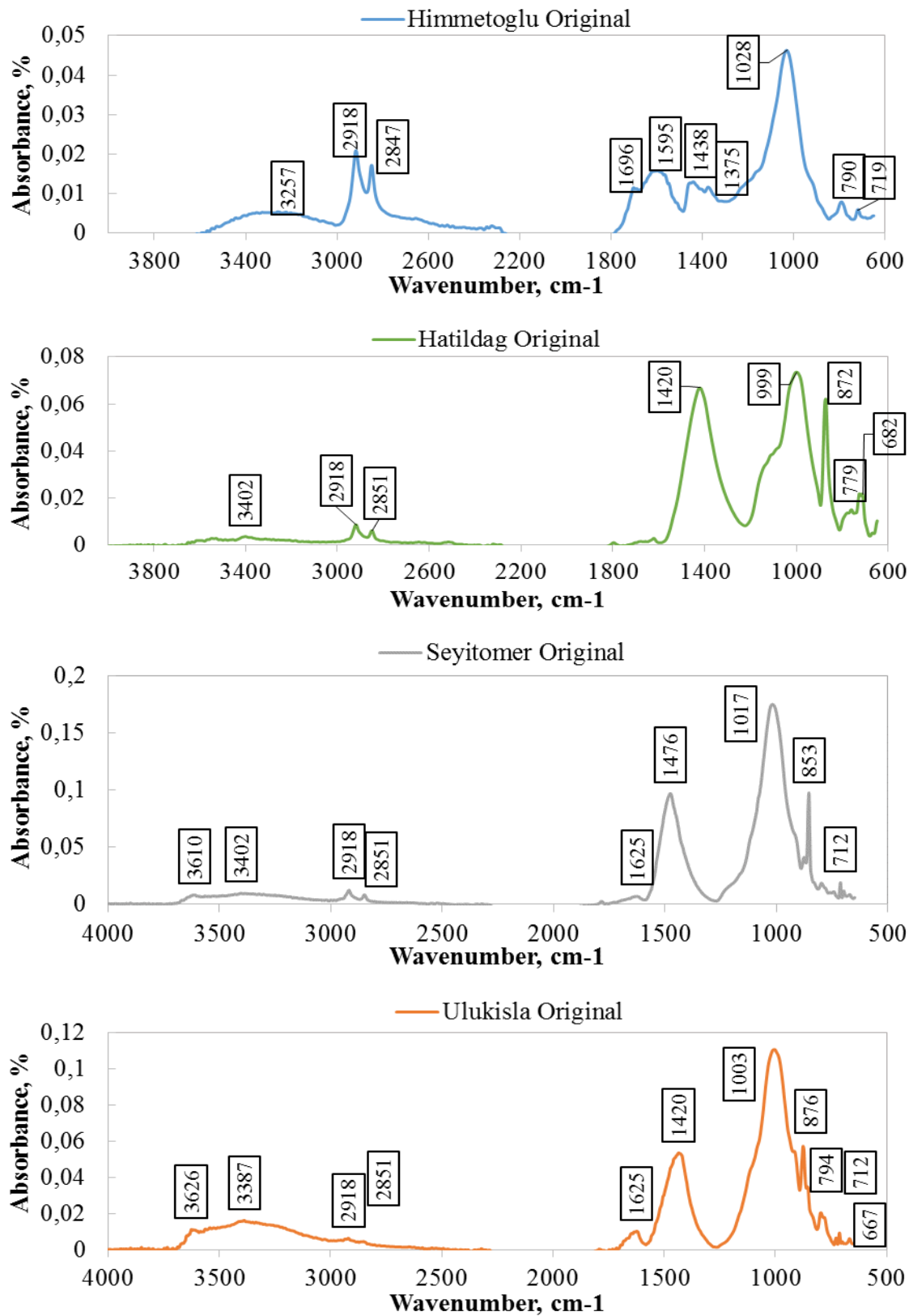


Figure 5-4 FTIR spectra of original oil shale samples

5.1.4 Thermal Gravimetric Analysis/Differential Scanning Calorimetry (TGA/DSC) Analysis Results of Original Samples

TGA/DSC analyses were conducted under nitrogen and air environments. In the first set, original samples, with and without iron powders, were subjected to same temperature program of retort experiments to mimic retort experiments under nitrogen environment. In the second set, original and iron powder added samples were subjected to identical heating under nitrogen; and in the third set under air environment. For simplicity, the samples from the first set will be named retort simulation samples; from the second set, combustion samples; and from the third set, pyrolysis samples.

5.1.4.1 Retort Simulation

In retort simulations, same temperature programs of retort experiments were used. Each sample was heated with different temperature program under nitrogen injection. Each program has dynamic and isothermal heating steps, respectively. In the first step, samples were heated up, and then the temperature kept constant during the isothermal heating step. In the third step, the temperature was increased and finally kept constant, again. Below figure shows the temperature program of retort experiments.

Table 5-2 Temperature program of retort experiments

(Hascakir, 2008)

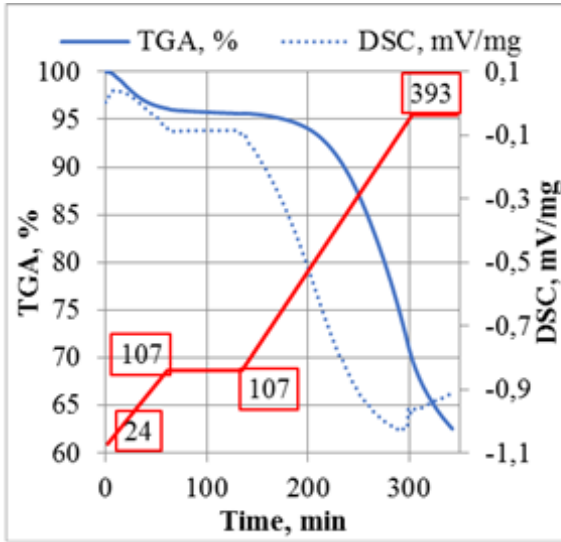
Hatildag		Himmetoglu		Seyitomer		Ulukisla	
Time (min)	Temp. (°C)	Time (min)	Temp. (°C)	Time (min)	Temp. (°C)	Time (min)	Temp. (°C)
0	30	0	24	0	30	0	30
70	140	60	107	37	150	86	120
100	140	132	107	127	150	131	120
229	430	297	393	298	423	504	515
260	430	342	393	330	423	506	515

Note that, the given temperature program of retort experiments in Fig 4-3 shows expected temperature profile; however, above program shows the simultaneous measured temperature values of real retort experiments.

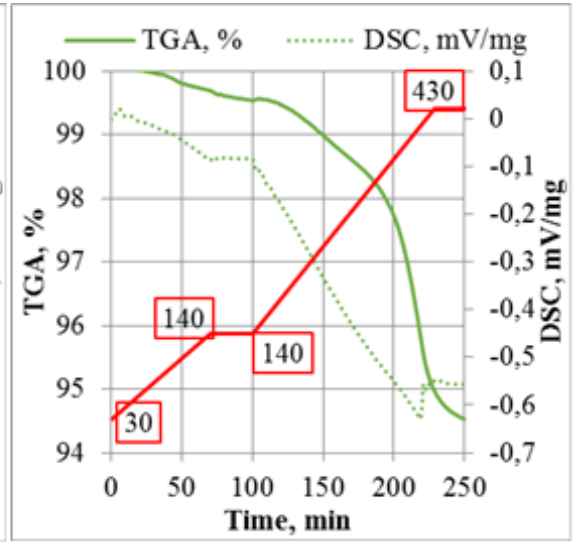
Figure 5-5 shows weight loss and heat flow versus time graphs of retort simulation processes under nitrogen environment. Red lines represent temperature program of each retort simulation. Himmetoglu oil shale has the lowest residuals with approximately 63%; which means 37% was produced during retort experiments. It is followed by Ulukisla with 15% weight loss, Seyitomer with 13% weight loss, and Hatildag with 5.5% weight loss, respectively. Unlike weight loss trend of retort simulations with TGA/DSC, retort experiments give different weight loss percentages.

According to the previous retort experiment results, Seyitomer has the highest weight loss percentages with 37%, followed by Ulukisla with 22%, Himmetoglu with 15%, and finally Hatildag with 7.5% (See Fig. 5-6). These inconsistent results can be explained by the heterogeneity of oil shale samples. On the other hand, as it can be recognized from below chart; Hatildag, Seyitomer, and Ulukisla oil shale samples has less weight loss after retort simulation than retort experiment. The reason for this situation may be explained by the mistaken measurements of the temperature. During the retort experiments, heat is supplied outside the sample. Temperature is measured inside the sample via thermocouple. Such system can cause some erroneous measurements; since, it takes some time to conduct heat from outside to inside.

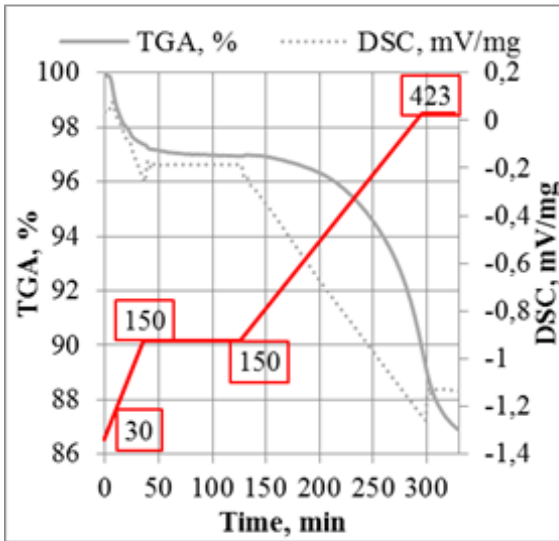
Moreover, sample amount of each sample is drastically different between retort experiments and TGA/DSC analysis. During the retort experiments sample amount is between 200 and 400 g; while, in TGA/DSC analysis between 30 and 60 mg. Therefore, sample amount can be another reason to explain the differences in weight loss of retort experiments and TGA/DSC analysis.



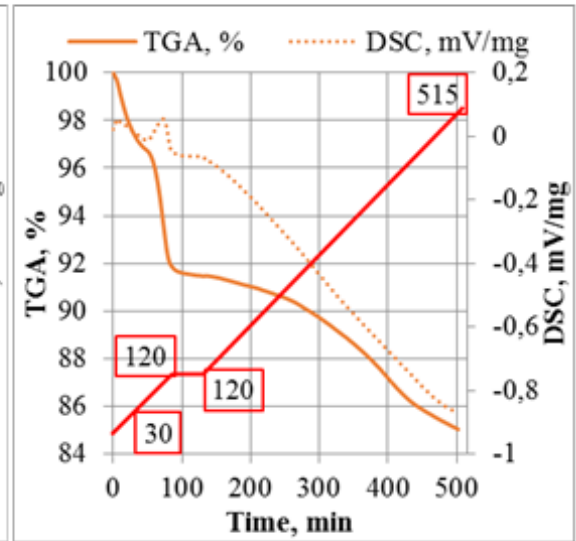
Himmetoglu Oil Shale



Hatildag Oil Shale



Seyitomer Oil Shale



Ulukisla Oil Shale

Figure 5-5 Retort simulation of original oil shale samples

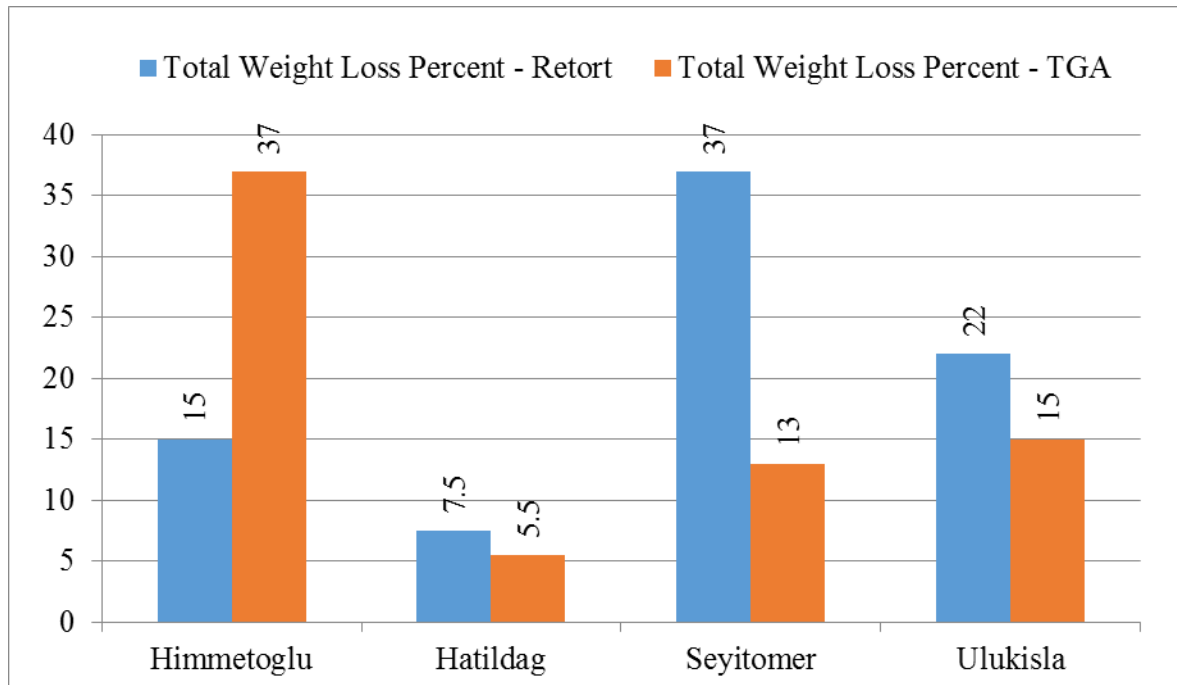


Figure 5-6 Weight loss comparison of retort experiment and retort simulation

For iron powder addition, same procedure with the retort experiments were followed. Each sample was heated with different temperature program under nitrogen injection after adding optimum dozed iron powders. Again, each program has dynamic and isothermal heating steps, respectively. In the first step, samples were heated up, and then the temperature kept constant during the isothermal heating step. In the third step, the temperature was increased and finally kept constant, again. Below table shows the temperature program.

Figure 5-7 shows weight loss and heat flow versus time graphs of retort simulation processes under nitrogen environment, after adding iron powder. Red lines represent temperature program of each retort simulation. Himmetoglu oil shale has the highest weight loss percentage with 54. Ulukisla follows it with 14% weight loss, Hatildag with 6% weight loss, and Seyitomer with 4.5% weight loss, respectively. According to the retort experiment results, Seyitomer has the highest weight loss percentages with 60%,

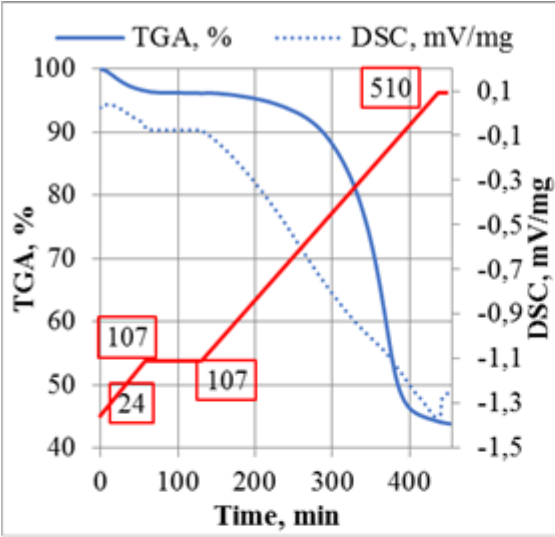
followed by Ulukisla with 19.5%, Himmetoglu with 12%, and finally Hatildag with 8% (See Fig. 5-8).

Table 5-3 Temperature program of retort experiments (with iron powder)
(Hascakir, 2008)

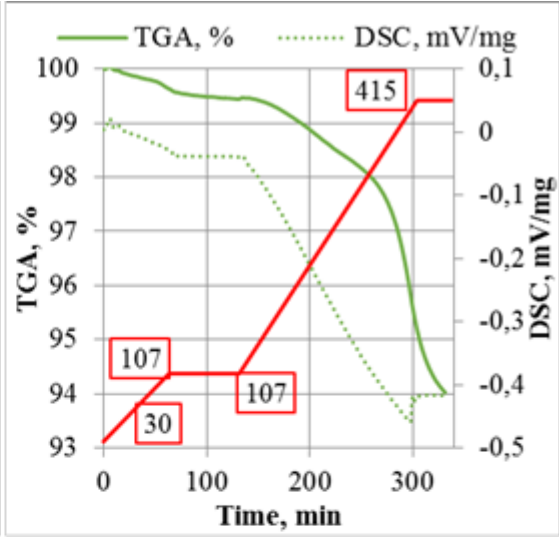
Hatildag + 0.1% Fe₂O₃		Himmetoglu + 0.1% Fe		Seyitomer + 0.5% Fe		Ulukisla + 0.1% Fe₂O₃	
Time (min)	Temp. (°C)	Time (min)	Temp. (°C)	Time (min)	Temp. (°C)	Time (min)	Temp. (°C)
0	30	0	24	0	30	0	30
63	107	60	107	79	120	86	120
129	107	132	107	134	120	131	120
296	415	441	510	280	395	430	519
330	415	454	510	300	395	459	519

These results show that, adding iron powder increases the production of Hatildag and Seyitomer during the retort experiments; while, decreases Himmetoglu and Ulukisla. On the other hand, when we compare retort simulations after adding iron powder, iron powder addition only increases the weight loss of Himmetoglu and Hatildag. Again, these inconsistent results can be explained by the heterogeneity of the oil shales, different mechanisms and sample amount of retort and thermal gravimetric analysis.

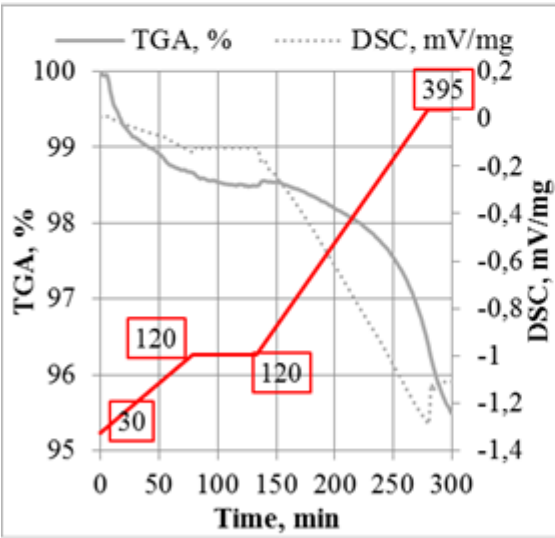
Surprisingly, Seyitomer oil shale shows different trend from previous retort simulation. Adding 0.5% Fe causes Seyitomer samples to lose less weight. As it seen from Figure 5-7, during first 140 min there is a fluctuation in TGA curve, which indicates additional reactions due to iron addition.



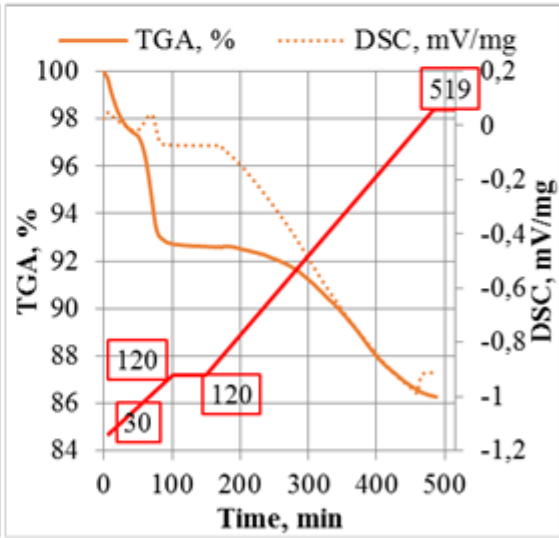
Himmetoglu Oil Shale (0.1% Fe)



Hatildag Oil Shale (0.1% Fe₂O₃)



Seyitomer Oil Shale (0.5% Fe)



Ulukisla Oil Shale (0.1% Fe₂O₃)

Figure 5-7. Retort simulation of original oil shale samples (with iron powder)

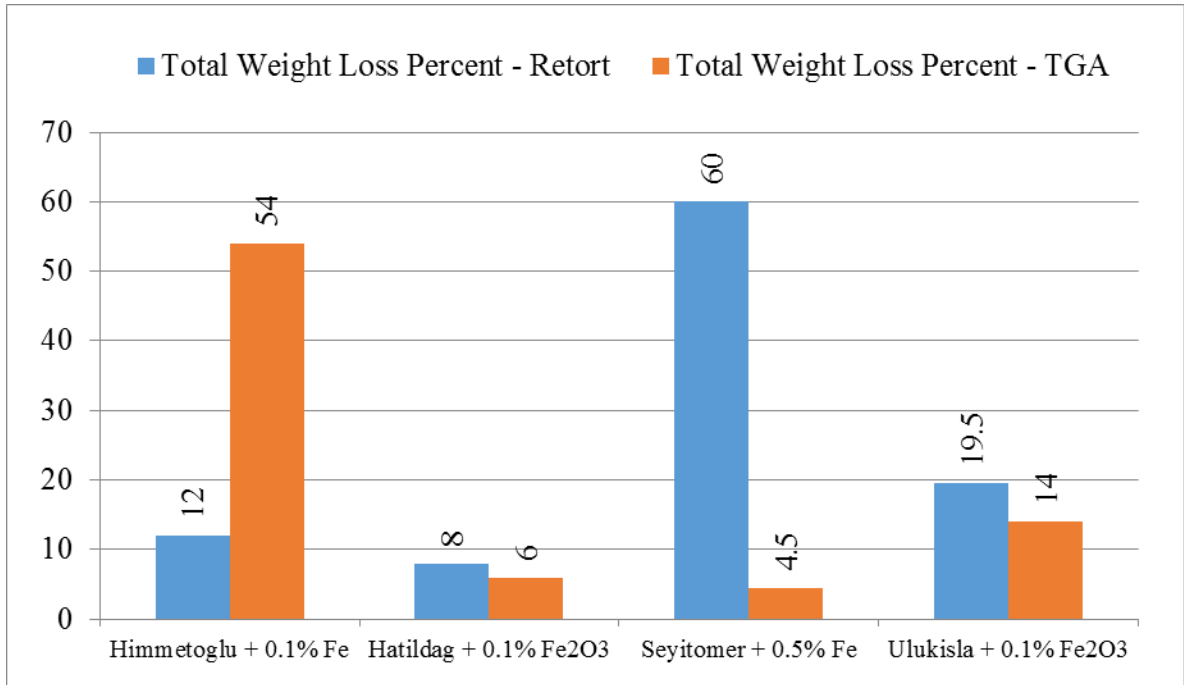


Figure 5-8 Weight loss comparison of retort experiment and retort simulation (with iron powder)

5.1.4.2 Identical Heating with Air

In this section, original oil shale samples are subjected to identical heating under air injection. The aim of this section is to understand the combustion trend and to visualize organic and inorganic amount of each oil shale sample.

TGA curves indicate weight loss percentages and DSC curves represent heat flow during the analysis. For all graphs of TGA/DSC analysis, y axis on the left hand side represents weight loss percentages and y axis on the right hand side gives heat flow behavior of oil shale samples. Therefore, the solid curves represent TGA curves and dashed curves represent heat flow.

Energy generation of Himmetoglu oil shale is increased under air injection, which might be due to its high organic content and the type of kerogen (Type I). Fuel formation reactions are observed in all but Ulukisla oil shale. This could be due to low organic content of Ulukisla oil shale. Complete thermal decomposition of kerogen is accomplished

in the ascending order for: Seyitomer, Hatildag, and Himmetoglu samples. As the thermal decomposition temperature increases, the energy generation increases.

Figure 5-9 shows the weight loss and heat flow curves of the combustion analyses from 24 °C to 900 °C. Derivative of the TG curve (DTG) helps to identify the weight loss periods of the combustion analysis (See Appendix A.3). We can say that there are two groups of peaks representing oxidation of the kerogen and the inorganic constituents.

First group of peaks between 200 and 600 °C are seen because of combustion of the aliphatic components of kerogen and the char - product of the aliphatic component's combustion. Second group of peaks (after 600 °C) represents the combustion of the inorganic components. The weight loss until 200 °C represents moisture content of the samples. Unlike other samples, Ulukisla oil shale has two sharp derivative peaks before 200 °C. First peak below 100 °C represents water content of the sample and the second peak between 100 and 200 °C represents the combustion of the light organic contents.

First derivative peak between 200 and 600 °C represents the oxidation of the aliphatic content of the kerogen. Later, the residuals of this oxidation process are dehydrogenated and polymerized into the char. The second peak represents the oxidation of char. The chemical reactions of the combustion analysis are so complex that each sample shows different mechanisms. Therefore, we cannot recognize every derivative peak of oxidation stages, or we can see additional peaks. For example, Seyitomer oil shale sample shows an additional derivative peak between 200 and 600 °C. Lithiophorite mineral of Seyitomer oil shale may cause this additional DTG peak. On the other hand, any chemical reaction between the inorganic matrix and the kerogen of the Seyitomer oil shale sample may cause this additional weight loss period.

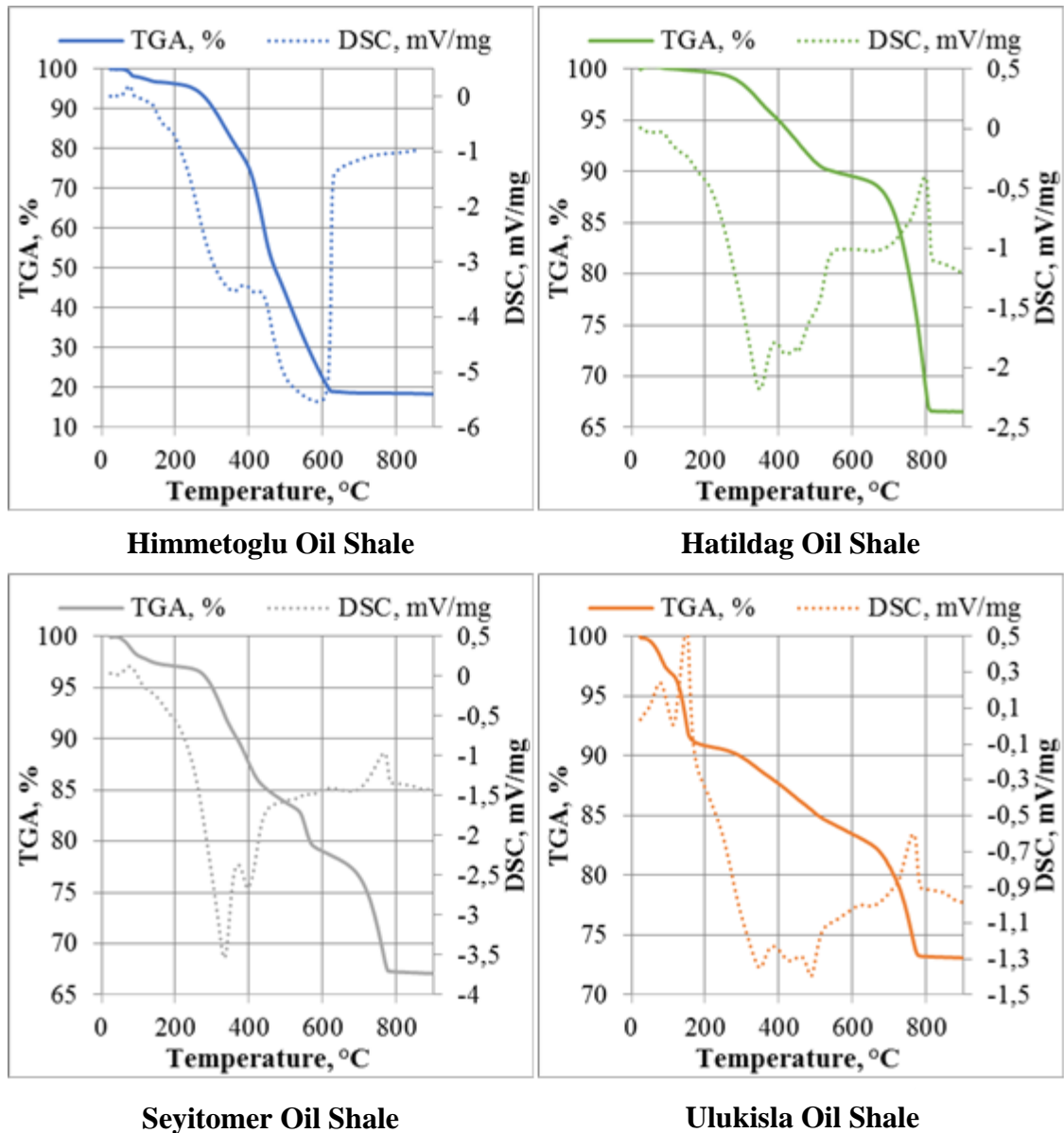


Figure 5-9 TGA/DSC results of identical heating under air injection

The oxidation of the inorganic matrix can be recognized above 600 °C. The oil shale samples that have high carbonate ion show high weight loss above 600 °C (Levy & Stuart, 1984). Hatildag, Ulukisla, and Seyitomer oil shale samples have distinctive peaks between 600 and 800 °C, indicating that the weight loss in this period is due to the calcite and dolomite decomposition (See Fig.5-9). On the other hand, Himmetoglu does not have typical DTG peak indicating that inorganic decomposition is taking place (See Appendix

A.3). Note that, Himmetoglu does not have any carbonate ion from calcite/dolomite (See Section 5.1.1 and 5.1.3).

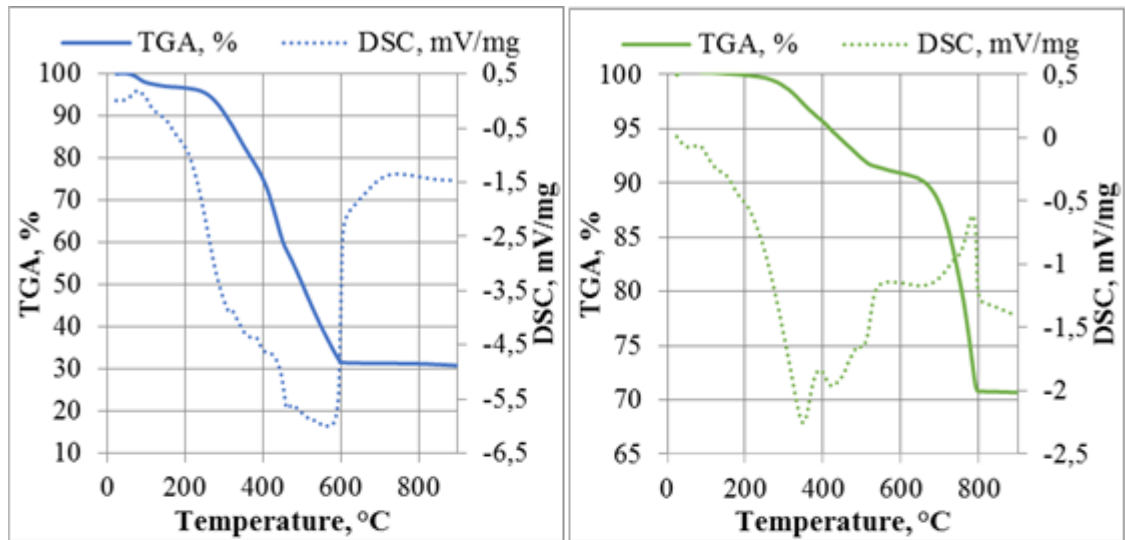
Table 5-4 shows the weight loss percentages of the oil shale samples during combustion analyses. Himmetoglu oil shale sample has the highest weight loss percentage. It is seen that Ulukisla oil shale sample has the lowest weight loss percentage during combustion with 26.9%.

Figure 5-10 shows the TGA/DSC curves after adding iron powder. For all samples, there is a decrease on weight loss after adding iron powder. For Himmetoglu oil shale, until 400 °C, weight loss curves show same trend; however, after 400 °C the weight loss is low after adding iron powder. Especially, the difference is high during inorganic combustion period. However, enthalpy change is higher after adding iron powder and combustion period takes short time when compared to the process without iron powder. TGA curves of Hatildag oil shale have almost same trend. Combustion process of organic and inorganic compounds end a bit earlier.

5.1.4.3 Identical Heating with Nitrogen

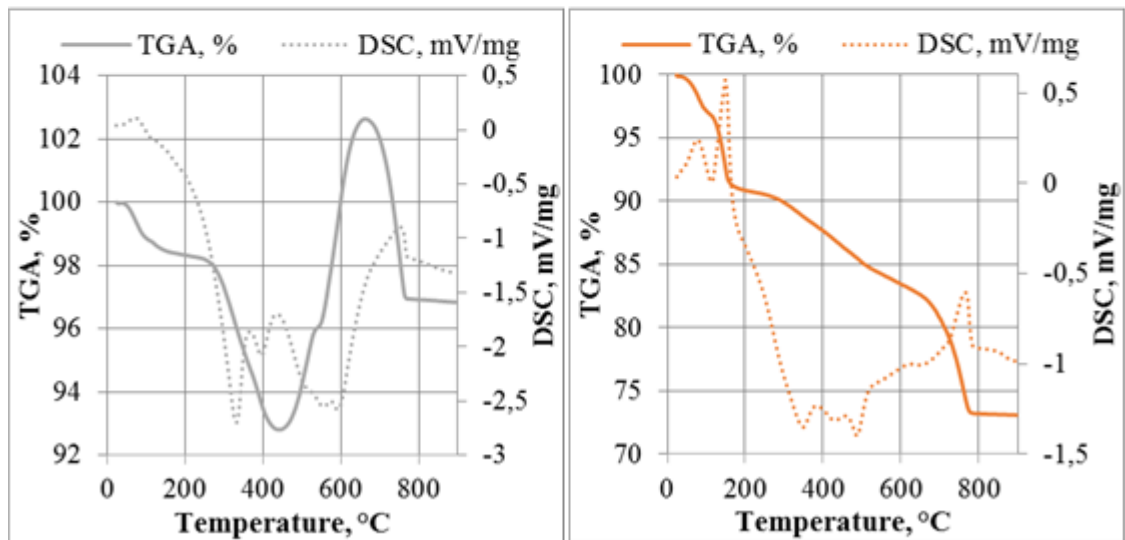
In the second set of identical heating experiments, pyrolysis takes place within nitrogen environment. Figure 5-11 shows the total weight loss and heat flow curves of pyrolysis analysis from 24 °C to 900 °C. There is no significant weight loss observed during pre-heating period (24-200 °C), indicating very low moisture content in the samples except for Ulukisla oil shale with 9% moisture content.

As explained by Alstadt et al. (2012), the relatively high hump between 3600 and 3000 cm^{-1} of the FTIR spectrum of original Ulukisla oil shale shows the H-OH hydrogen bonds from water also supports the presence of moisture content. Table 5-4 shows the moisture contents of the samples separately.



Himmetoglu Oil Shale (0.1% Fe)

Hatildag Oil Shale (0.1% Fe₂O₃)



Seyitomer Oil Shale (0.5% Fe)

Ulukisla Oil Shale (0.1% Fe₂O₃)

Figure 5-10 TGA/DSC results of identical heating under air injection (with iron powder)

Two stages during pyrolysis process are identified as organic and inorganic decomposition periods. The first stage occurs roundly between 200 °C and 600 °C and represents organic decomposition; where degradation of kerogen and bitumen molecules occurs (Al-Harashseh et al., 2011). During organic decomposition, kerogen decomposition occurs generally until 350 °C. Then, the produced gas, bitumen, and carbon residue of kerogen

devolatilization are decomposed into oil, coke (char), and gas between 350 and 600 °C. The organic decomposition stage is completed with these two stages.

However, several studies show that, sometimes according to the type of the oil shale the organic decomposition stage can be completed with one-stage (Al-Harashseh et al., 2009; Fang-Fang, Ze, Wei-Gang, & Wen-Li, 2010; Qing, Baizhong, Aijuan, Jingru, & Shaohua, 2007).

The second stage refers to inorganic decomposition period and takes place generally between 600 °C and 800 °C. In the second stage, weight loss is seen due to the decomposition of the inorganic compounds of oil shale like carbonates. At high temperatures, the produced carbon dioxide during carbonate decomposition reacts with residual char and forms carbon monoxide. This process results in additional weight loss (Qing et al., 2007). For DTG curves of pyrolysis, see Appendix A.3.

Total weight losses during pyrolysis are shown in Table 5-4. As seen from Table 5-4, the total weight loss of Himmetoglu oil shale is high (67%); while, Ulukisla has the lowest (29.6%) weight loss. Weight loss due to the organic decomposition is also highest in Himmetoglu oil shale; which indicates Himmetoglu oil shale has the highest organic content. As Bhargava et al. (2005) stated, this situation can be confirmed by FTIR spectra (See Section 5.1.3). The intensity of the peaks showing asymmetric and symmetric stretching methylene bridge, carbonyl C=O stretch and C=C aromatic structure bands of kerogen verifies that Himmetoglu oil shale has the highest organic content (See, Fig. 5-4). Other oil shales (Seyitomer, and Hatildag) that have methylene bridge bands also have relatively high organic decomposition. Similarly, the oil shale samples that have significantly high carbonate minerals (from dolomite and calcite) show high inorganic decomposition. Hatildag oil shale has the highest weight loss for the inorganic decomposition with 24.9%. Ulukisla and Seyitomer are the other oil shales that have high inorganic decomposition due to dolomite and calcite decomposition (See Table 5-4).

As expected, lack of carbonate ion results in the low inorganic decomposition period for Himmetoglu oil shale. The effect of the other common minerals such as, pyrite, cannot be recognized during the pyrolysis stage as Ballice (2005) reported in his study on Turkish oil shales.

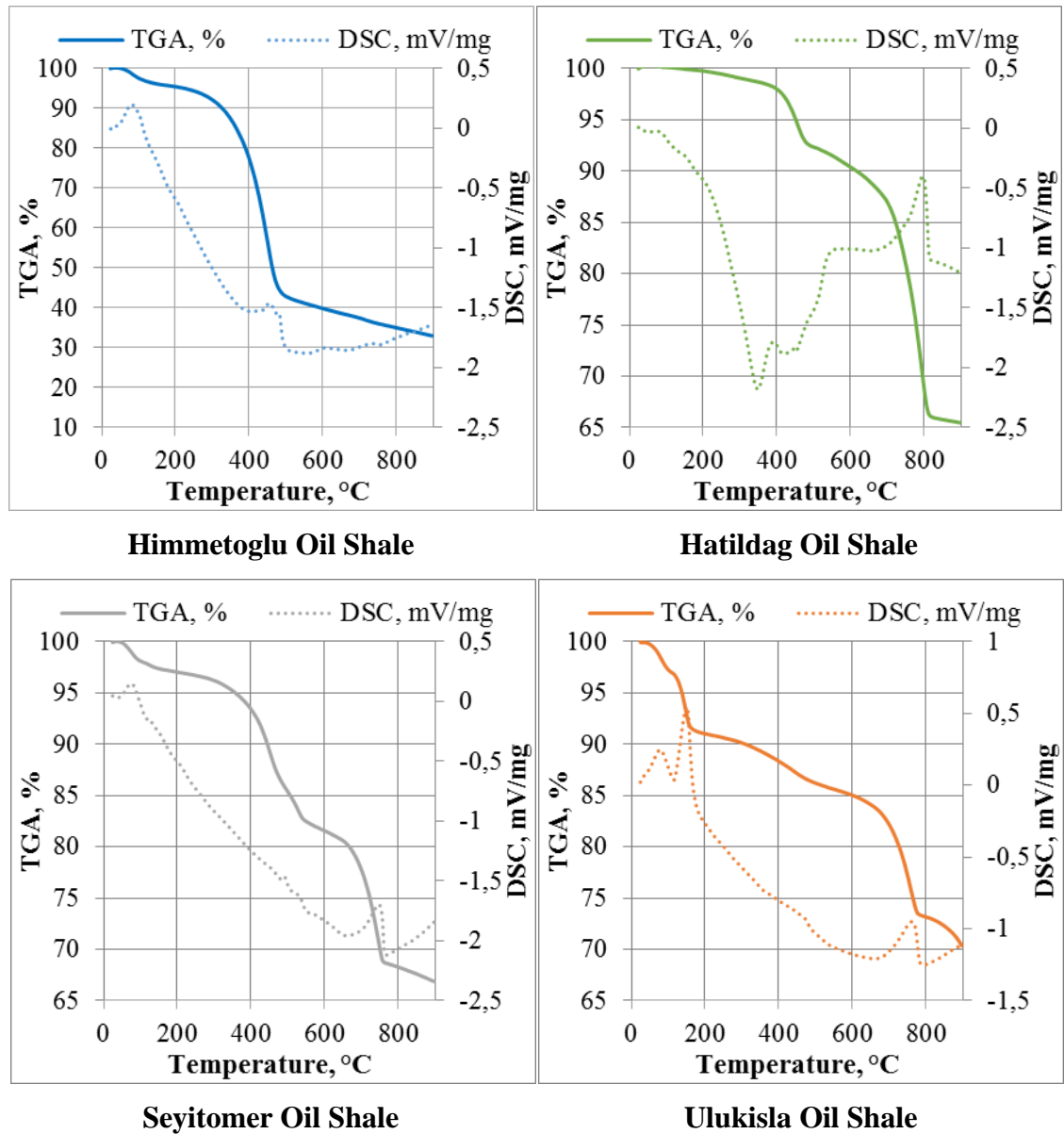


Figure 5-11 TGA/DSC results of identical heating under nitrogen injection

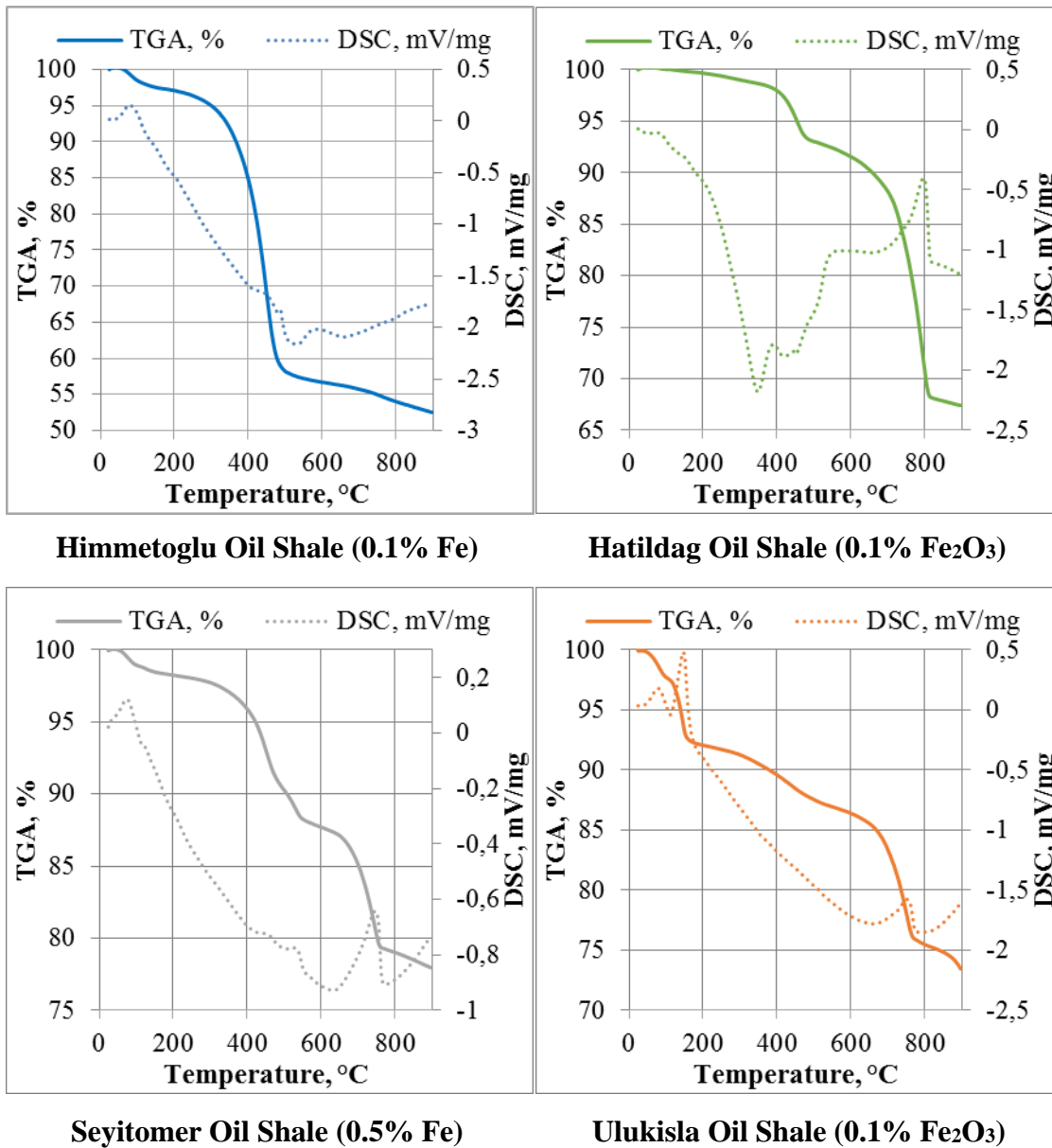


Figure 5-12 TGA/DSC results of identical heating under nitrogen injection (with iron powder)

Same trend with TGA curves of each oil shale sample can be seen after adding iron powder under nitrogen injection; however, there is a decrease on weight loss after adding iron powder similar to combustion analysis. Below table shows the weight loss percentages of each oil shale sample during pyrolysis and combustion analyses.

Table 5-4 Weight loss percentages

Oil Shale \ %	Moisture Content*	Weight Loss During Pyrolysis	Organic Decomp.*	Inorganic Decomp.*	Weight Loss During Combustion
Himmetoglu	4.5	67.0	55.6	6.8	81.6
Himmetoglu + 0.1% Fe	3.0	47.5	40.4	4.2	69.2
Hatildag	0.2	34.5	9.4	24.9	33.5
Hatildag + 0.1% Fe₂O₃	0.3	32.6	8.1	24.1	29.3
Seyitomer	3.0	33.1	15.5	14.7	32.9
Seyitomer + 0.5% Fe	1.8	22.0	10.5	9.7	3.0
Ulukisla	9.0	29.6	6.0	14.7	26.9
Ulukisla + 0.1% Fe₂O₃	7.9	26.5	5.7	12.9	24.4

*From pyrolysis data

5.1.4.4 Kinetic Analysis of Pyrolysis and Combustion

In this section, kinetic analyses of original oil shale sample with and without iron powder are presented. The aim of the kinetic analyses are to compare the activation energies of each sample under air and nitrogen environments, and to understand the effect of iron powder. During the kinetic analyses, Arrhenius Model was used; since, it requires one heating rate. The main assumption of the model is that rate of mass loss depends on temperature, rate constant, and mass of the residual sample:

$$dw/dt = kw^n; \quad \text{and } k = A \exp\left(-E_a/RT\right) \quad (5-1)$$

Therefore;

$$dw/dt = A \exp\left(-E_a/RT\right)w \quad (5-2)$$

Finally, after taking logarithm of both sides, Arrhenius equation gets the form below:

$$\log\left(dw/dt/w\right) = \log A - \left(E_a/2.303RT\right) \quad (5-3)$$

After plotting $\log((dw / dt) / w)$ versus $1 / T$ graph, the slope of the linear parts is equal to the $(E_a / 2.303RT)$. In addition, the intercept ($\log A$) gives the Arrhenius constant.

Below tables show the peak temperature and activation energy for combustion and pyrolysis, respectively. As seen, iron powder decreases the activation energy of each oil shale sample.

Table 5-5 Activation energies of combustion calculated from Arrhenius Method at a heating rate of 10 °C min⁻¹

Sample	Low Temperature Oxidation LTO			High Temperature Oxidation HTO		
	Peak T, °C	E _a , kJ·mol ⁻¹	R ²	Peak T, °C	E _a , kJ·mol ⁻¹	R ²
Himmetoglu	312	48.6	0.9574	442	122.4	0.9820
Himmetoglu 0.1%Fe	323	38.3	0.9708	433	85.2	0.9942
Hatildag	376	39.9	0.7459	456	106.4	0.7666
Hatildag 0.1%Fe ₂ O ₃	356	24.7	0.4950	431	89.7	0.6800
Seyitomer	317	66.4	0.8226	556	66.4	0.7349
Seyitomer 0.5%Fe	329	52.7	0.8801	-	-	-
Ulukisla	356	35.2	0.7683	429	42.8	0.3026
Ulukisla 0.1%Fe ₂ O ₃	341	20.5	0.6681	441	46.1	0.4097

Table 5-6 Activation energies of pyrolysis calculated from Arrhenius Method at a heating rate of 10 °C min⁻¹

Sample	Peak T, °C	E _a , kJ·mol ⁻¹	R ²
Himmetoglu	451	70.0	0.9809
Himmetoglu 0.1%Fe	450	69.3	0.9792
Hatildag	466	102.7	0.9878
Hatildag 0.1%Fe ₂ O ₃	461	97.0	0.9833
Seyitomer	461 – 526	53.5 – 69.2*	0.9329 – 0.8159
Seyitomer 0.5%Fe	451 - 526	52.4 – 65.2*	0.9537 – 0.8867
Ulukisla	446	37.6	0.9539
Ulukisla 0.1%Fe ₂ O ₃	426	19.9	0.6619

*E_{a1} and E_{a2} for two-pyrolysis region, respectively

5.1.4.5 Effect of Temperature Program

The aim of this section is to understand the effect of the temperature program by comparing identical heating under nitrogen injection. To do so, the weight loss percentages at final temperature of the retort experiments were compared with the weight loss percentages of the corresponding temperature at identical heating results.

Constant rates (identical heating) were commonly used during TGA/DSC analysis; since, they can easily and rapidly give results. However, to get good determination from TGA/DSC analysis, lower rates or retention times are needed (Salin & Seferis, 1993). Therefore, we expected to see higher weight loss percentage with the temperature program (Table 5-3) of Hascakir (2008) which provides both lower heating rates and retention times.

Consequently, as seen from Table 5-7, weight loss percentages of retort analysis results were higher than the weight loss percentages of identical heating (10 °C/min) for the corresponding temperature values.

Table 5-7 Effect of temperature program

Type	Temperature °C	Weight Loss (%)	Oil Shale
Retort	393	37.0	Himmatoglu
Identical	393	20.0	
Retort + 0.1% Fe	510	54.0	
Identical + 0.1% Fe	510	42.0	
Retort	430	5.5	Hatildag
Identical	430	3.0	
Retort + 0.1% Fe ₂ O ₃	415	6.0	
Identical + 0.1% Fe ₂ O ₃	415	2.5	
Retort	423	13.0	Seyitomer
Identical	423	8.0	
Retort + 0.5% Fe	395	4.5	
Identical + 0.5% Fe	395	4.0	
Retort	519	15.0	Ulukisla
Identical	519	14.0	
Retort + 0.1% Fe ₂ O ₃	519	14.0	
Identical + 0.1% Fe ₂ O ₃	519	13.0	

5.2 Postmortems

In this section, XRD, TGA/DSC, FTIR and SEM analysis results of retort, microwave, combustion, pyrolysis, and retort simulation postmortems are mentioned and discussed. The main purpose of this section is to discuss the results of recovery part of our study.

For simplicity, we labeled the samples from Hascakir's (2008) retort experiments as retort postmortems, samples from microwave heating experiments as microwave postmortems, samples from identical heating under air and nitrogen injection as combustion and pyrolysis postmortems, and samples from TGA/DSC instrument after mimicking the temperature program of the retort experiment of Hascakir's (2008) study as retort simulation postmortems.

Note that, microwave-heating experiments were conducted according to the experimental procedure mentioned in Section 4.4. Only for Himmetoglu oil shale with iron powder, the heating time was 3 minutes instead of 10 minutes. The reason is that after adding 0.1% Fe to the Himmetoglu oil shale sample, we obtained shale oil production and stopped the heating period. As microwave postmortems, the samples from microwave heating experiments were used.

5.2.1 X-Ray Diffraction (XRD) Analysis Results of Postmortems

In this section XRD results of retort and microwave (Himmetoglu, only) postmortems are shown. The minerals of the postmortems obtained from XRD analysis show that again quartz and dolomite/calcite are still the leading minerals. Table 5-5 shows the XRD results of retort and microwave postmortems of the samples with and without iron powder. As seen from Appendix D, XRD spectra after retort experiments show that the humps indicating amorphous content of kerogen decreased. This also indicates the production of kerogen during the retort experiments. Moreover, it can be seen that clay minerals which can be noticed from original sample disappeared after retort experiments showing that clays were also decomposed during the experiments.

5.2.2 Scanning Electron Microscope Analysis Results of Postmortems

Retort and microwave heating experiments' postmortems are analyzed with SEM. It is seen that retort experiments cause drastic changes on oil shale samples. Because almost all of the retort postmortems became char after the experiments, the SEM images shows the easily dispersible surface of char (See Fig. 5-13). Although, retort experiments creates drastic changes on surface, still some fossils can be seen on the shale surface (See Appendix C.3). On the other hand, microwave heating creates minor changes on surface area of oil shale samples. The common change on all oil shale samples is that microwave heating increases surface area, leastwise (See Fig. 5-13). For all SEM images of retort and microwave heating postmortems, please see Appendix C.3.

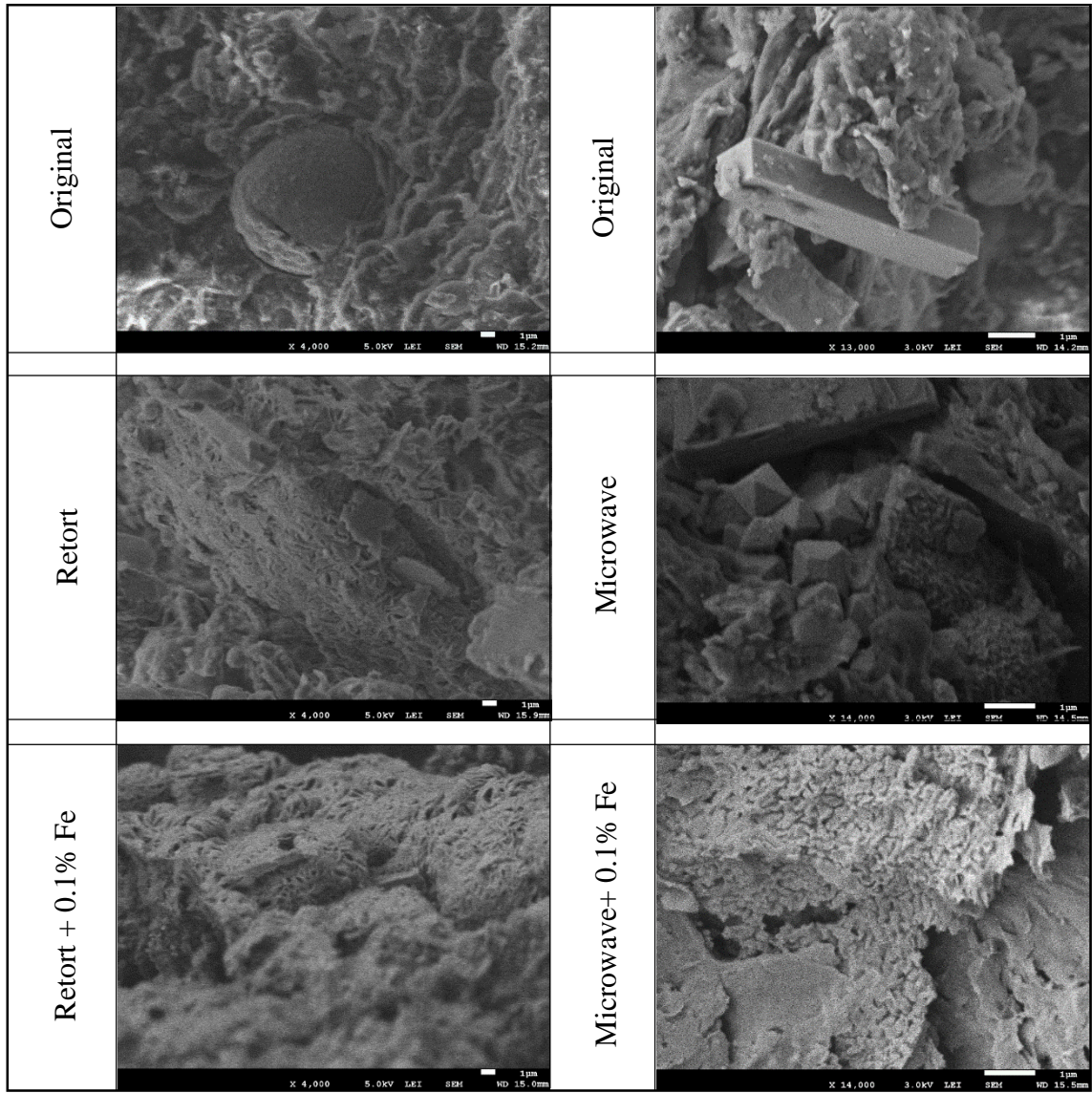


Figure 5-13 Retort and microwave postmortems of Himmetoglu oil shale

Table 5-8 Minerals from XRD analysis of postmortems

<i>Himmetoglu</i>	<i>Minerals with chemical formula</i>
After Retort	Pyrrhotite [FexS], Pyrite [FeS ₂], Albite [NaAlSi ₃ O ₈], Quartz [SiO ₂]
After Retort (0.1% Fe)	Pyrrhotite [FexS], Albite [NaAlSi ₃ O ₈], Quartz [SiO ₂]
Hatildag	Minerals with chemical formula
After Retort	Quartz [SiO ₂], Pyrite [FeS ₂], Dolomite [CaMg(CO ₃) ₂], Albite [NaAlSi ₃ O ₈], Analcime [Na ₂ (Al ₂ Si ₄ O ₁₂)·2H ₂ O], Illite [K _{0.65} Al ₂ (Al _{0.65} Si _{3.35} O ₁₀)(OH) ₂]
After Retort (0.1% Fe₂O₃)	Dolomite [CaMg(CO ₃) ₂], Quartz [SiO ₂], Pyrite [FeS ₂], Illite [K _{0.65} Al ₂ (Al _{0.65} Si _{3.35} O ₁₀)(OH) ₂], Albite [NaAlSi ₃ O ₈], Analcime [Na ₂ (Al ₂ Si ₄ O ₁₂)·2H ₂ O], Muscovite [KAl ₂ (AlSi ₃ O ₁₀)(OH) ₂]
Seyitomer	Minerals with chemical formula
After Retort	Aragonite [CaCO ₃], Quartz [SiO ₂], Illite [K _{0.65} Al ₂ (Al _{0.65} Si _{3.35} O ₁₀)(OH) ₂], Pyrite [FeS ₂], Sudoite [Mg ₂ Al ₃ (Si ₃ Al)O ₁₀ (OH) ₈], Gaudefroyite [Ca ₄ Mn ₂]
After Retort (0.05% Fe)	Dolomite [CaMg(CO ₃) ₂], Quartz [SiO ₂], Illite [K _{0.65} Al ₂ (Al _{0.65} Si _{3.35} O ₁₀)(OH) ₂], Pyrite [FeS ₂], Albite [NaAlSi ₃ O ₈], Analcime [Na ₂ (Al ₂ Si ₄ O ₁₂)·2H ₂ O]
Ulukisla	Minerals with chemical formula
After Retort	Clinochlore [CaSO ₄ ·2H ₂ O], Aragonite [CaCO ₃], Quartz [SiO ₂], Dolomite [CaMg(CO ₃) ₂], Illite [K _{0.65} Al ₂ (Al _{0.65} Si _{3.35} O ₁₀)(OH) ₂], Polyhalite [K ₂ Ca ₂ Mg(SO ₄) ₄ ·2H ₂ O]
After Retort (0.1% Fe₂O₃)	Clinochlore [CaSO ₄ ·2H ₂ O], Quartz [SiO ₂], Marshite [CuI], Dolomite [CaMg(CO ₃) ₂], Illite [K _{0.65} Al ₂ (Al _{0.65} Si _{3.35} O ₁₀)(OH) ₂], Polyhalite [K ₂ Ca ₂ Mg(SO ₄) ₄ ·2H ₂ O], Albite [NaAlSi ₃ O ₈]

Himmetoglu after Microwave (cont'd Table 5-5)

<i>After Microwave</i>	<i>Dolomite, Pyrite [FeS₂], Albite [NaAlSi₃O₈],</i>
After Microwave (0.1% Fe)	Pyrite [FeS ₂], Albite [NaAlSi ₃ O ₈], Liottite (Na,Ca,K) ₂₄ (Si,Al) ₃₆ O ₇₂ [SO ₄ ,Cl,F] ₁₀ ,

5.2.3 Fourier Transform Infrared Spectroscopy (FTIR) Analysis Results of Postmortems

This section mainly includes three parts. First part is the FTIR results of retort and microwave postmortems. The results are used to identify produced and remained components after the experiments by comparing original samples. Second part is the FTIR results of combustion and pyrolysis postmortems that show residual inorganic content after TGA/DSC analysis. Finally, FTIR results of retort simulation postmortems which are used to compare the original retort postmortems and the simulation ones.

Figures in Appendix B.1 show the FTIR spectra of the samples after the retort experiments. When we compare with the FTIR spectra of original oil shale sample of Himmetoglu oil shale, it is seen that without iron powder we were not able to produce all the organic content during the experiments. However, it is seen from Figure B-2 that iron powder addition helped to produce almost all the aliphatic content at 2917 and 2847 cm⁻¹ (little amount of aromatic and carbonyl groups remains, at 1561 and 1438 cm⁻¹). For Seyitomer oil shale, retort experiments were sufficient to produce all of the organic content (with and without iron powder). Retort experiments of Seyitomer oil shale were able to produce all of the organic content; however, after adding iron powder some organic content remains after the analysis. As seen from Figure B-7 & B-8, during the retort experiments, all of the organic content of Hatildag and Ulukisla was produced. Note that, all the inorganic content remains after the retort experiments since the maximum temperature of retort experiments did not reach the required temperature for inorganic decomposition.

Figures in Appendix B.2 show spectra of original and microwave heated samples. After microwave heating experiment of Himmetoglu oil shale, it is seen that all the organic content remains same. As mentioned before, after adding iron powder microwave heating experiments caused to produce shale oil. From Figure B-10, we can see all the aliphatic, aromatic and carbonyl content (from 2914, 2847, 1695, 1573, and 1435 cm^{-1}). However, as it can be recognized clearly, the intensity of Si-O bond from quartz seems to increase. The reason for this is that, since we produce some organic content, the bonds of inorganic content can easily be detected by FTIR.

Figure B-11 shows the FTIR spectra of the produced shale oil from microwave heating experiments after adding 0.1% Fe in Himmetoglu oil shale sample. All the bonds of the kerogen inside Himmetoglu oil shale can easily be seen from this spectra; which means that with microwave heating we are able to produce the organic components that oil shale includes, without creating any change on its kerogen.

FTIR spectra of other oil shale samples (except Seyitomer); however, do not show any remarkable change after microwave heating experiments, even after adding iron powder. It is observed that iron powder addition leads production of some organic content of Seyitomer oil shale during microwave experiment (See Fig. B-15).

In Appendix B.3, figures represent the FTIR spectra of the samples after combustion analysis. Each of the FTIR spectra of the combustion postmortems show similar peaks: the only remaining minerals are Si-O stretch of quartz and silica ($\sim 1000 \text{ cm}^{-1}$), and little calcite ion ($\sim 1420 \text{ cm}^{-1}$). As expected, the analysis produced all organic content and calcite ions during the identical heating under air injection until 900 °C. However, with the iron powder added samples, combustion analyses were not sufficient to produce all carbonate minerals ($\sim 1420 \text{ cm}^{-1}$), maybe due to the reactions taken place.

FTIR spectra of pyrolysis postmortems in Appendix B.4 show that almost all of the asymmetric and symmetric CH_2 bridge bands of kerogen (~ 2920 and 2850 cm^{-1}) and

carbonyl stretch ($\sim 1696\text{ cm}^{-1}$) disappear after pyrolysis. Carbonate minerals of Hatildag, Seyitomer and Ulukisla oil shales are almost decomposed after the identical heating under nitrogen injection until $900\text{ }^{\circ}\text{C}$.

Finally, the comparison of the FTIR results of retort experiment and simulation postmortems are seen in Appendix B.5. In this section, it is helpful to compare the analysis results with retort experiment's results (Appendix B.1).

From retort postmortem we can see the asymmetric and symmetric methylene bridge (~ 2918 and 2845 cm^{-1}) of Himmetoglu oil shale; however, from results of simulation we see that they were produced. As mentioned in Section 5.1.4.1, the production from retort experiment is 15% and the production of simulation is 37%. Therefore, these production percentages explain the loss of components after the simulation process (See Fig. 5-6). As seen from Fig. B-35, only common difference is the loss of C-H bending of CH_3 . Again, when we compare the production percentages, we see more weight loss percentages from simulation (See Fig. 5-8).

For Hatildag oil shale, the production amounts of experiment and simulation are almost same. Likewise, FTIR spectra of retort postmortems and simulations show parallel trend and show that all of the organic content decomposed during the analyses and experiments.

From FTIR figures of Seyitomer oil shale, the residuals of the simulation and analysis (with and without iron powder) are almost same. It is seen that retort experiments and simulations are able to produce all the organic content ($\sim 2921, 2851\text{ cm}^{-1}$). However, the FTIR results cannot explain the differences in production percentages (See, Fig. 5-6 & 5-8).

For Ulukisla oil shale, it is seen that like retort experiments, simulation also produced all organic content. Yet, the carbonate ion peaks looks remain same after simulation ($\sim 1420, 872\text{ cm}^{-1}$), (See, Fig. B-40 & B-41); although, they decomposed during retort experiments (See, Fig. B-7 & B-8).

5.2.4 Thermal Gravimetric Analysis/Differential Scanning Calorimetry (TGA/DSC) Analysis Results of Postmortems

In this section, retort and microwave postmortems are subjected to identical heating under air injection. The aim of this section is to understand the effects of retort and microwave heating experiments by comparing TGA/DSC analysis behaviors of original samples and postmortems.

5.2.4.1 Identical Heating of Retort Postmortems with Air

Each retort postmortem is subjected to identical heating from 24 to 900 °C under air injection. The graphs (Fig. A-1 & A-2) in Appendix A show the weight loss and heat flow curves with respect to temperature of retort postmortems with and without iron powder addition.

From TGA curves of retort postmortems, it is seen that organic decomposition periods are shorter than TGA results of original samples, at first sight. The results show that circa there are 22%, 5%, 11%, and 1% weight loss differences of organic content between originals and postmortems of Himmetoglu, Hatildag, Seyitomer and Ulukisla, respectively. These differences indicate the production percent during the retort experiments, roughly. When we compare the production results with the retort simulation by TGA, except Ulukisla, the results are more consistent with the real retort experiment results conducted by Hascakir (2008). Actually, like other samples, organic decomposition period of Ulukisla retort postmortem is drastically shorter than original sample. However, the weight loss during inorganic decomposition period of retort postmortem is remarkably high, which creates inconsistent results.

TGA analysis of the postmortem of iron powder added Himmetoglu oil shale again gives promising results with %11 production; which is very similar to results of Hascakir (2008). However; TGA analysis of Hatildag, Seyitomer, and Ulukisla do not give reliable results with retort experiments. Same trend is observed with Ulukisla postmortem, during

inorganic decomposition period, can be seen from Hatildag postmortem; that creates high total weight loss percentages. Moreover, as we recognize from previous results, iron powder cause precipitation with Seyitomer oil shale under air injection, which makes impossible to compare original and retort postmortems weight loss percentages (For total weight loss percentages of retort experiments, See Fig. 5-6 & 5-8).

5.2.4.2 Identical Heating of Microwave Postmortems with Air

Each microwave postmortem is subjected to identical heating from 24 to 900 °C under air injection. Figure A-3 shows the weight loss and heat flow curves with respect to temperature of microwave postmortems without iron powder. At first sight, (by comparing with TGA/DSC results of original samples) it is seen that microwave heating just cause to produce moisture content in 10 minutes. The enthalpy change (area under DSC curve) of Himmetoglu oil shale is decreased after subjected to microwave heating. The TGA and DSC curves of other oil shale samples almost remain same, indicating that microwave heating does not cause drastic changes on the samples (Also, See Fig. 5-9)

Figure A-4 shows the TGA/DSC curves of the microwave postmortems with iron powder. The TGA and DSC curves of Himmetoglu postmortems show difference with originals (See Fig. 5-10). There is approximately 15% total weight loss difference between original and microwave postmortem, which is attributed to shale oil production during microwave experiments. Both weight loss and enthalpy changes are lower, indicating production during microwave heating after adding iron powder. Unfortunately, the effect of iron powder cannot be seen from TGA/DSC curves of other oil shale samples.

CHAPTER 6

CONCLUSIONS

This study was carried out to understand mechanism of retort and microwave heating experiments by analyzing the reactivity and extraction potential of the oil shale samples. To do so, spectral and thermal analyses methods were used.

In the first part of the study, characterization studies were conducted by using XRD, TGA/DSC, FTIR and SEM analysis methods. It was found that combination of TGA/DSC and FTIR was useful to detect organic content, and combination of XRD and FTIR to detect inorganic content.

To understand the pyrolysis and combustion behaviors of the samples, identical heating under air and nitrogen environments were conducted. From TGA/DSC analyses, it was seen that the more carbonate ion had the oil shale, the more weight loss occurred during inorganic stage. Similarly, the more organic content, the more weight loss occurred during organic decomposition stage. However, the effect of clay minerals during the decomposition stages was not observed. The highest total weight loss arose from Himmetoglu oil shale due to its high organic content; however, it was understood that the total weight loss of other oil shale samples were mostly from their inorganic content. Moreover, kinetic analyses were carried and the catalyst effect of iron powder on pyrolysis and combustion was seen clearly.

With TGA/DSC, retort experiments were mimicked by using the temperature program of the experiments. The different final weight loss percentages of experiments and

simulations were attributed to the different heating and measuring mechanisms of retort apparatus and TGA/DSC instrument.

Identical heating and retort simulation results were compared. For the final temperature of the retort experiments, corresponding weight loss percentages of identical heating were specified and it was comprehended that temperature program causes more weight loss percentages; since, it provides more retention time.

SEM images of oil shale samples confirmed the existence of some minerals identified by XRD analysis. Moreover, the noticed fossil images indicated that the depositional environment of Seyitomer and Himmetoglu oil shales were marine.

In the second part of the study, postmortems of the experiments were further analyzed by TGA/DSC, FTIR, XRD and SEM, to see the effects of retort and microwave heating methods. XRD showed that heating experiments caused to produce some clay minerals. However, again the effect of clay minerals could not be noticed with the used analyses.

From FTIR results of retort postmortems it was seen that, except Himmetoglu oil shale, all organic content of oil shale samples were produced during experiments. This means that, for Himmetoglu oil shale, the used temperature program was not sufficient to produce all its organic content; as it comprised high kerogen content. However, it was seen that after adding iron powder, for all oil shale samples, organic content was produced during the retort analyses, entirely.

From microwave postmortems, we did not notice significant changes on the spectra after microwave heating, even from spectra of Himmetoglu with iron powder. It was understood that our microwave heating method was not able to produce all organic content during the experiments. On the other hand, the produced oil from Himmetoglu oil shale after adding iron powder during microwave heating experiments were analyzed by FTIR. It was seen that the fingerprints of the shale oil and the kerogen peaks of oil shale were

same. This indicated that microwave heating did not change the characteristics of kerogen during production.

FTIR spectra of pyrolysis and combustion postmortems showed the residual components after heating until 900 °C. The residuals were only the inorganic content, especially quartz. FTIR was found to be effective when comparing retort experiment and retort simulation. The results were used to understand the differences between the production percentages of the experiment and simulation. Generally, we obtained similar peaks from FTIR results of the postmortems of retort experiment and retort simulations.

TGA/DSC was used to burn the postmortems to see the residuals after the experiments. It was seen that retort experiments were able to produce some organic and inorganic content; while, microwave experiments not.

Finally, SEM analyses on retort and microwave postmortems showed that, retort experiments created char-like surfaces, and microwave heating caused to increase surface area of oil shale samples.

REFERENCES

- Abbasov, V. M., Mamedov, F. F., & Ismailov, T. a. (2008). Heats of combustion of oil shale, bitumen, and their mixtures. *Solid Fuel Chemistry*, 42(4), 248–250. doi:10.3103/S0361521908040113
- Abernethy, E. R. (2013). Production Increase of Heavy Oils By Electromagnetic Heating. *Journal of Canadian Petroleum Technology*, 15(03). doi:10.2118/76-03-12
- Al-Harashsheh, M., Al-Ayed, O., Robinson, J., Kingman, S., Al-Harashsheh, A., Tarawneh, K., ... Barranco, R. (2011). Effect of demineralization and heating rate on the pyrolysis kinetics of Jordanian oil shales. *Fuel Processing Technology*, 92(9), 1805–1811. doi:10.1016/j.fuproc.2011.04.037
- Al-Harashsheh, M., Kingman, S., Saeid, A., Robinson, J., Dimitrakakis, G., & Alnawafleh, H. (2009). Dielectric properties of Jordanian oil shales. *Fuel Processing Technology*, 90(10), 1259–1264. doi:10.1016/j.fuproc.2009.06.012
- Alomair, O., Alarouj, M., Althenayyan, A., Alsaleh, A., & Mohammad, H. (2012). Improving Heavy Oil Recovery by Unconventional Thermal Methods. In *SPE Kuwait International Petroleum Conference and Exhibition* (p. 16). Kuwait City, Kuwait: Society of Petroleum Engineers.
- Alstadt, K. N., Katti, D. R., & Katti, K. S. (2012). An in situ FTIR step-scan photoacoustic investigation of kerogen and minerals in oil shale. *Spectrochimica Acta. Part A, Molecular and Biomolecular Spectroscopy*, 89, 105–13. doi:10.1016/j.saa.2011.10.078
- Altun, N. E., Hiçyılmaz, C., Hwang, J. Y., Bağcı, A. S., & Kök, M. V. (2006). Oil Shales in the World and Turkey; Reserves, Current Situation and Future Prospects: A Review. *Oil Shale*, 23(3), 211–227.
- Ballice, L. (2005). Effect of demineralization on yield and composition of the volatile products evolved from temperature-programmed pyrolysis of Beypazari (Turkey) Oil Shale. *Fuel Processing Technology*, 86(6), 673–690. doi:10.1016/j.fuproc.2004.07.003
- Bhargava, S., Awaja, F., & Subasinghe, N. (2005). Characterisation of some Australian oil shale using thermal, X-ray and IR techniques. *Fuel*, 84(6), 707–715. doi:10.1016/j.fuel.2004.11.013

- Biglarbigi, K., Mohan, H., & Killen, J. (2009). Oil Shale 1: US, World Possess Rich Resource Base. *Oil & Gas Journal*.
- Bradhurst, D. H., & Worner, H. K. (1996). Evaluation of oil produced from the microwave retorting of Australian shales. *Fuel*, 75(3), 285–288. doi:10.1016/0016-2361(95)00232-4
- Bridges, J. E., Stresty, G., Taflove, A., & Snow, R. H. (1979). Radio-Frequency Heating to Recover Oil from Utah Tar Sands. In R. F. Meyer & C. . Steele (Eds.), *The Future of Heavy Cruse Oils and Tar Sands* (pp. 396–409). New York: Mining Informational Services, McGraw-Hill, Inc. Retrieved from <http://ds.heavyoil.utah.edu/dspace/handle/123456789/7967>
- Bridges, J. E., Taflove, A., & Snow, R. H. (1978). Net Energy Recoveries for the in-situ Dielectric Heating of Oil Shale. In J. H. Gary (Ed.), *Eleventh Oil Shale Symposium Proceedings*.
- Briggs, W. E., Lewis, J. E., & Tranquilla, J. M. (1983). Dielectric Properties of New Brunswick Oil Shale. *Journal of Microwave Power*, 18(1), 75–82.
- Burnham, A. K., & Mcconaghy, J. R. (2006). Comparison of the Acceptability of Various Oil Shale Processes. In *26th Oil Shale Symposium* (pp. 1–11). Golden, CO: Colorado School of Mines.
- Butts, J. R., Lewis, J. E., & Steward, F. R. (1983). Microwave Heating of New Brunswick Oil Shale. *Journal of Microwave Power*.
- Carlson, R. D., Blase, E. F., & Mclendon, T. R. (1981). Development of The IIT Research Institut RF Heating Process for in-situ Oil Shale/Tar Sand Fuel Extraction. Retrieved January 2, 2014, from <http://content.lib.utah.edu/utills/getfile/collection/ir-eua/id/2906/filename/2720.pdf>
- Chen, C., Wang, W., Sun, Y., Guo, W., & Yan, X. (2013). Influence of the Heat Transfer Efficiency of Oil Shale in-situ Fragmentation. In F. Wang, M. Miyajima, T. Li, W. Shan, & T. F. Fathani (Eds.), *Progress of Geo-Disaster Mitigation Technology in Asia* (pp. 577–583). Berlin: Springer-Verlag Berlin Heidelberg. doi:10.1007/978-3-642-29107-4
- Coates, J., & Ed, R. A. M. (2000). Interpretation of Infrared Spectra , A Practical Approach Interpretation of Infrared Spectra , A Practical Approach, 10815–10837.
- Das, S. C. (2009). *A Study of Oxidation Reaction Kinetics During an Air Injection Process*. University of Adelaide. Retrieved from <https://digital.library.adelaide.edu.au/dspace/handle/2440/60192>

- Downs, R. T. (2006). An Integrated Study of the Chemistry, Crystallography, Raman and Infrared Spectroscopy of Minerals. In *The RRUFF Project*. Kobe, Japan: 19th General Meeting of the International Mineralogical Association.
- El harfi, K., Mokhlisse, A., Chanaa, M. B., & Outzourhit, A. (1999). Pyrolysis of the Moroccan (Tarfaya) Oil Shales under Microwave Irradiation. *Fuel*, 79(2000), 733–742.
- Fang-Fang, X., Ze, W., Wei-Gang, L., & Wen-Li, S. (2010). Study on Thermal Conversion of Huadian Oil Shale Under N₂ and Co₂ Atmospheres. *Oil Shale*, 27(4), 309. doi:10.3176/oil.2010.4.04
- Fernandez, Y., Arenillas, A., & Menendez, J. A. (2011). Microwave Heating Applied to Pyrolysis. In S. Grundas (Ed.), *Advances in Induction and Microwave Heating of Mineral and Organic Materials* (pp. 723–752). Spain: InTech. doi:10.5772/562
- Güleç, K., & Önen, A. (1992). Turkish Oil Shales: Reserves, Characterization and Utilisation Studies. In *Eastern Oil Shale Symposium* (pp. 12–24).
- Hakala, J. A., Stanchina, W., Soong, Y., & Hedges, S. (2011). Influence of Frequency, Grade, Moisture and Temperature on Green River Oil Shale Dielectric Properties and Electromagnetic Heating Processes. *Fuel Processing Technology*, 92(1), 1–12. doi:10.1016/j.fuproc.2010.08.016
- Hascakir, B. (2008). Investigation of Productivity of Heavy Oil Carbonate Reservoirs and Oil Shales using Electrical Heating Methods (Doctoral thesis, Middle East Technical University, Ankara, Turkey). Retrieved from <http://etd.lib.metu.edu.tr/upload/3/12609804/index.pdf>
- Hascakir, B., & Akin, S. (2010). Recovery of Turkish Oil Shales by Electromagnetic Heating and Determination of the Dielectric Properties of Oil Shales by an Analytical Method. *Energy & Fuels*, 24(1), 503–509. doi:10.1021/ef900868w
- International Energy Agency. (2010). *World Energy Outlook*. Paris, France.
- Laherrere, J. (2005). Review on Oil Shale Data. Retrieved March 25, 2015, from http://ecolo.org/documents/documents_in_english/OilShaleReview.pdf
- Largeau, C., Derenne, S., Casadevall, E., Berkaloff, C., Corolleur, M., Lugardon, B., ... Connan, J. (1990). Occurrence and origin of “ultralaminar” structures in “amorphous” kerogens of various source rocks and oil shales. *Organic Geochemistry*, 16(4-6), 889–895. doi:10.1016/0146-6380(90)90125-J
- Lee, S. (1990). *Oil Shale Technology*. CRC Press. Retrieved from <https://books.google.com/books?id=ojovooEaWhgC&pgis=1>

- Levy, J. H., & Stuart, W. I. (1984). Thermal Properties of Australian Oil Shales: Characterization by Thermal Analysis and Infrared Spectrophotometry. In *Symposium on Characterization and Chemistry of Oil Shales Presented before the Divisions of Fuel Chemistry and Petroleum Chemistry, Inc.* (pp. 61–70).
- Mallon, R. G. (1980). *Economics of Shale Oil Production by Radio Frequency Heating*. Retrieved from <http://www.osti.gov/scitech/biblio/5358198>
- Meredith, R. J. (1998). *Engineers' Handbook of Industrial Microwave Heating*. London, United Kingdom: The Institution of Electrical Engineers. Retrieved from <http://www.google.com.tr/books?hl=tr&lr=&id=fKXHVc8W64oC&pgis=1>
- Pan, Y., Zhang, J., Wang, X., & Yang, S. (2012). Research on Electric Heating Technology In-situ Oil Shale Mining, 2(8), 39–44.
- Parker, H. W. (1964). In-situ Electrolinking of Oil Shale. Oklahoma, USA. Retrieved from <http://www.google.com.tr/books?hl=tr&lr=&id=fKXHVc8W64oC&pgis=1>
- Pringle, F. G., Everleigh, C., & Forthe, J. (2010). *Microwave Processing of Oil Shale and Coal*. USA.
- Qing, W., Baizhong, S., Aijuan, H., Jingru, B., & Shaohua, L. (2007). Pyrolysis characteristics of Huadian oil shales. *Oil Shale*, 24(2), 147–157.
- Rouxhet, P. G., Robin, P. L., & Nicaise, G. (1980). Characterization of kerogens and of their evolution by infrared spectroscopy. In *Kerogen: Insoluble Organic Matter from Sedimentary Rocks* (pp. 165–190).
- Salin, I. M., & Seferis, J. C. (1993). Kinetic analysis of high-resolution TGA variable heating rate data. *Journal of Applied Polymer Science*, 47(5), 847–856. doi:10.1002/app.1993.070470512
- Sarapuu, E. (1957). *Method of Underground Electrolinking and Electrocarbonization of Mineral Fuels*. Minneapolis, USA.
- Savage, K. D. (1985). *Method of Heating an Oil Shale Formation*. Texas, USA.
- Smith, M. W., Shadle, L. J., & Hill, D. (2007). Oil Shale Development from the Perspective of NETL's Unconventional Oil Resource Repository. In *26th Oil Shale Symposium*. Golden, CO: Colorado Energy Research Institute, Colorado School of Mines. Retrieved from <http://ceri-mines.org/documents/A12b-MWSmithetalJB.pdf>
- Speight, J. G. (1999). Kerogen. In *The Chemistry and Technology of Petroleum, Fourth Edition* (Third., p. 123). USA: CRC Press.

- Speight, J. G. (2012). *Shale Oil Production Processes*. Elsevier. Retrieved from http://www.google.com.tr/books?hl=tr&lr=&id=MeF43dYp_4YC&pgis=1
- Şener, M., Şengüler, I., & Kök, M. V. (1995). Geological Considerations for the Economic Evaluation of Oil Shale Deposits in Turkey. *Fuel*, 74(7), 999–1003. doi:10.1016/0016-2361(95)00045-7
- Vinegar, H. J., Bass, R. M., & Hunsucker, B. G. (2005). Heat Sources with Conductive Material for in-situ Thermal Processing of an Oil Shale Formation. Texas, USA.
- Wilson, R. (1987). Well Production Method Using Microwave Heating. California, USA.
- World Energy Council. (2010). *2010 Survey of Energy Resources*. London, United Kingdom. Retrieved from http://www.worldenergy.org/wp-content/uploads/2012/09/ser_2010_report_1.pdf
- Yen, T. F. (1976). *Science and Technology of Oil Shale*. Michigan, USA: Ann Arbor Science Publishers. Retrieved from <https://books.google.com/books?id=RMb5AAAAIAAJ&pgis=1>
- Yen, T. F., & Chilingarian, G. V. (1976). *Oil Shale*. The Netherlands: Elsevier.
- Zheng, D., Li, S., Ma, G., & Wang, H. (2012). Autoclave Pyrolysis Experiments of Chinese Liushuhe Oil Shale To Simulate in-Situ Underground Thermal Conversion. *Oil Shale*, 29(2), 103. doi:10.3176/oil.2012.2.02

APPENDIX A

THERMAL GRAVIMETRIC ANALYSIS

A.1 Identical Heating of Retort Postmortem with Air

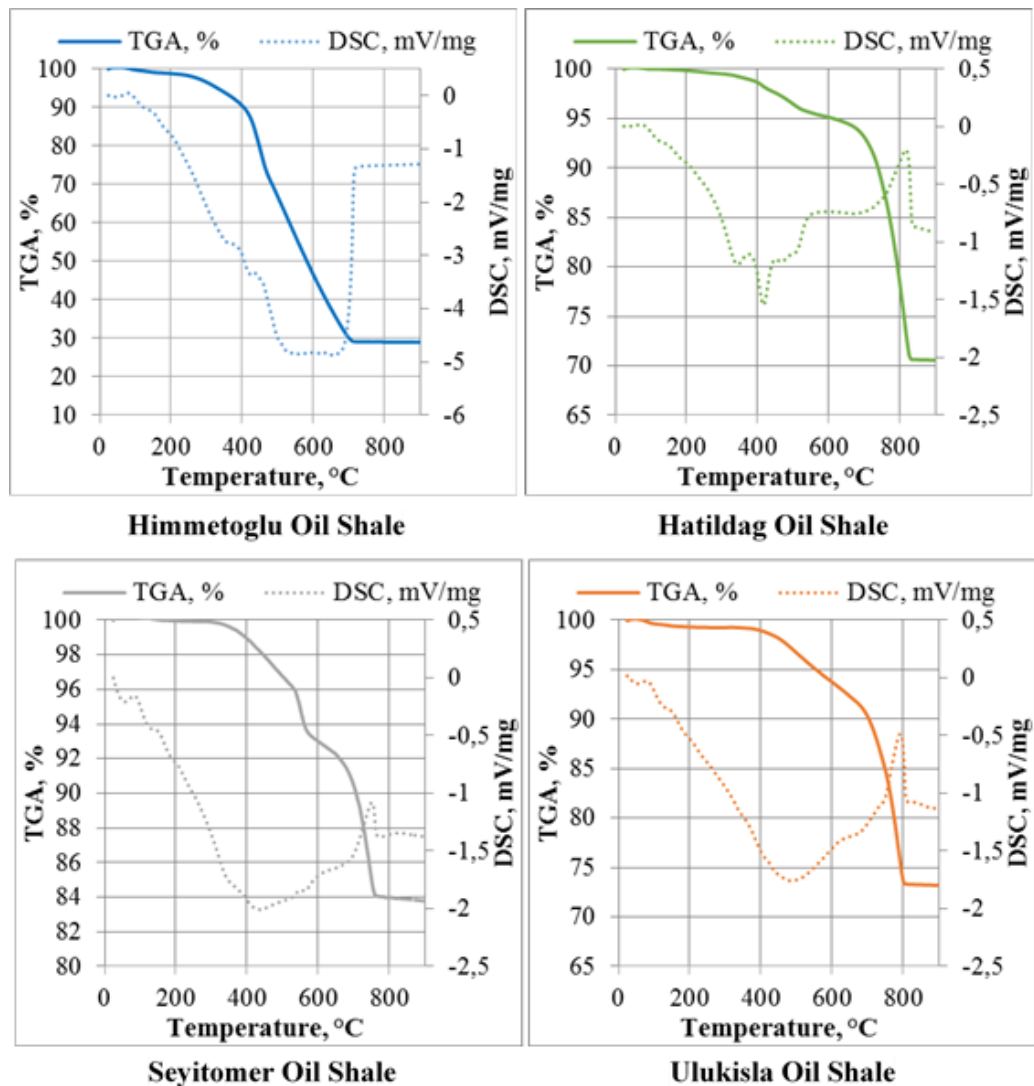
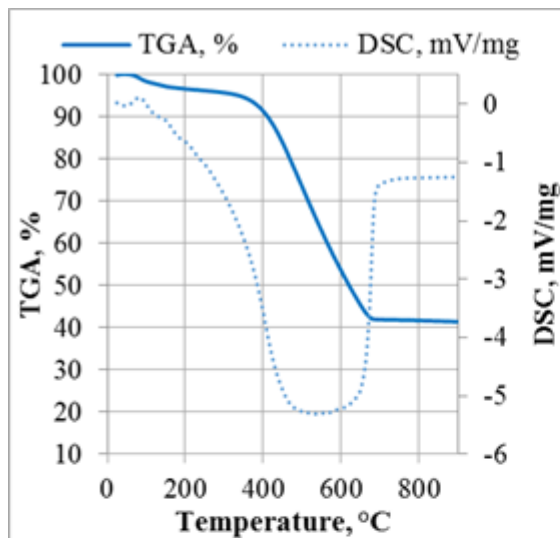
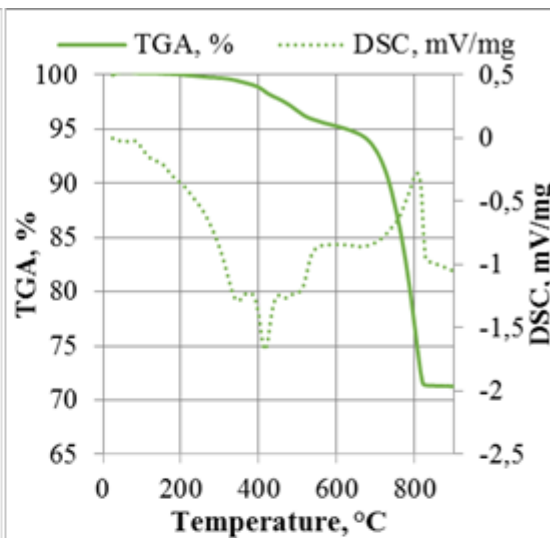


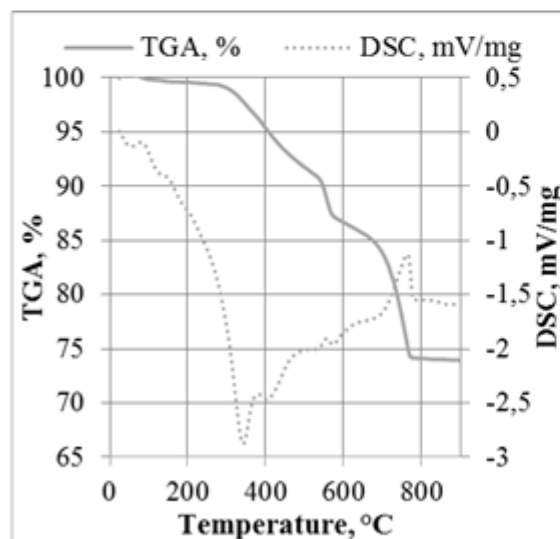
Figure A-1 TGA/DSC results of identical heating of retort postmortems



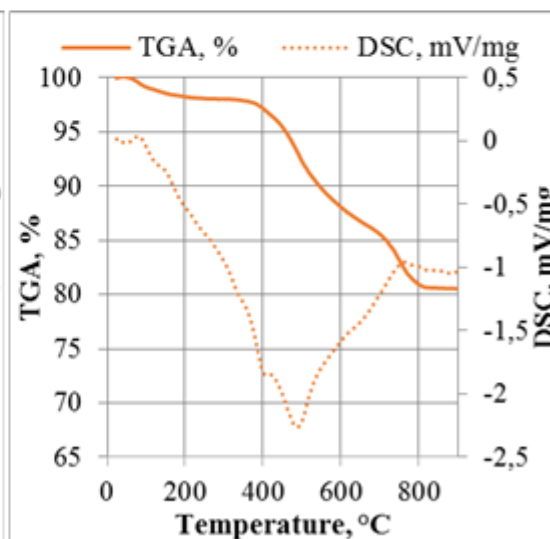
Himmetoglu Oil Shale (0.1% Fe)



Hatildag Oil Shale (0.1% Fe₂O₃)



Seyitomer Oil Shale (0.5% Fe)



Ulukisla Oil Shale (0.1% Fe₂O₃)

Figure A-2 TGA/DSC results of identical heating of retort postmortems (with iron powder)

A.2 Identical Heating of Microwave Postmortem with Air

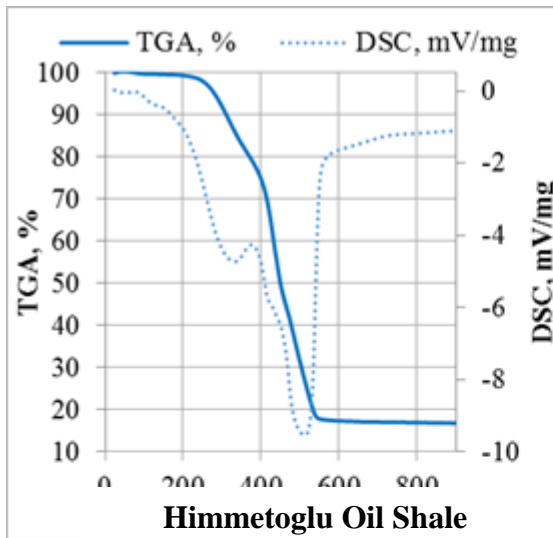


Figure AA. Himmetoglu Oil Shale

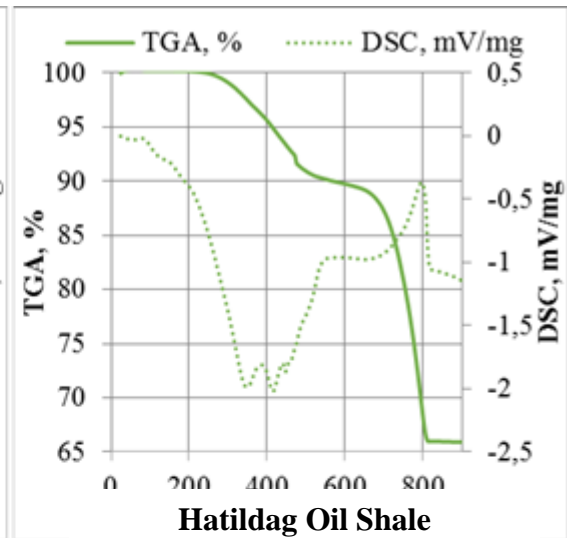


Figure AA. Hatildag Oil Shale

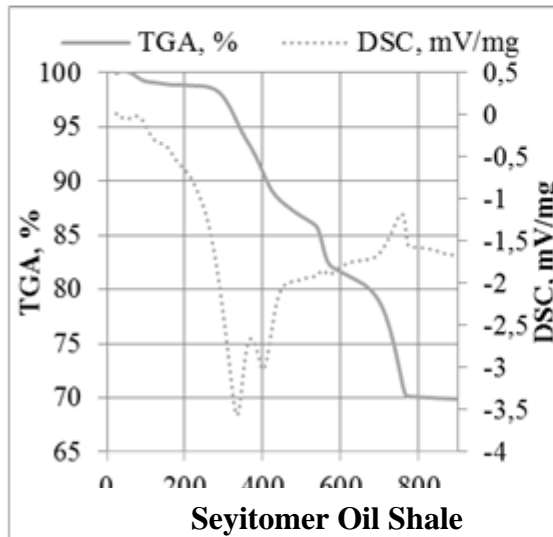


Figure AA. Seyitomer Oil Shale

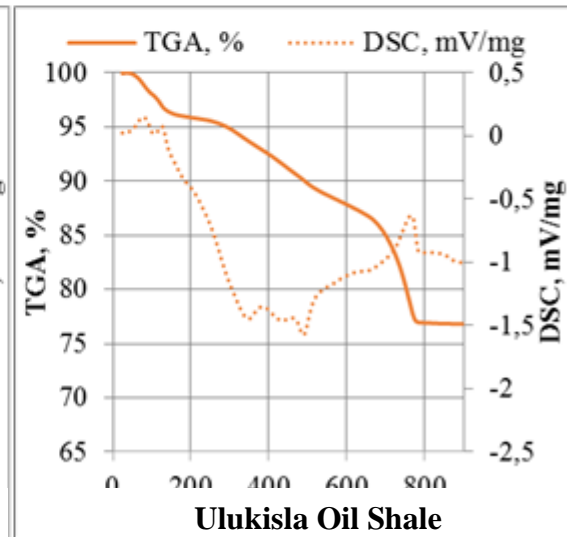


Figure AA. Ulukisla Oil Shale

Figure A-3 TGA/DSC results of identical heating of microwave postmortems

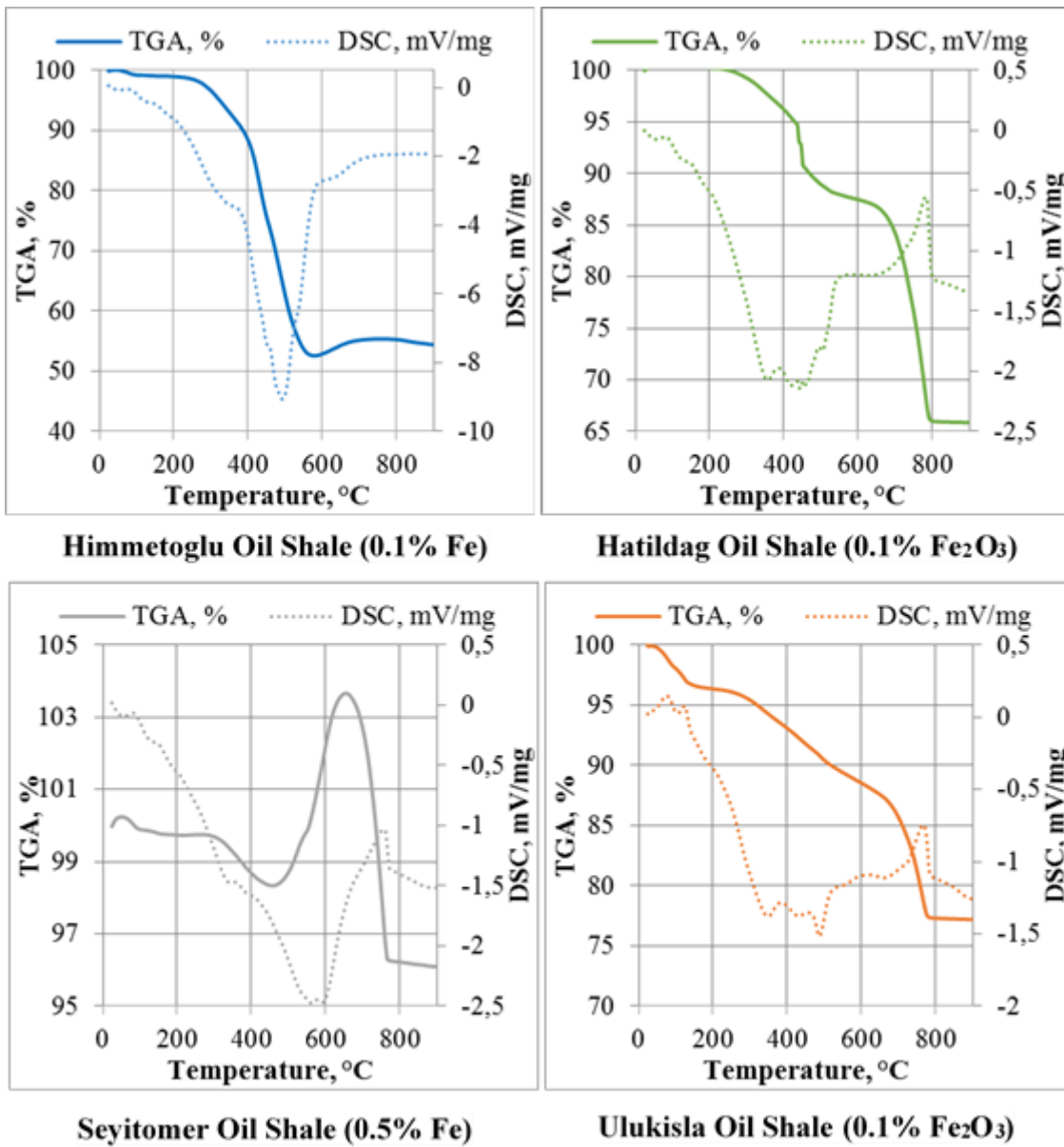


Figure A-4 TGA/DSC results of identical heating of microwave postmortems (with iron powder)

A.3 Differential Thermal Gravimetric Analysis (DTG)

Himmetoglu

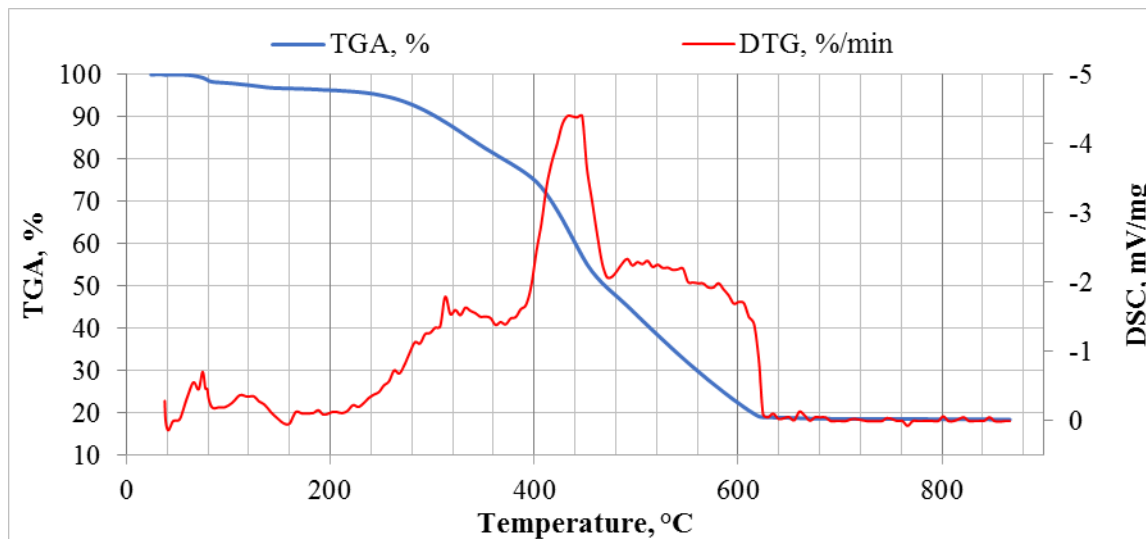


Figure A-5 TG vs. DTG curves of Himmetoglu under air injection

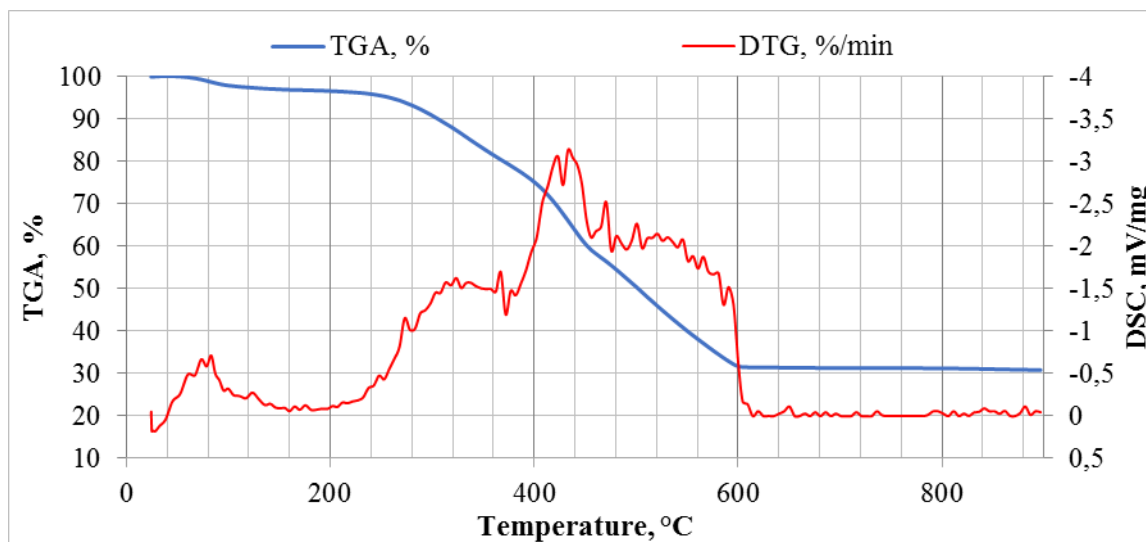


Figure A-6 TG vs. DTG curves of Himmetoglu under air injection (with iron powder)

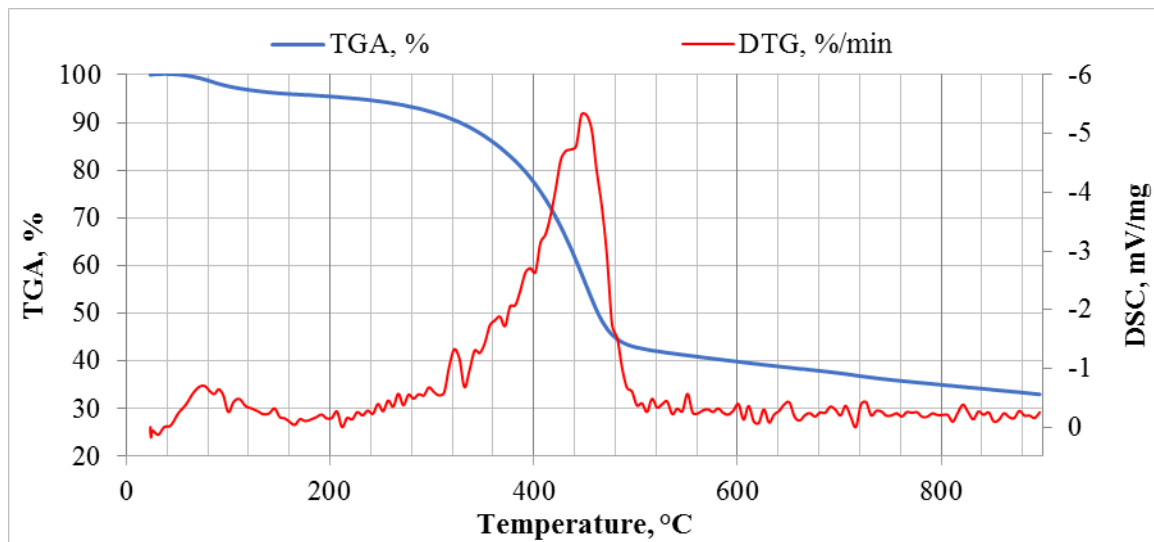


Figure A-7 TG vs. DTG curves of Himmetoglu under nitrogen injection

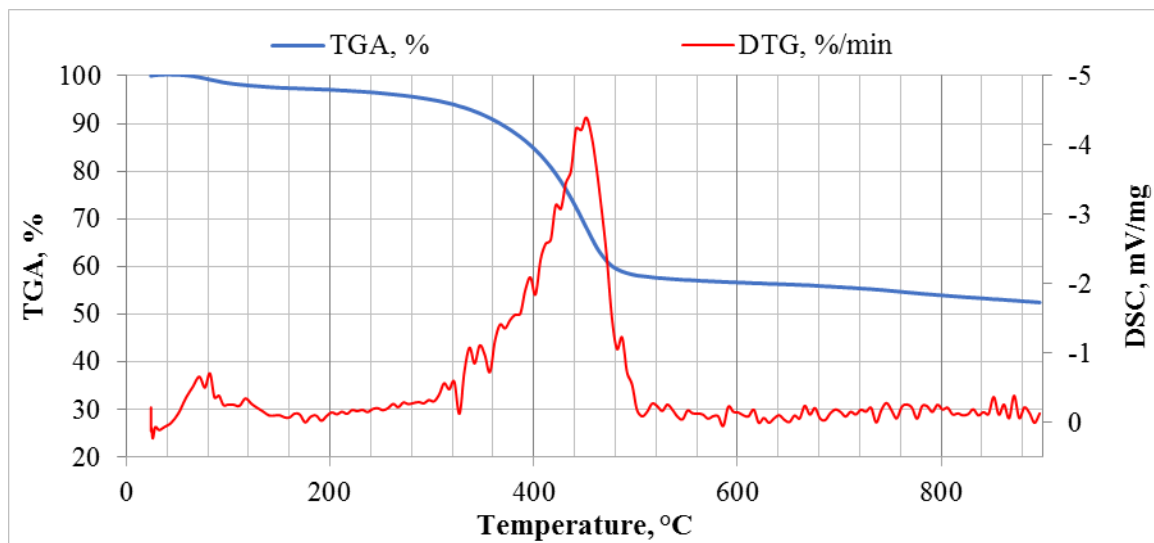


Figure A-8 TG vs. DTG curves of Himmetoglu under nitrogen injection (with iron powder)

Hatildag

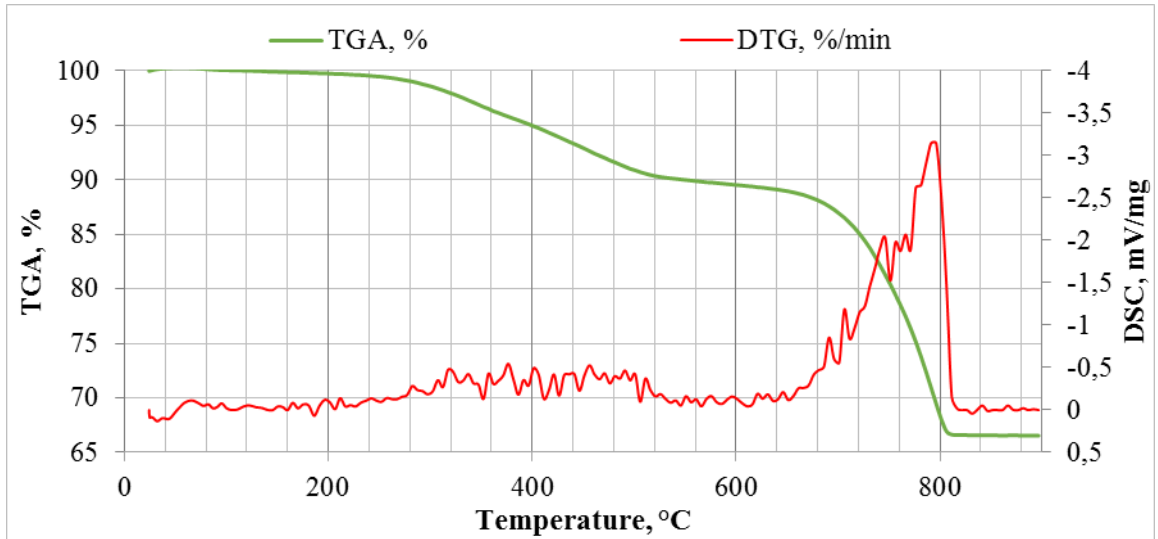


Figure A-9 TG vs. DTG curves of Hatildag under air injection

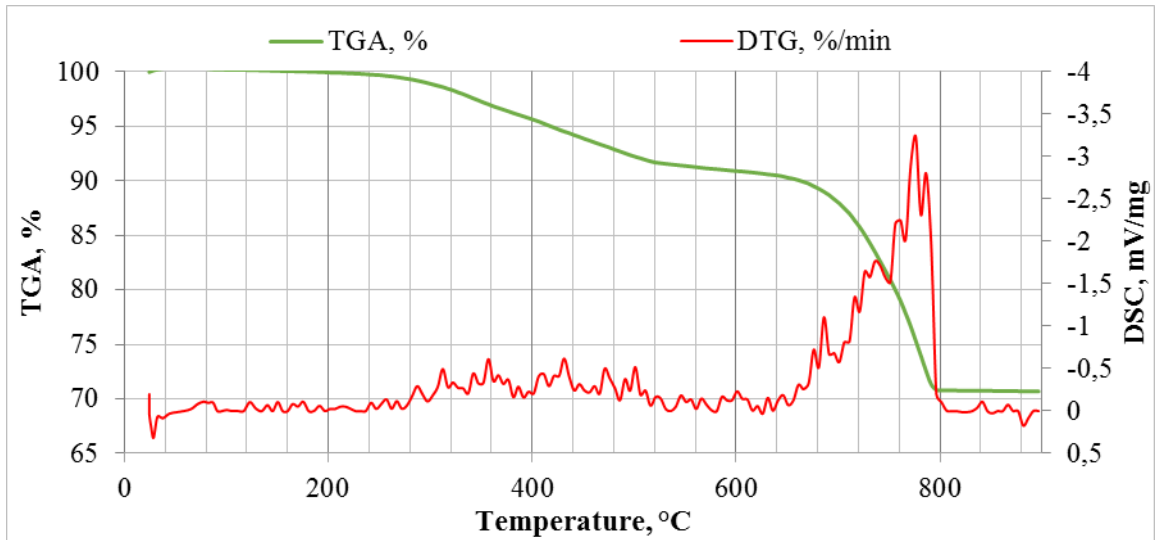


Figure A-10 TG vs. DTG curves of Hatildag under air injection (with iron powder)

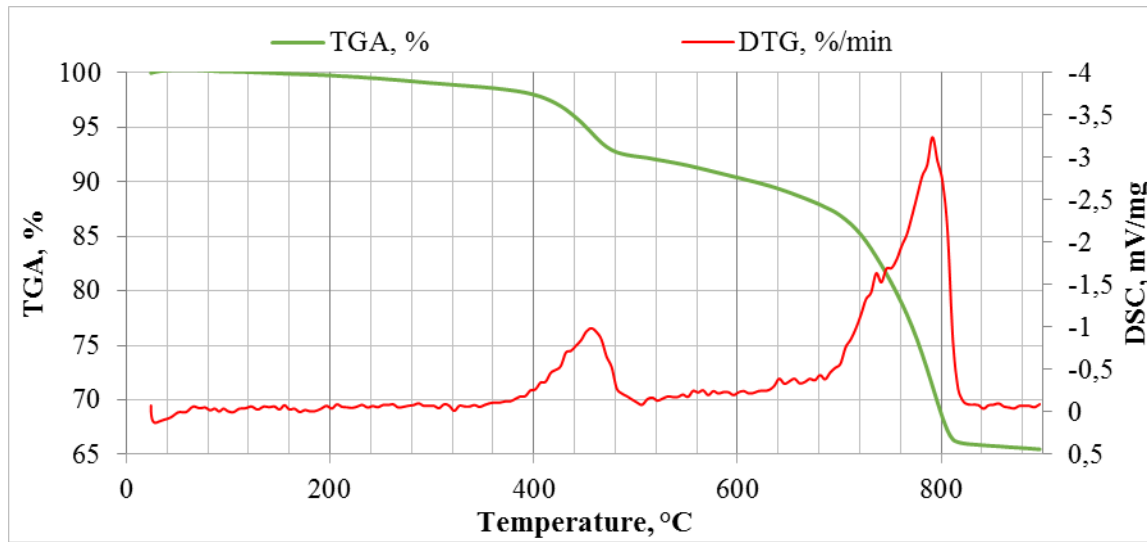


Figure A-11 TG vs. DTG curves of Hatildag under nitrogen injection

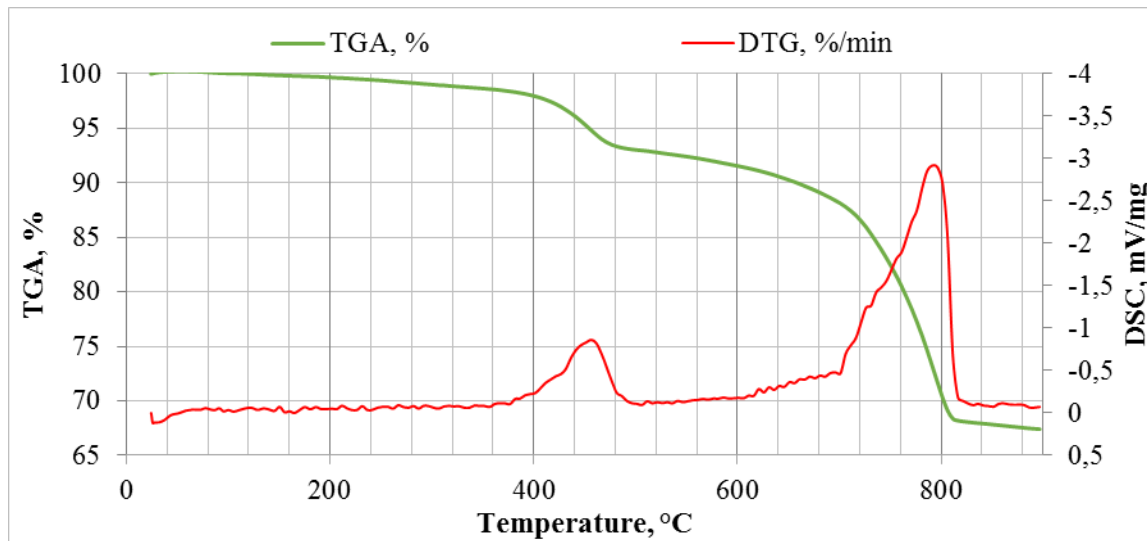


Figure A-12 TG vs. DTG curves of Hatildag under nitrogen injection (with iron powder)

Seyitomer

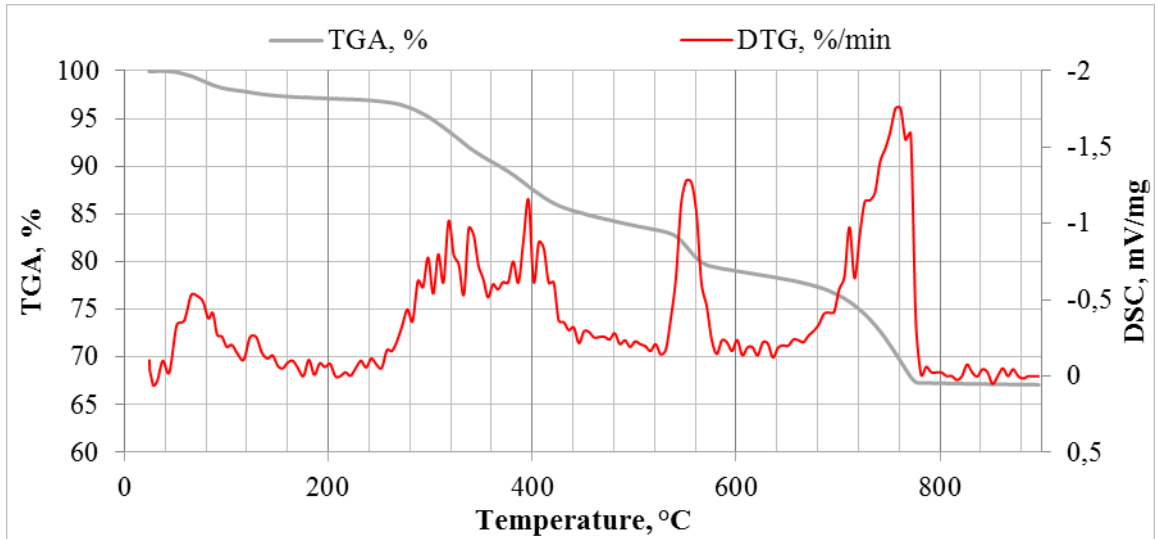


Figure A-13 TG vs. DTG curves of Seyitomer under air injection

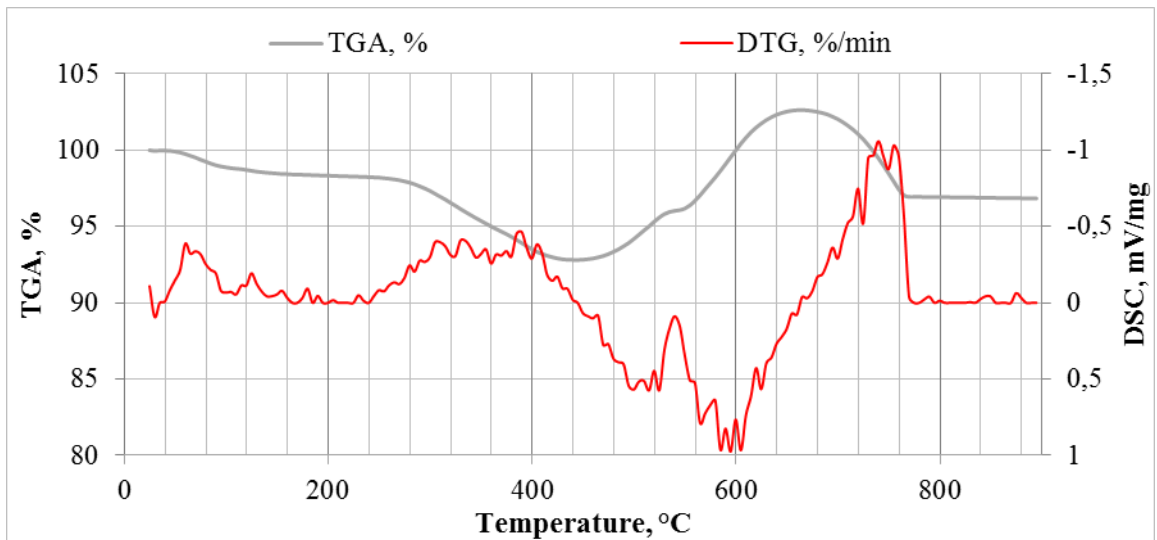


Figure A-14 TG vs. DTG curves of Seyitomer under air injection (with iron powder)

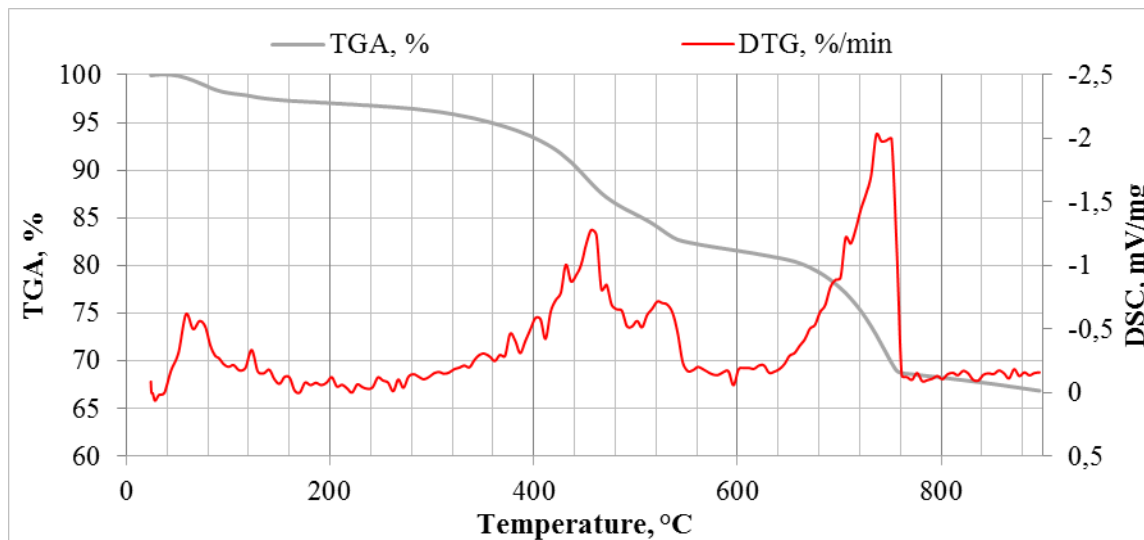


Figure A-15 TG vs. DTG curves of Seytomer under nitrogen injection

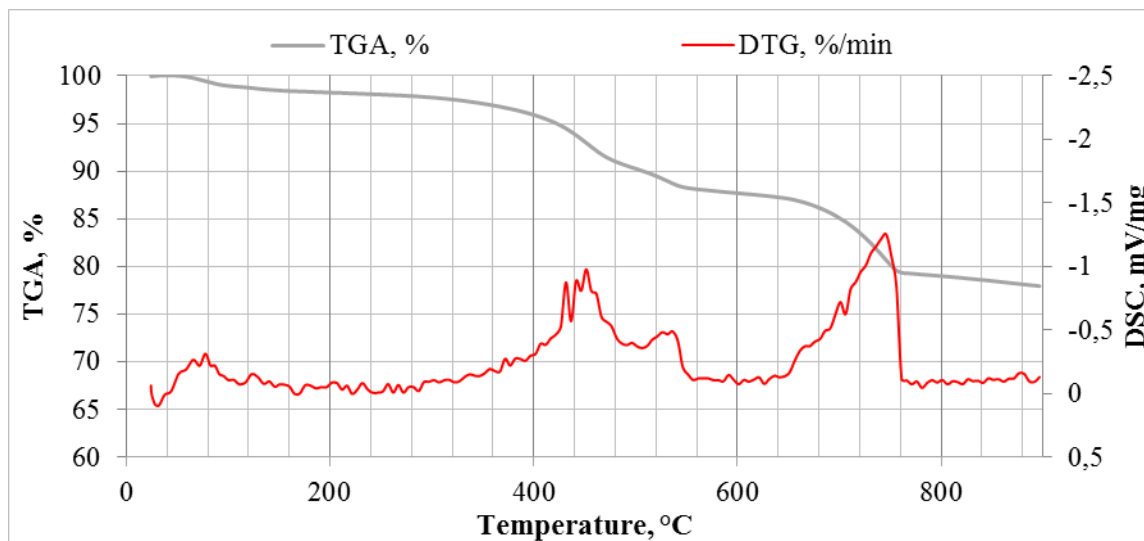


Figure A-16 TG vs. DTG curves of Seytomer under nitrogen injection (with iron powder)

Ulukisla

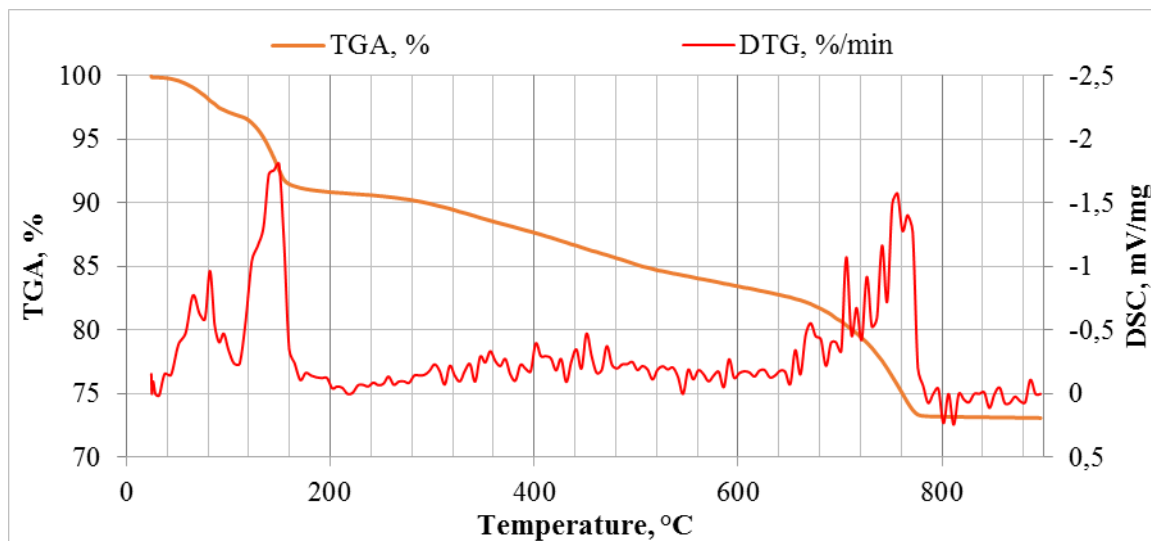


Figure A-17 TG vs. DTG curves of Ulukisla under air injection

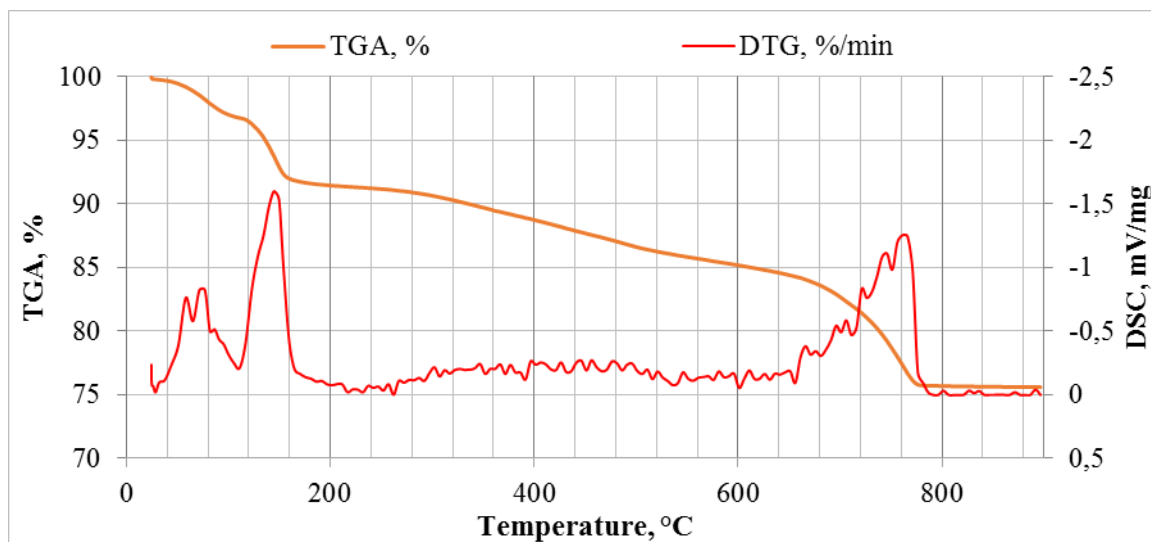


Figure A-18 TG vs. DTG curves of Ulukisla under air injection (with iron powder)

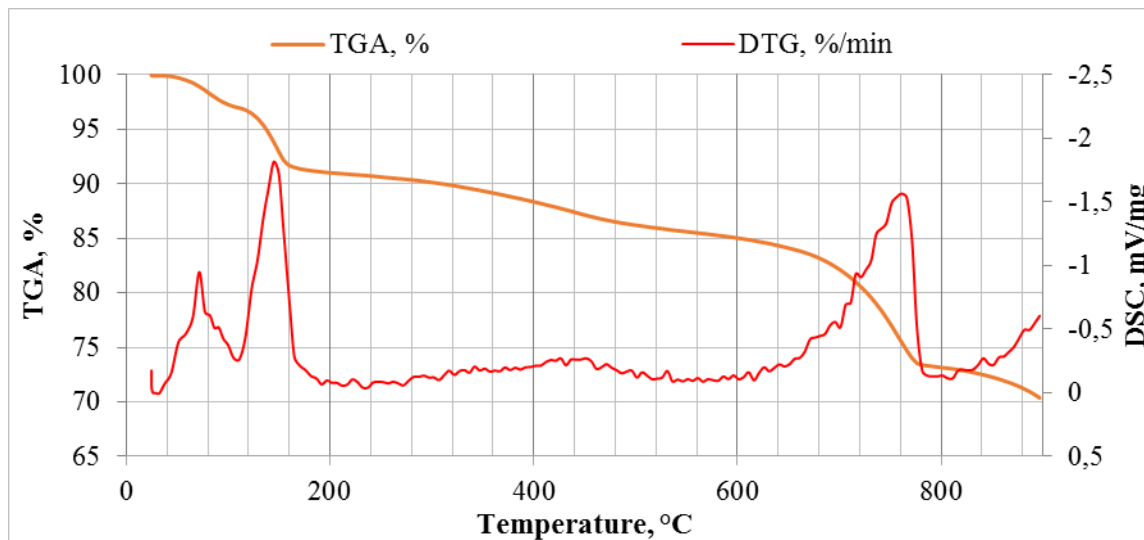


Figure A-19 TG vs. DTG curves of Ulukisla under nitrogen injection

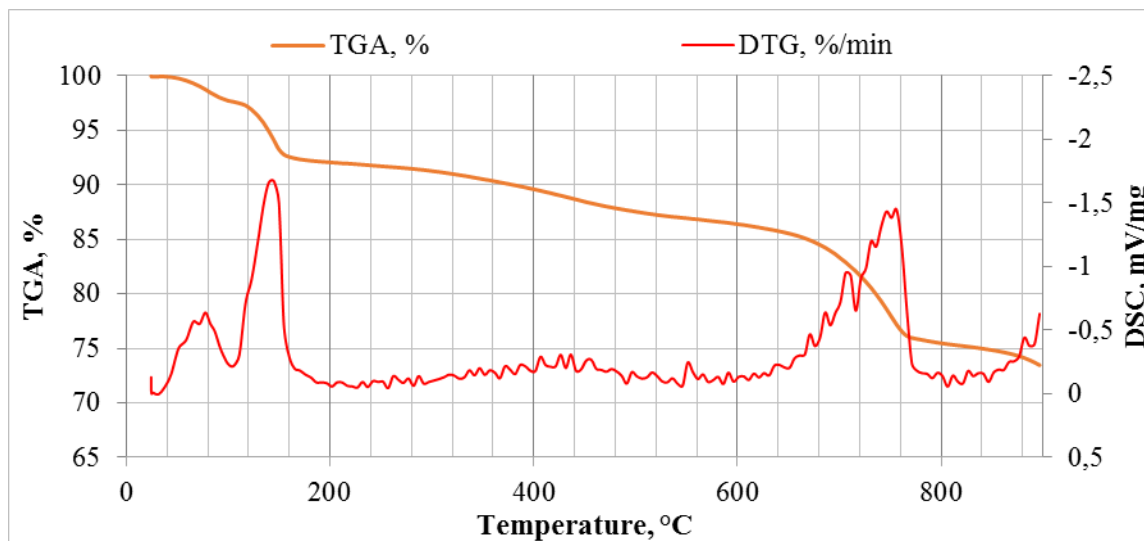


Figure A-20 TG vs. DTG curves of Ulukisla under nitrogen injection (with iron powder)

A.4 Arrhenius Model Plots

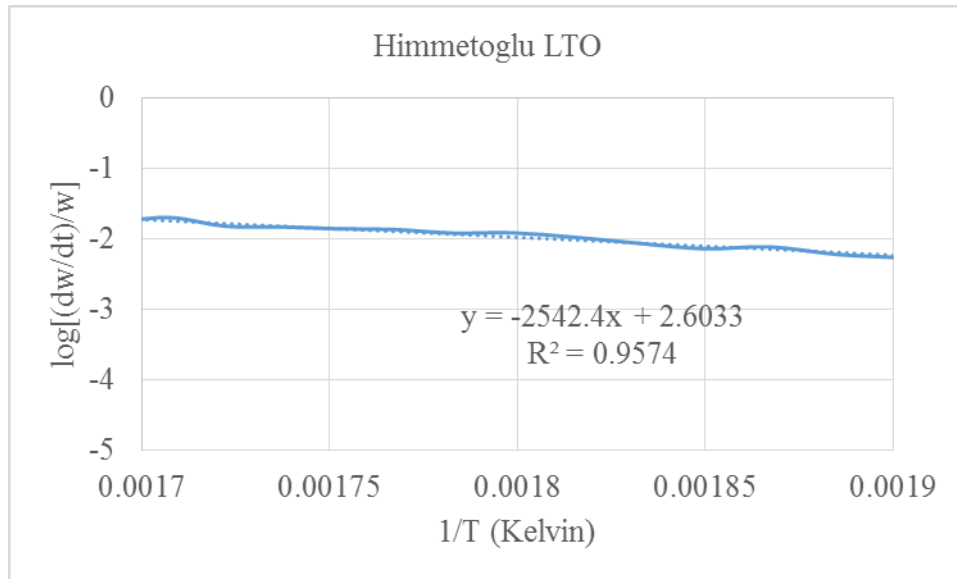


Figure A-21 Arrhenius plot of Himmetoglu for LTO at 10 °C/min

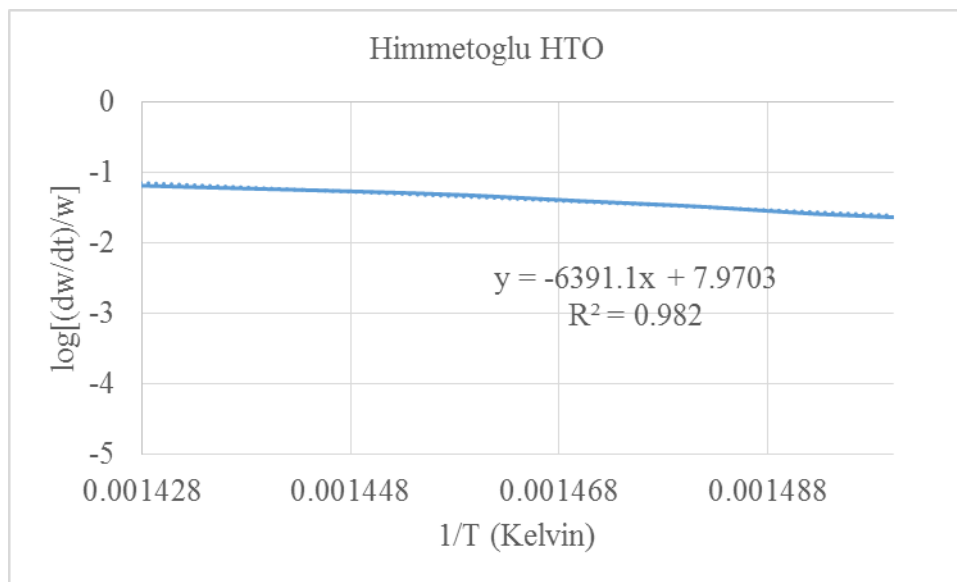


Figure A-22 Arrhenius plot of Himmetoglu for HTO at 10 °C/min

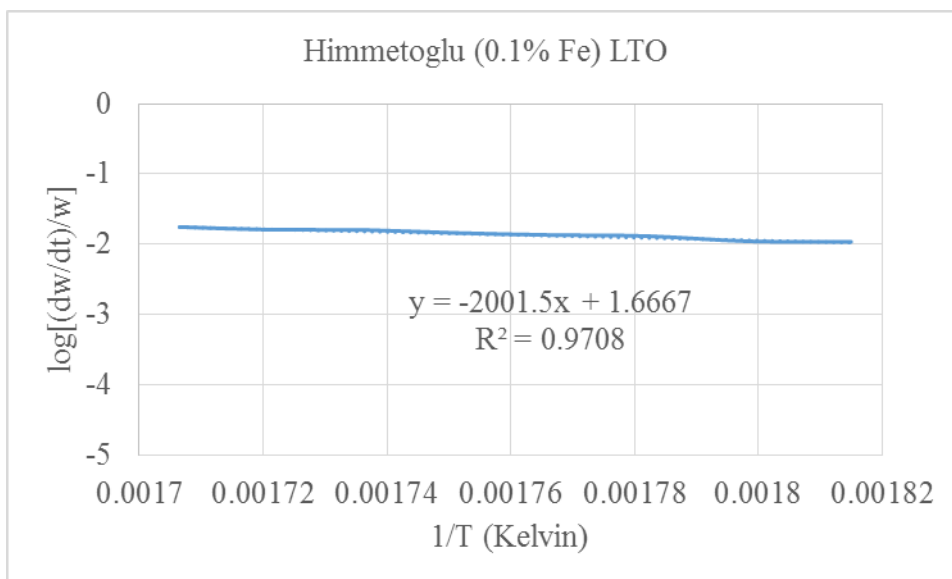


Figure A-23 Arrhenius plot of Himmetoglu (with iron powder) for LTO at 10 °C/min

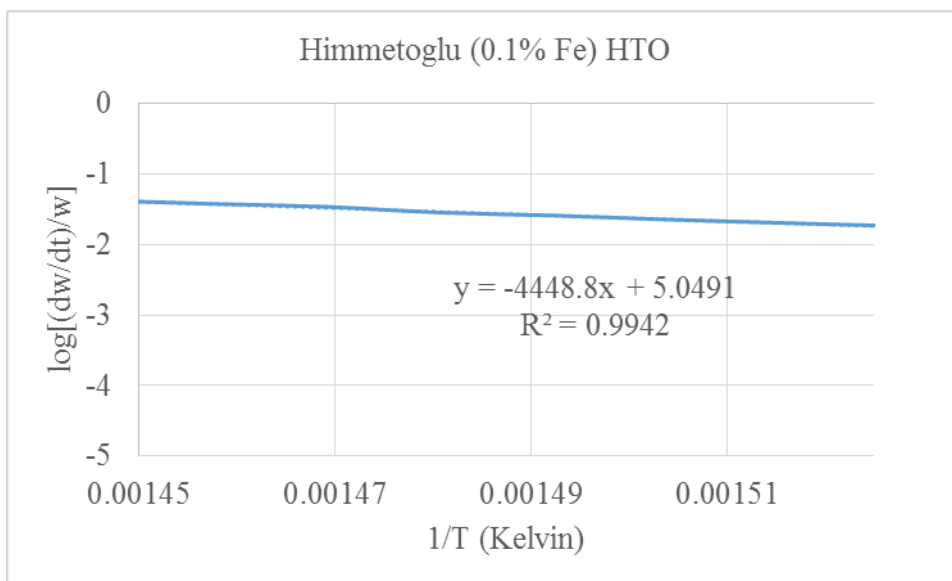


Figure A-24 Arrhenius plot of Himmetoglu (with iron powder) for HTO at 10 °C/min

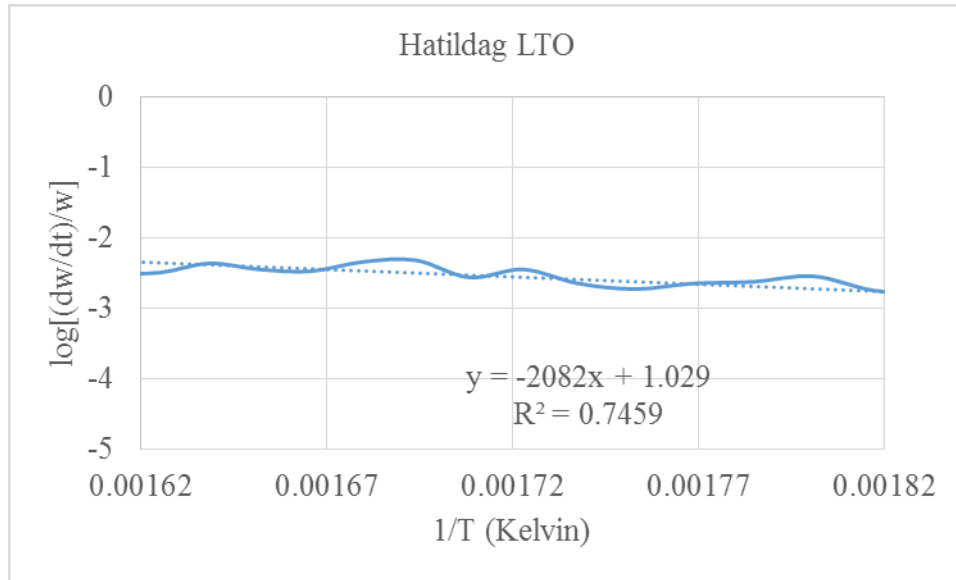


Figure A-25 Arrhenius plot of Hatildag for LTO at 10 °C/min

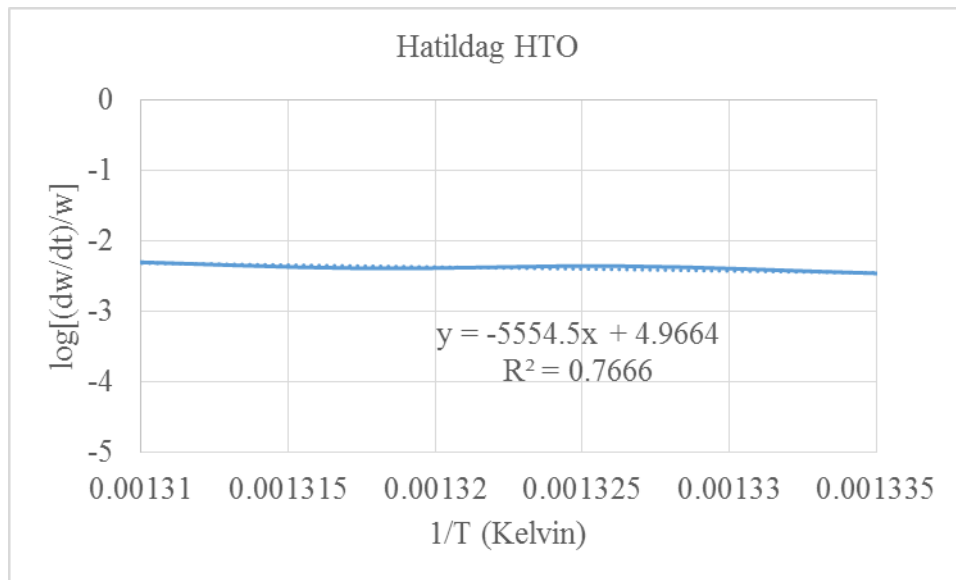


Figure A-26 Arrhenius plot of Hatildag for HTO at 10 °C/min

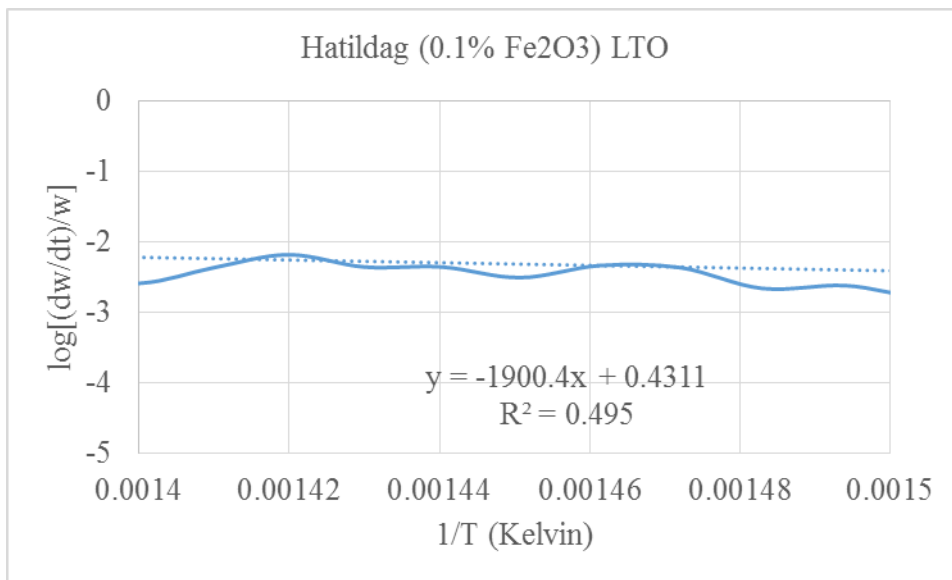


Figure A-27 Arrhenius plot of Hatildag (with iron powder) for LTO at 10 °C/min

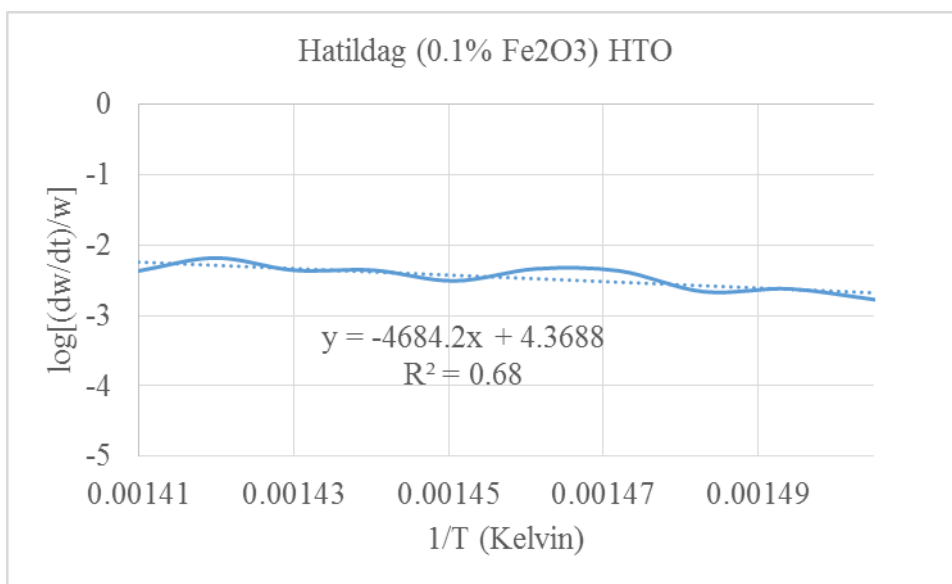


Figure A-28 Arrhenius plot of Hatildag (with iron powder) for HTO at 10 °C/min

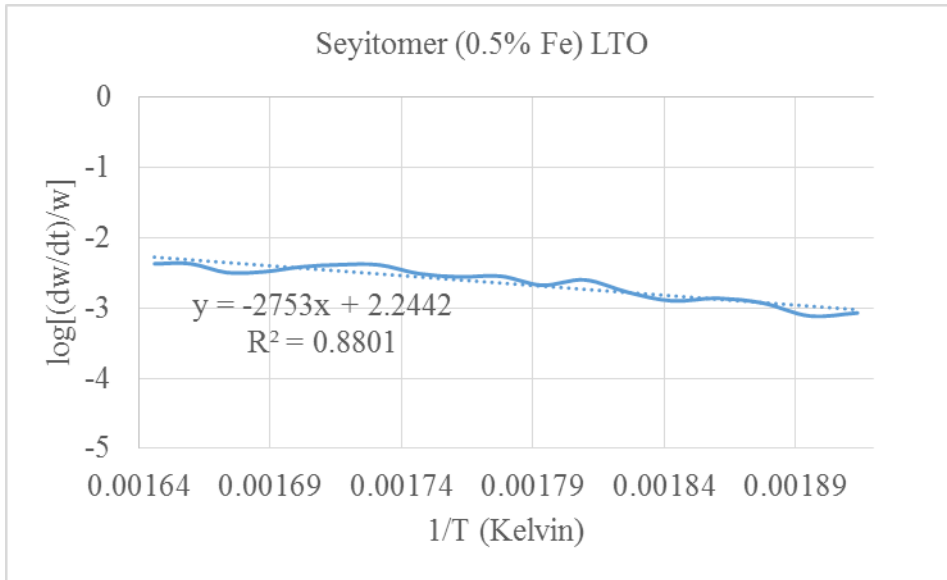


Figure A-31 Arrhenius plot of Seyitomer (with iron powder) for LTO at 10 °C/min

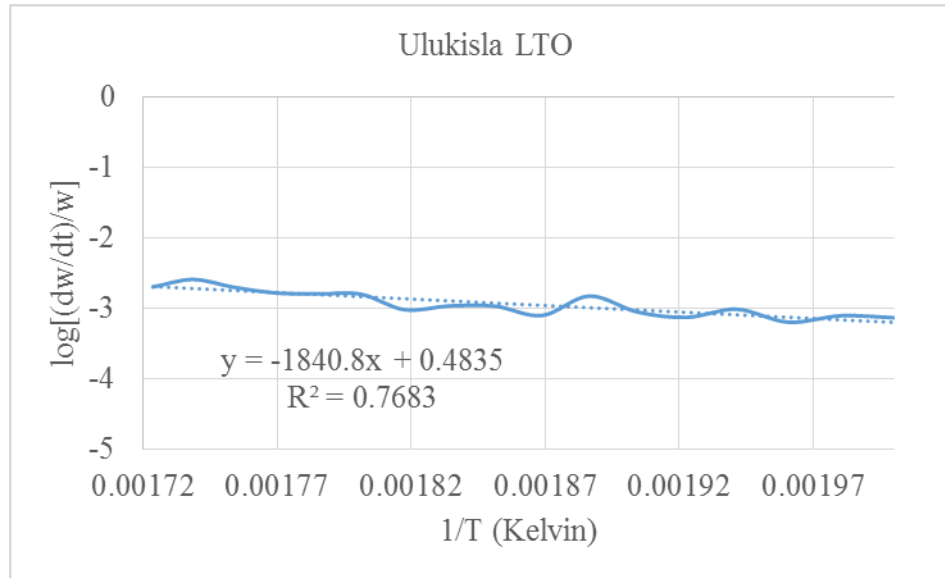


Figure A-32 Arrhenius plot of Ulukisla for LTO at 10 °C/min

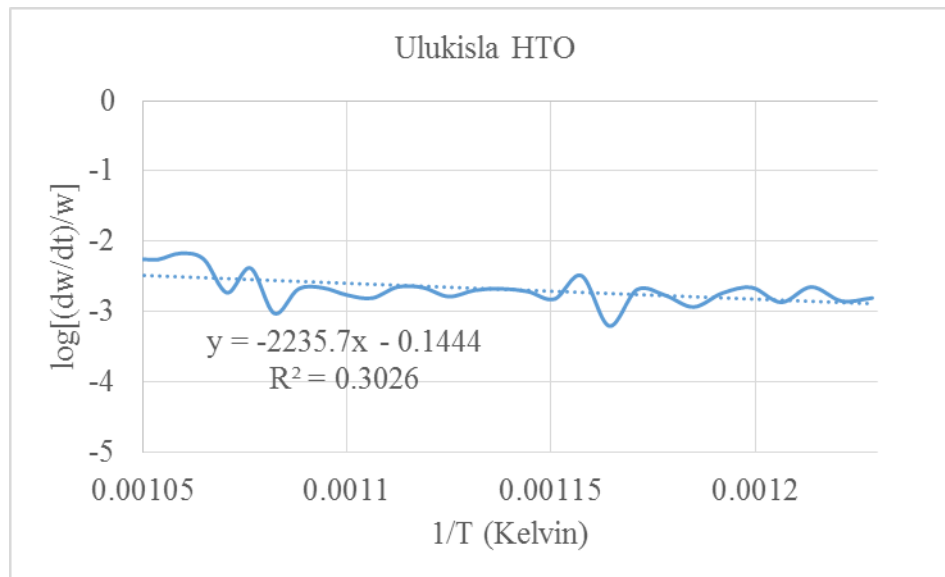


Figure A-33 Arrhenius plot of Ulukisla for HTO at 10 °C/min

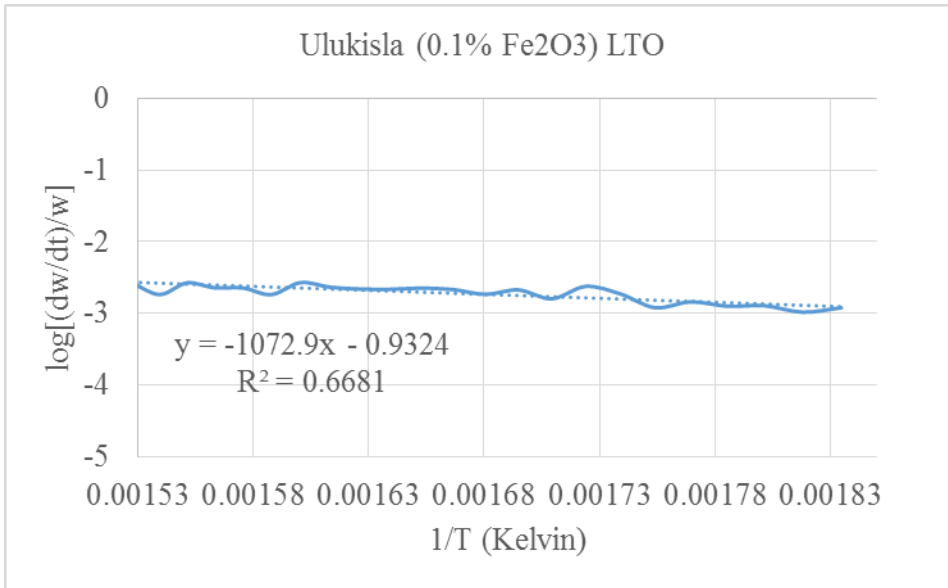


Figure A-34 Arrhenius plot of Ulukisla (with iron powder) for LTO at 10 °C/min

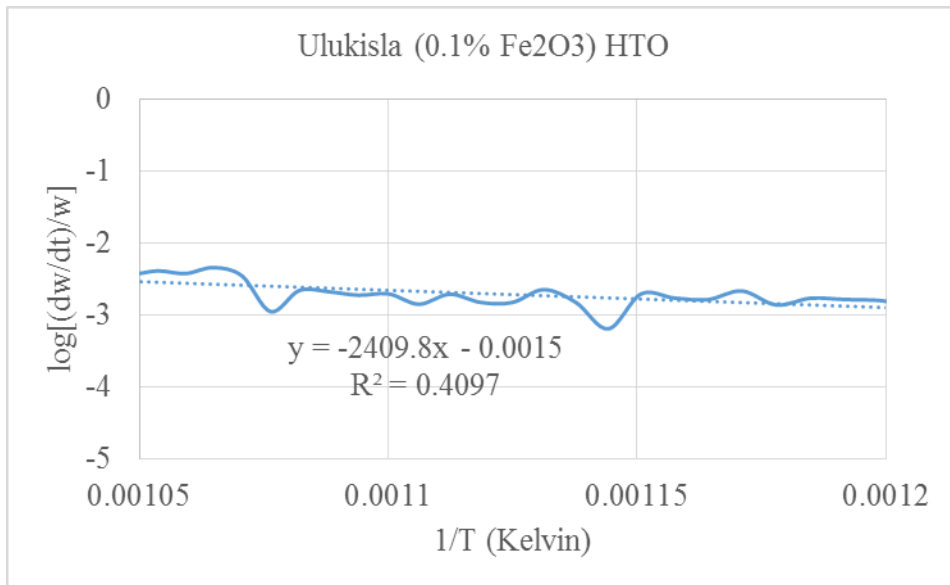


Figure A-35 Arrhenius plot of Ulukisla (with iron powder) for HTO at 10 °C/min

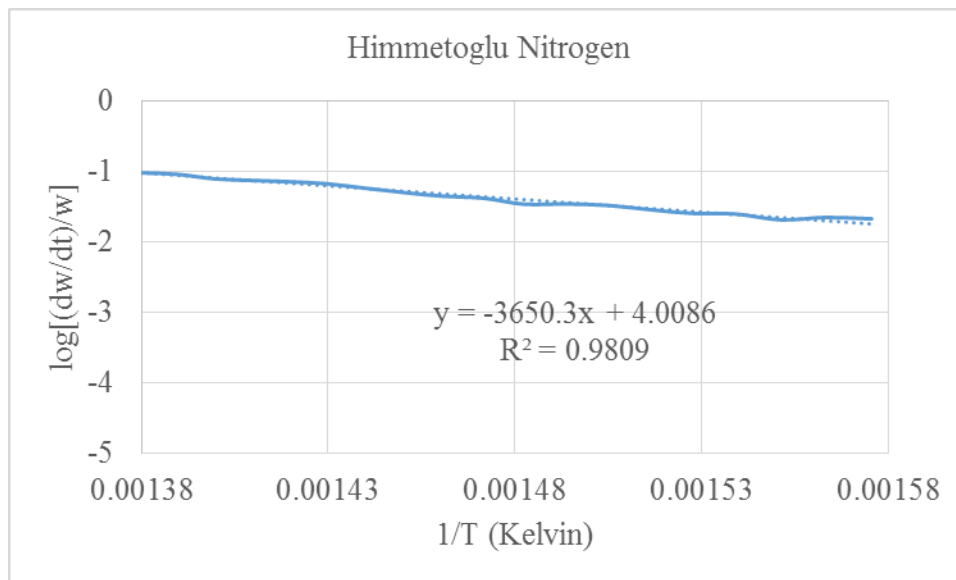


Figure A-36 Arrhenius plot of Himmetoglu for pyrolysis at 10 °C/min

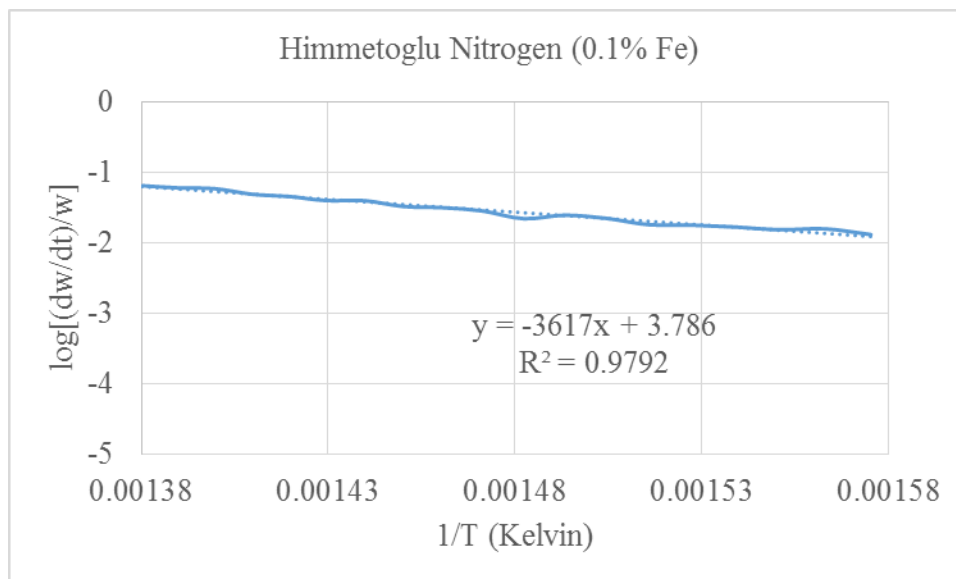


Figure A-37 Arrhenius plot of Himmetoglu (with iron powder) for pyrolysis at 10 °C/min

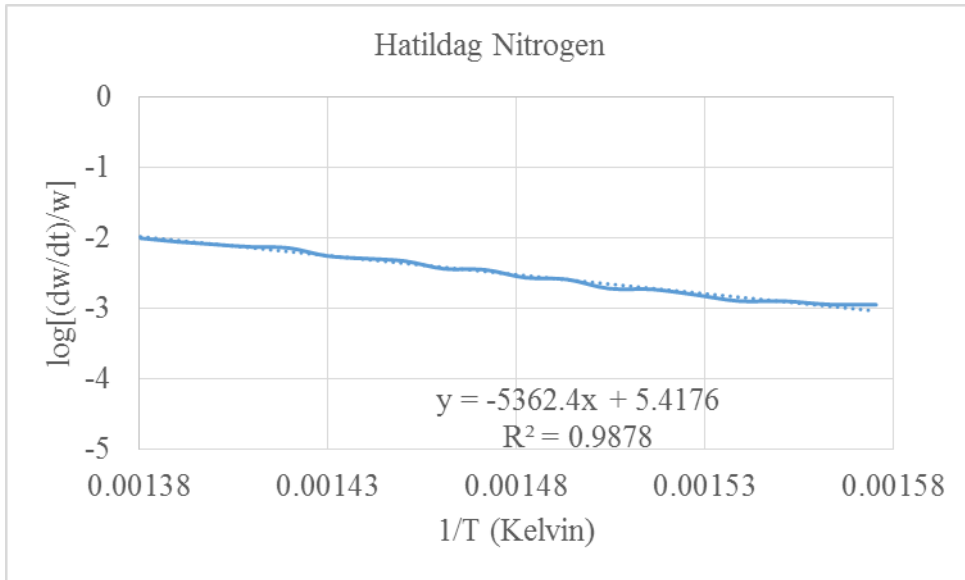


Figure A-38 Arrhenius plot of Hatildag for pyrolysis at 10 °C/min

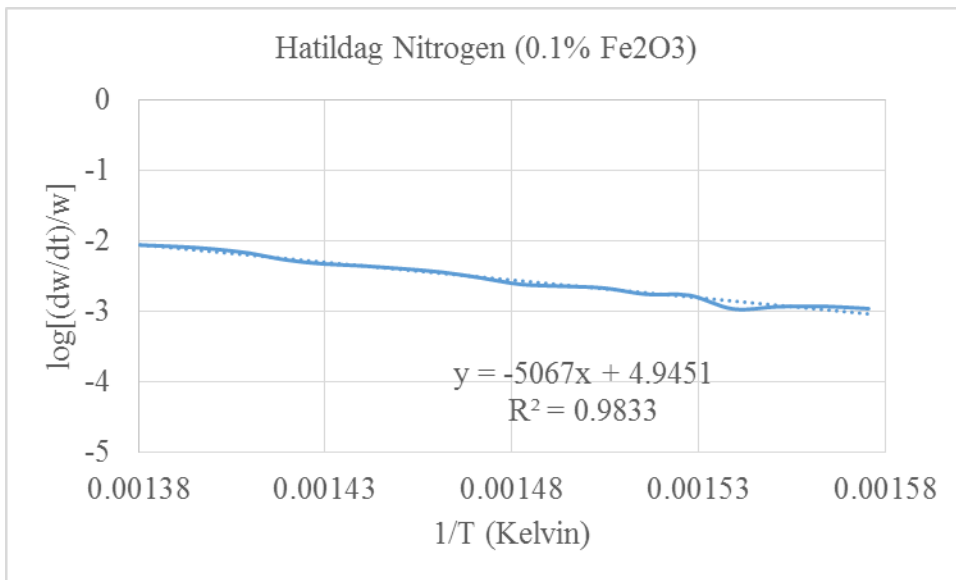


Figure A-39 Arrhenius plot of Hatildag (with iron powder) for pyrolysis at 10 °C/min

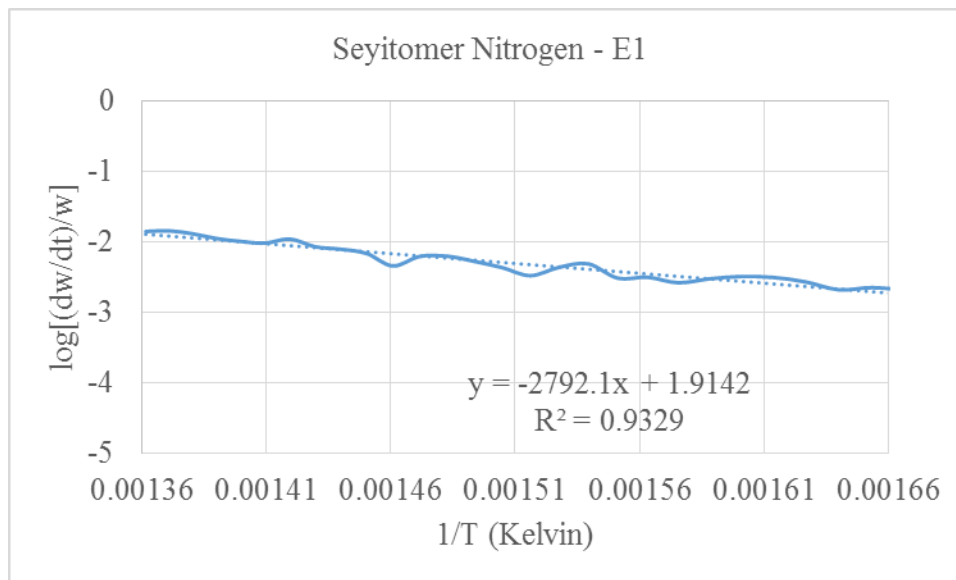


Figure A-40 Arrhenius plot of Seyitomer for pyrolysis (I. region) at 10 °C/min

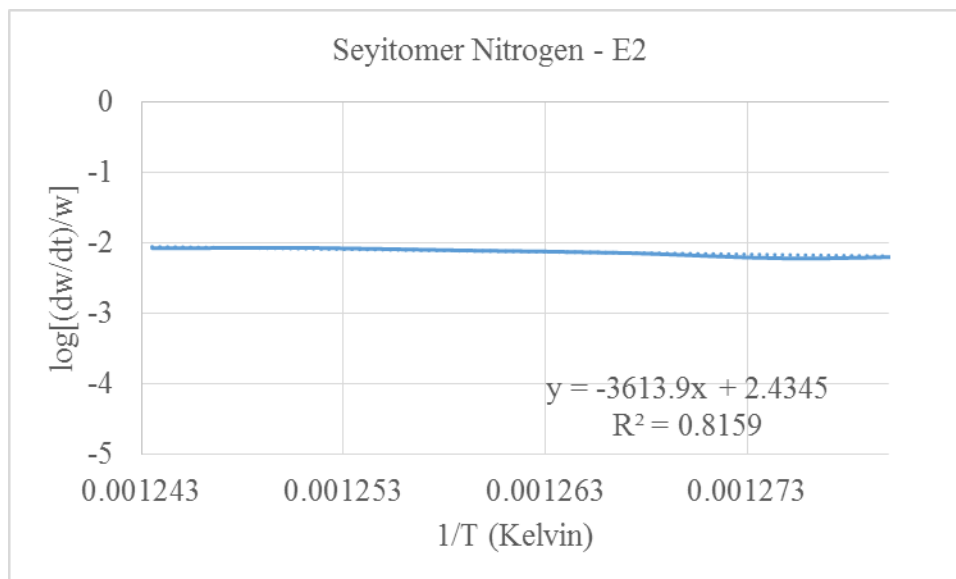


Figure A-41 Arrhenius plot of Seyitomer for pyrolysis (II. region) at 10 °C/min

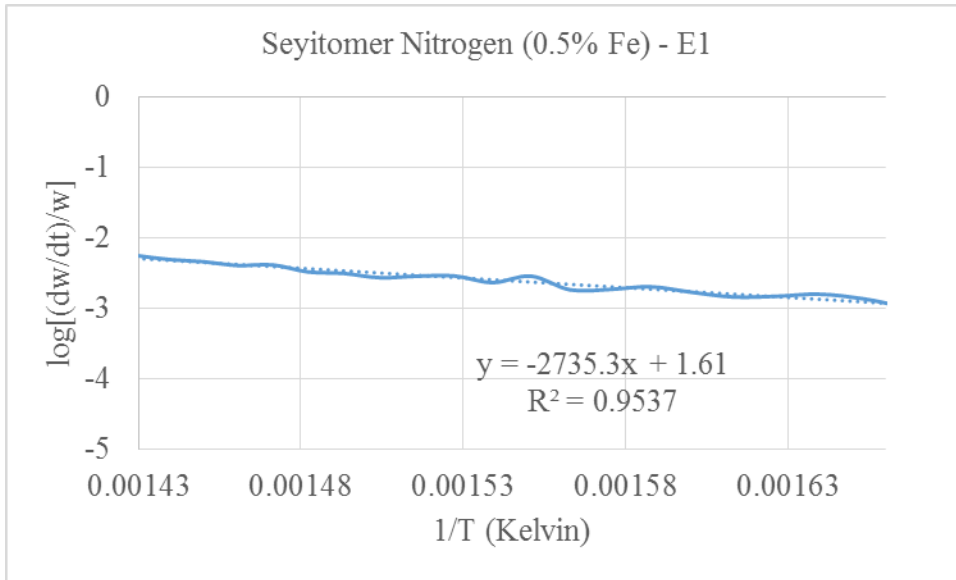


Figure A-42 Arrhenius plot of Seyitomer (with iron powder) for pyrolysis (I. region) at 10 °C/min

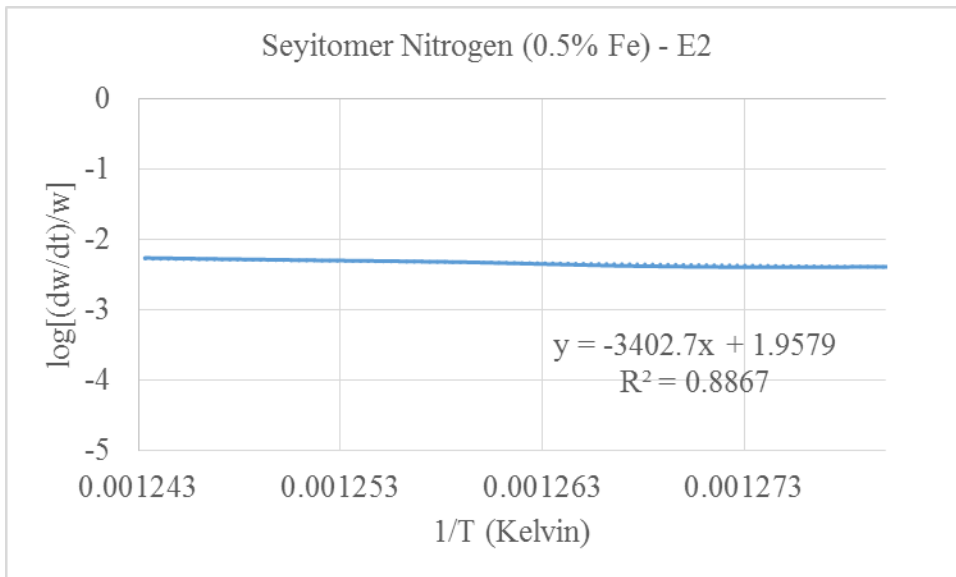


Figure A-43 Arrhenius plot of Seyitomer (with iron powder) for pyrolysis (II. region) at 10 °C/min

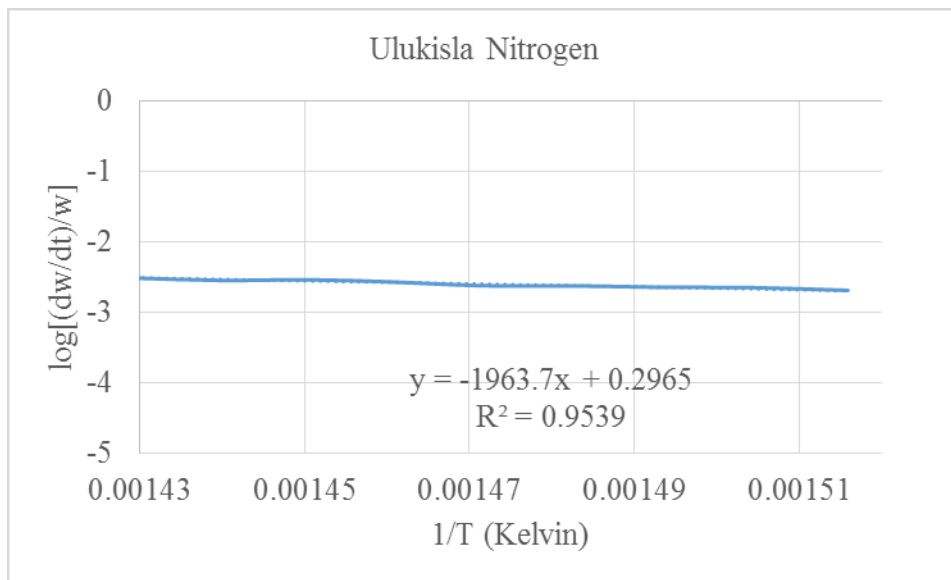


Figure A-44 Arrhenius plot of Ulukisla for pyrolysis at 10 °C/min

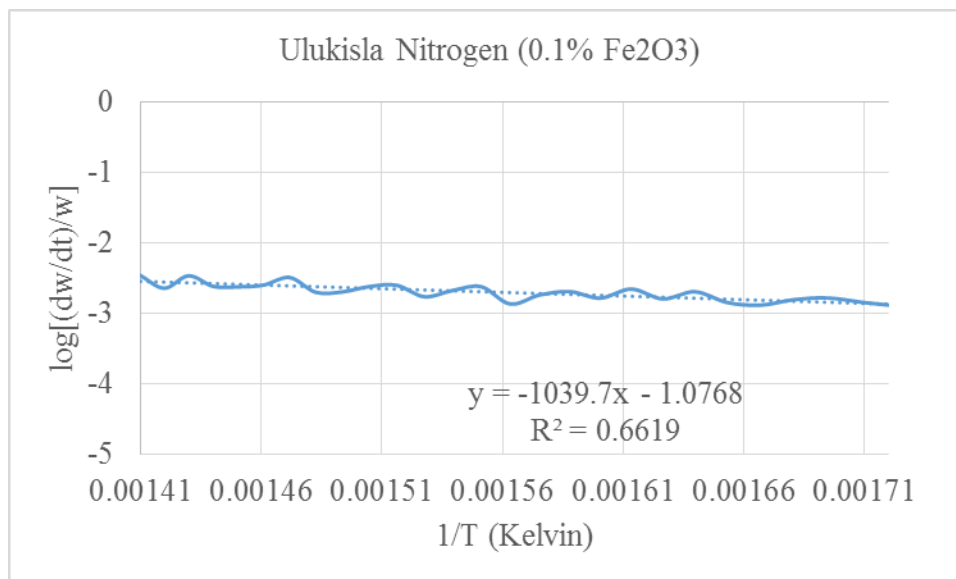


Figure A-45 Arrhenius plot of Ulukisla (with iron powder) for pyrolysis at 10 °C/min

APPENDIX B

FOURIER TRANSFORM INFRARED SPECTROSCOPY

B.1 Retort Postmortems

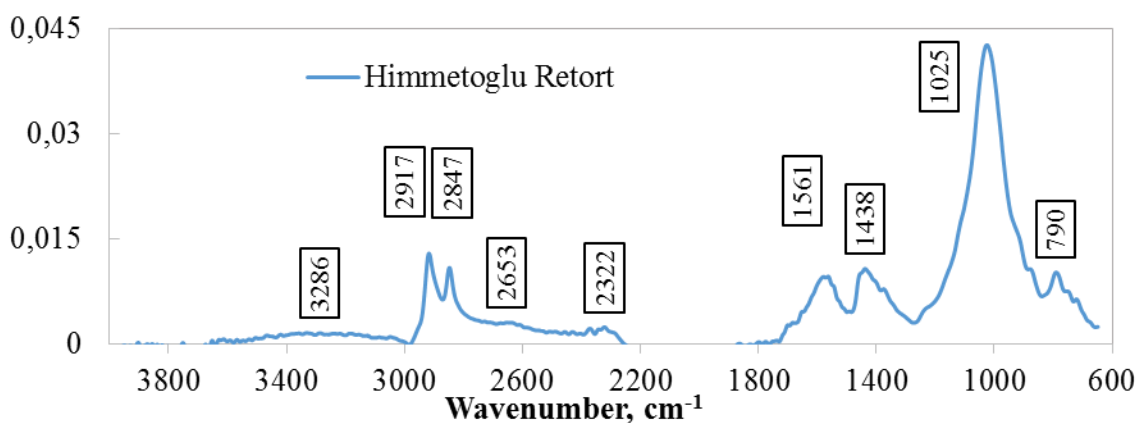


Figure B-1 FTIR spectra of Himmetoglu retort postmortem

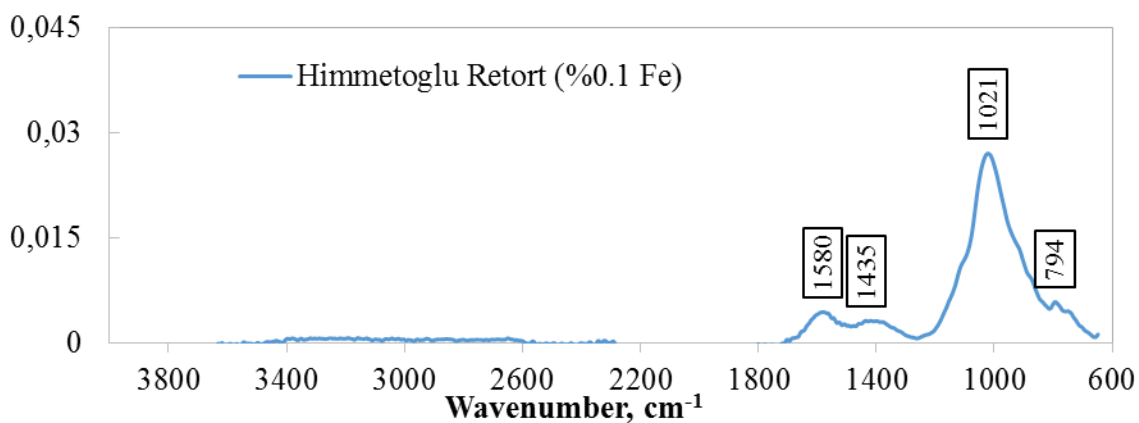


Figure B-2 FTIR spectra of Himmetoglu retort postmortem (with iron powder)

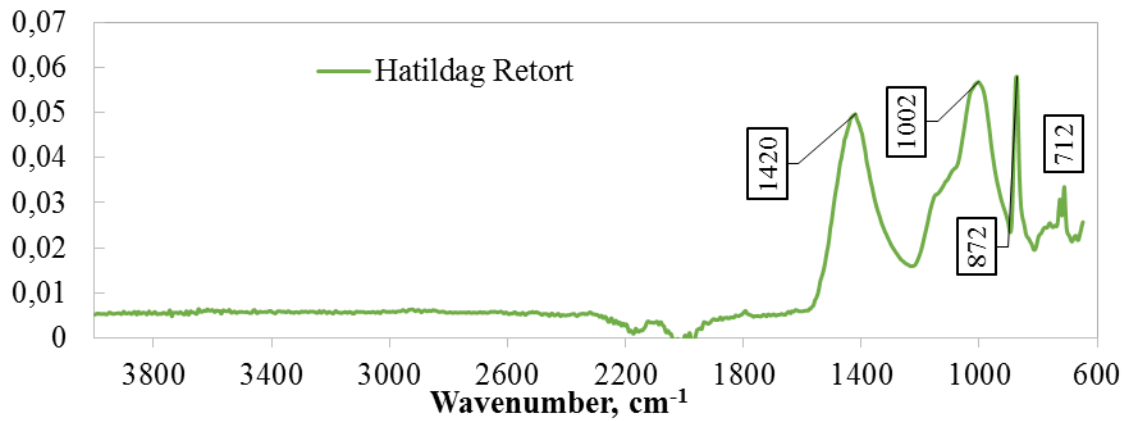


Figure B-3 FTIR spectra of Hatildag retort postmortem

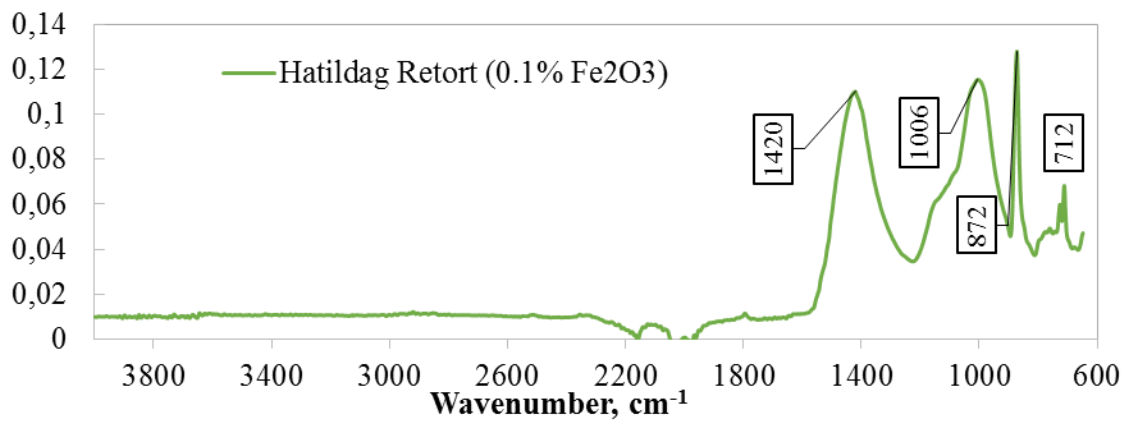


Figure B-4 FTIR spectra of Hatildag retort postmortem (with iron powder)

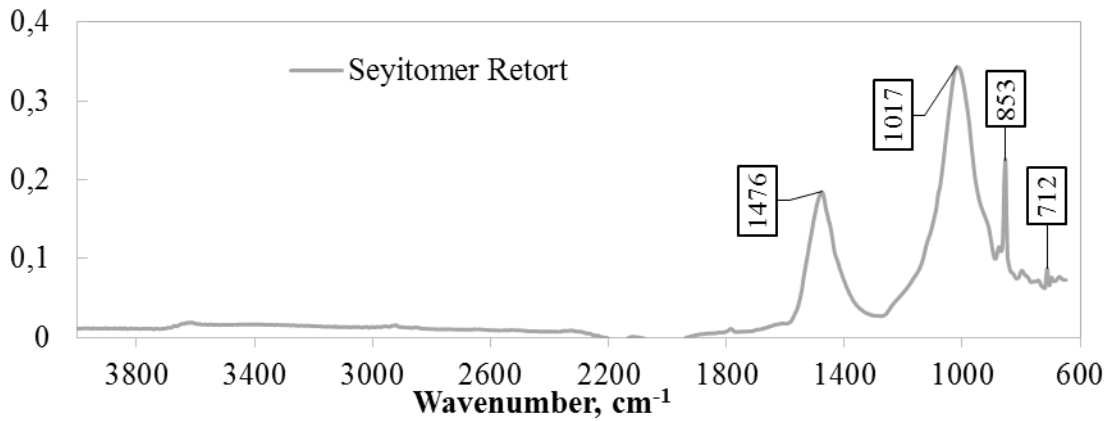


Figure B-5 FTIR spectra of Seyitomer retort postmortem

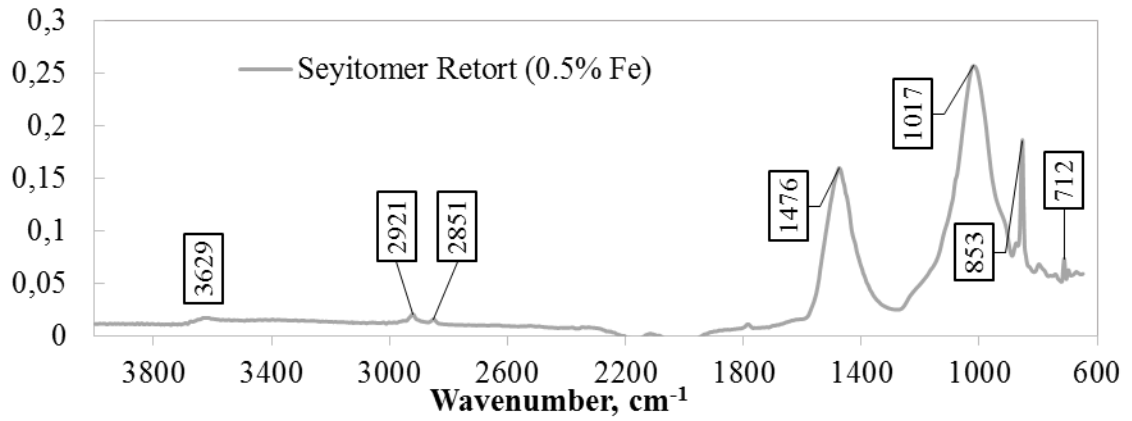


Figure B-6 FTIR spectra of Seyitomer retort postmortem (with iron powder)

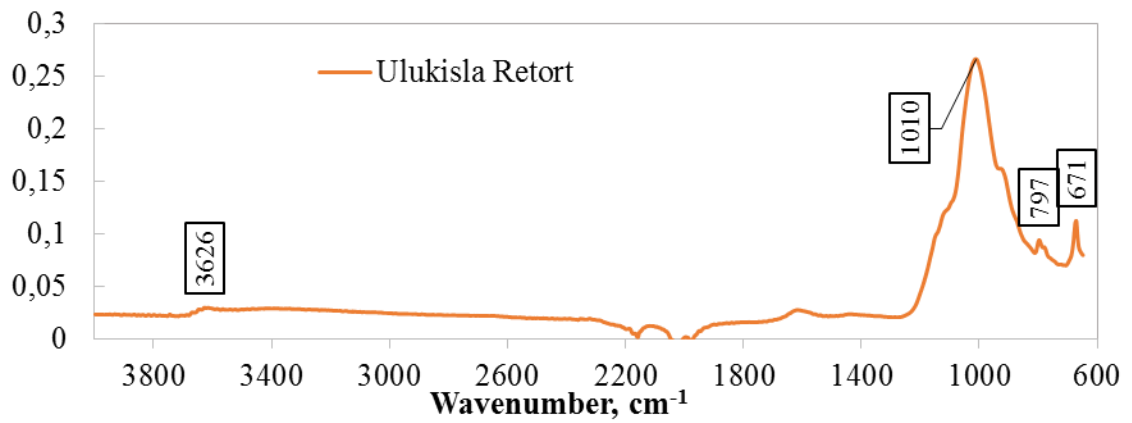


Figure B-7 FTIR spectra of Ulukisla retort postmortem

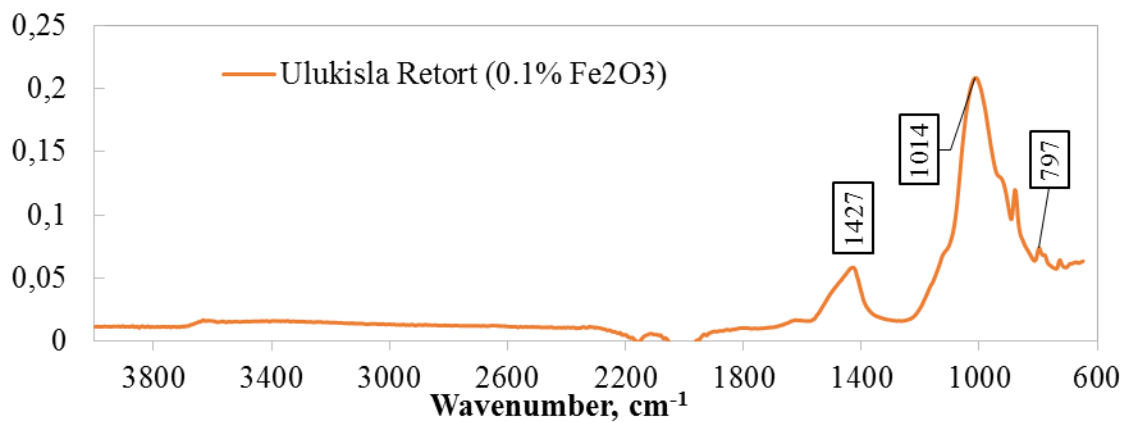


Figure B-8 FTIR spectra of Ulukisla retort postmortem (with iron powder)

B.2 Microwave Postmortems

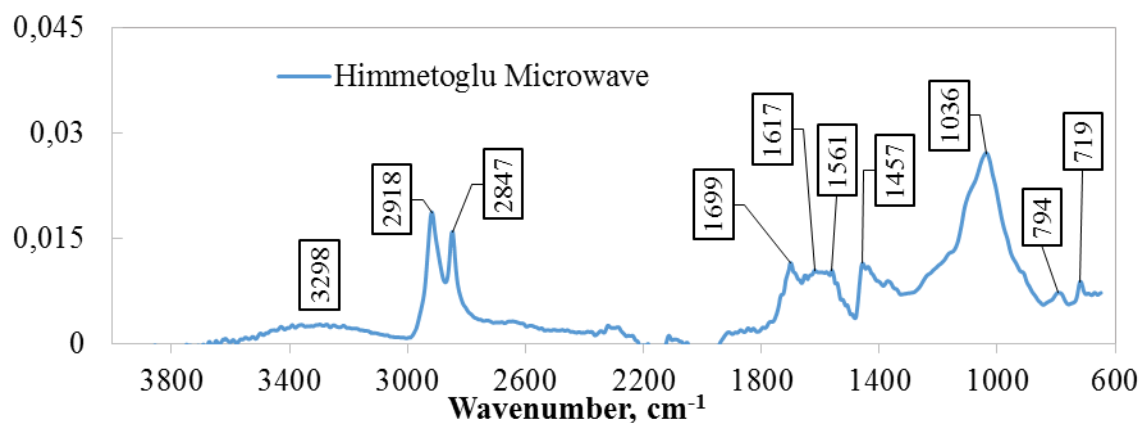


Figure B-9 FTIR spectra of Himmetoglu microwave postmortem

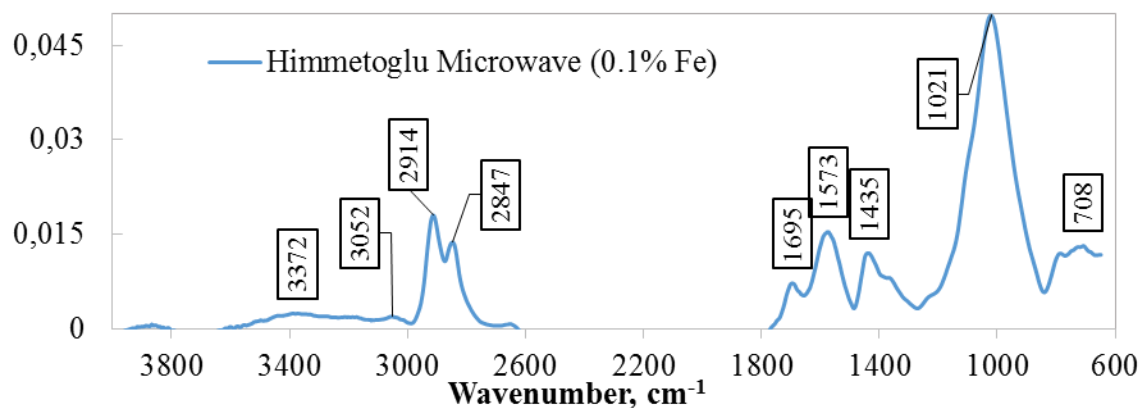


Figure B-10 FTIR spectra of Himmetoglu microwave postmortem (with iron powder)

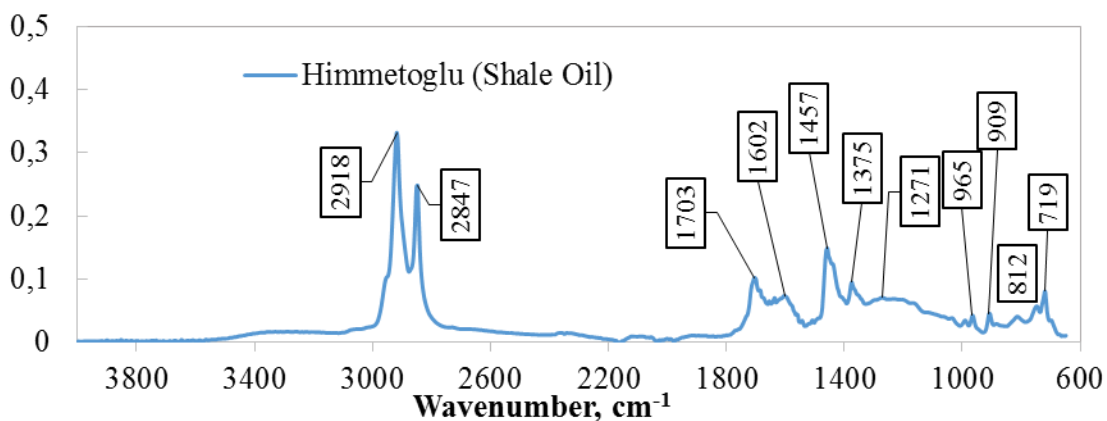


Figure B-11 FTIR spectra of Himmetoglu Shale Oil

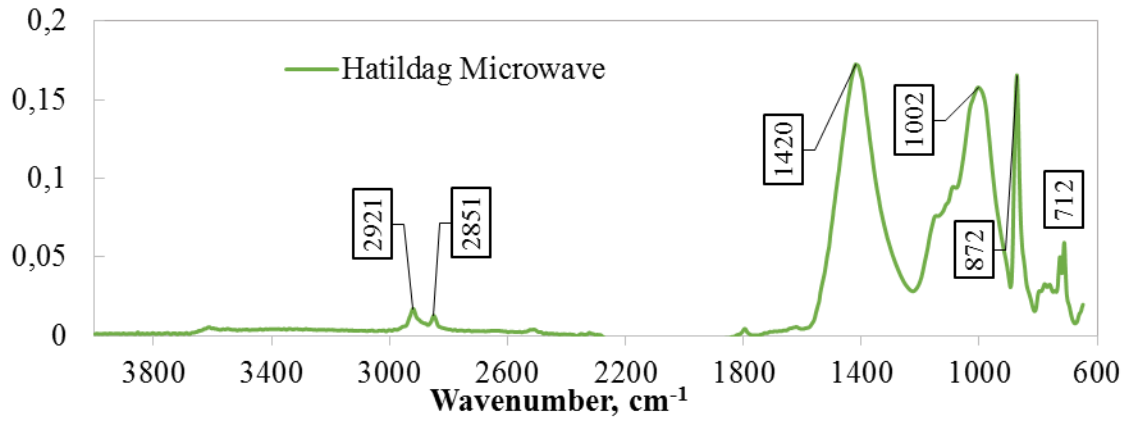


Figure B-12 FTIR spectra of Hatildag microwave postmortem

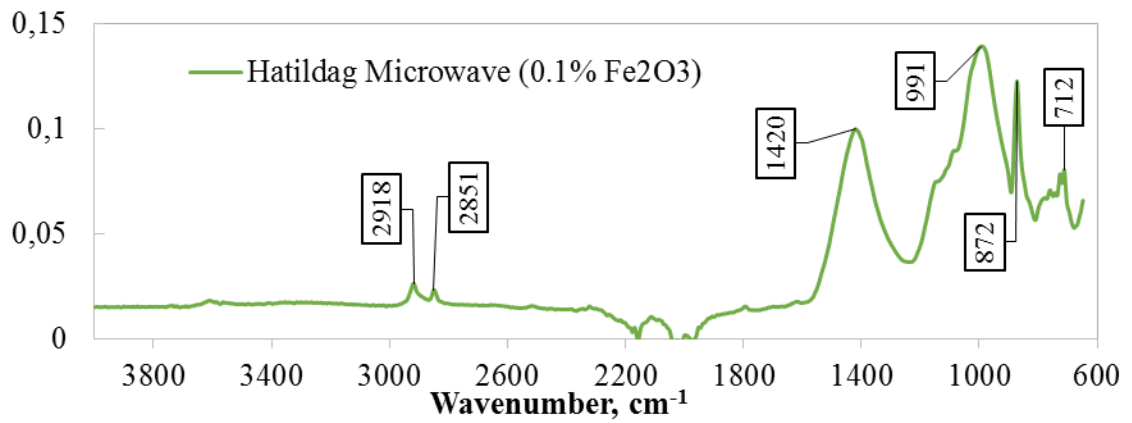


Figure B-13 FTIR spectra of Hatildag microwave postmortem (with iron powder)

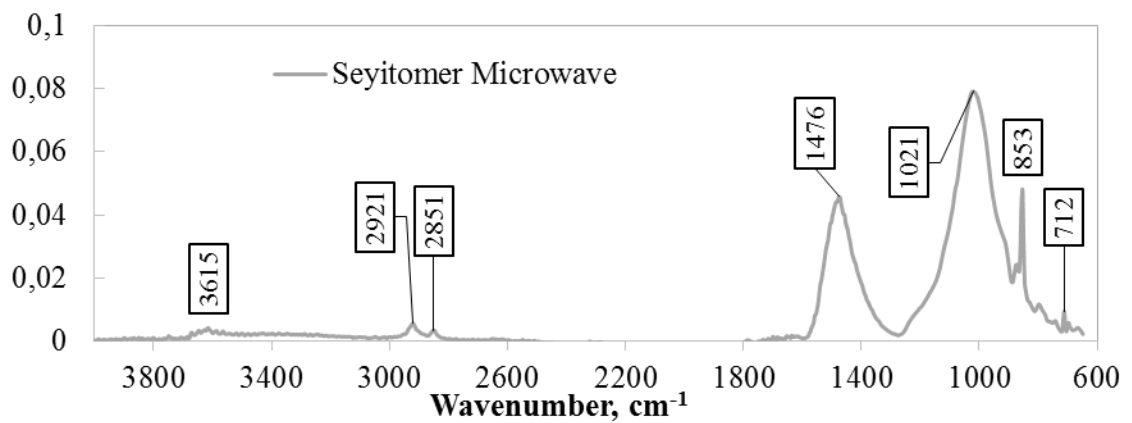


Figure B-14 FTIR spectra of Seyitomer microwave postmortem

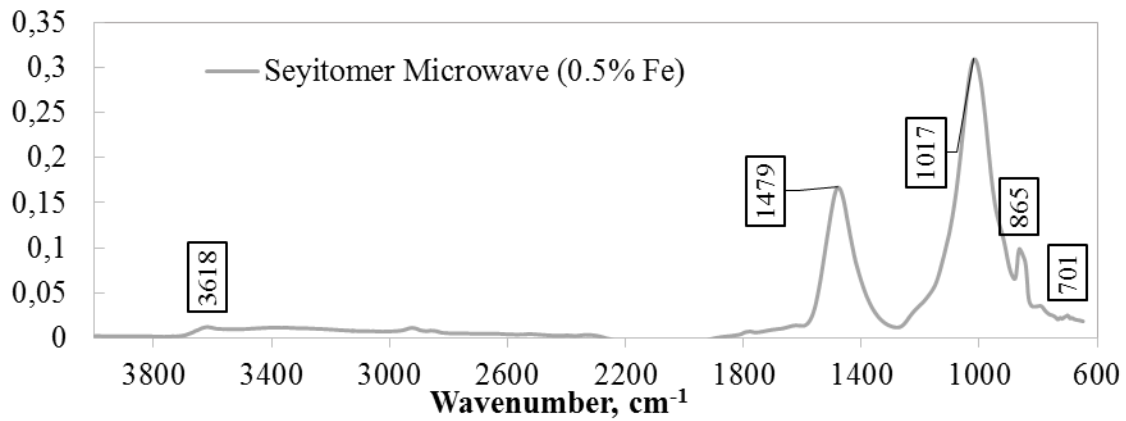


Figure B-15 FTIR spectra of Seyitomer microwave postmortem (with iron powder)

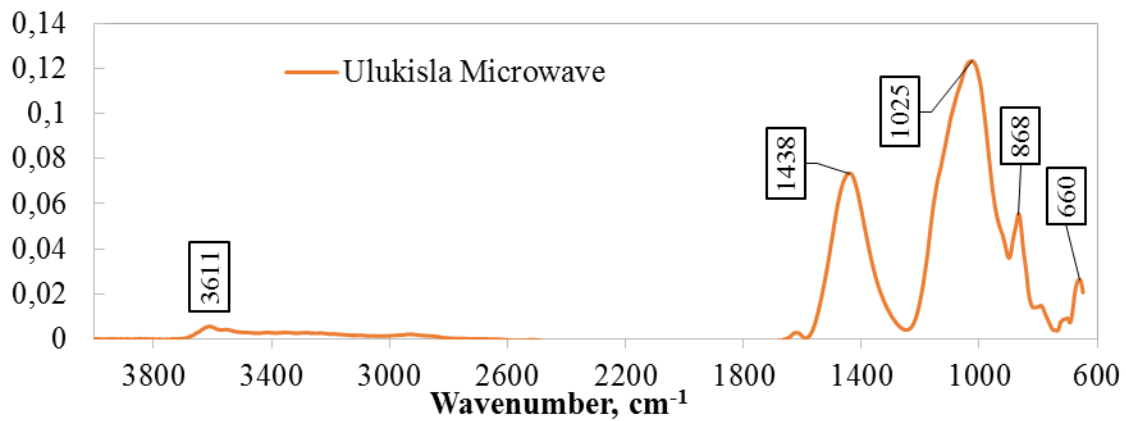


Figure B-16 FTIR spectra of Ulukisla microwave postmortem

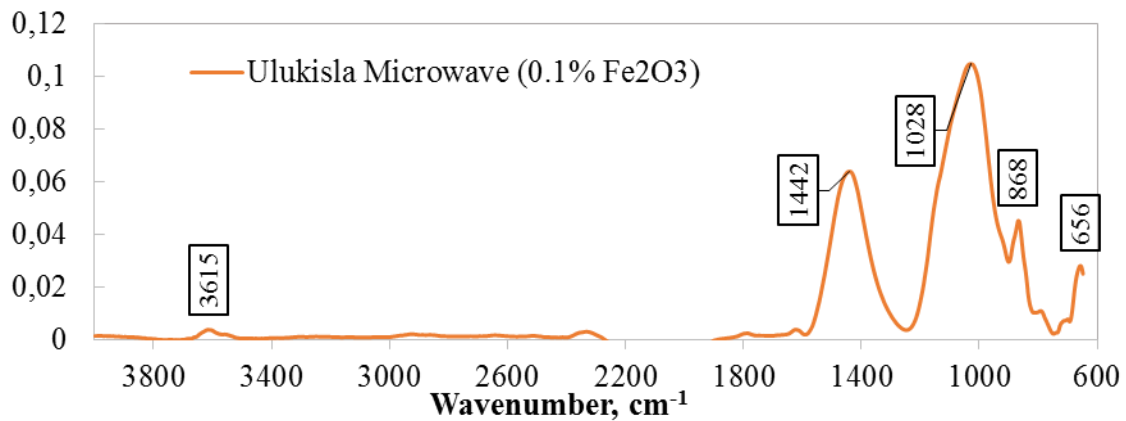


Figure B-17 FTIR spectra of Ulukisla microwave postmortem (with iron powder)

B.3 Combustion Postmortems

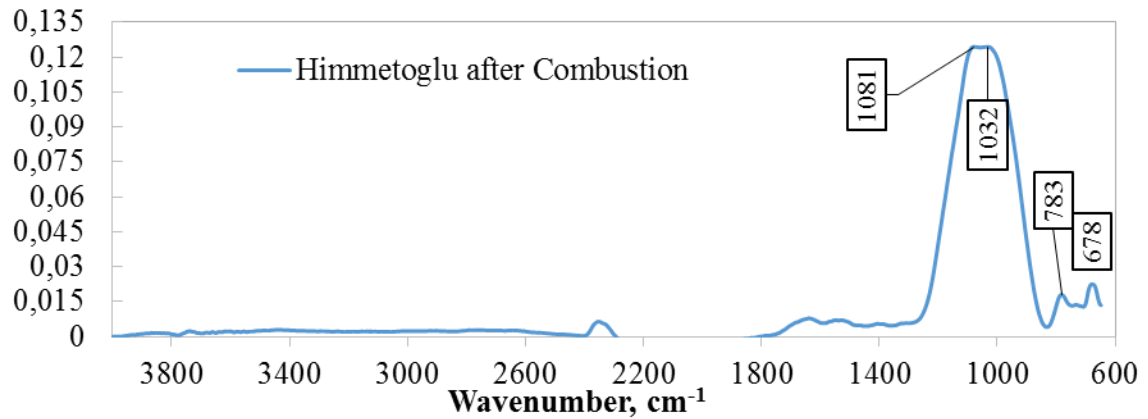


Figure B-18 FTIR spectra of Himmetoglu combustion postmortem

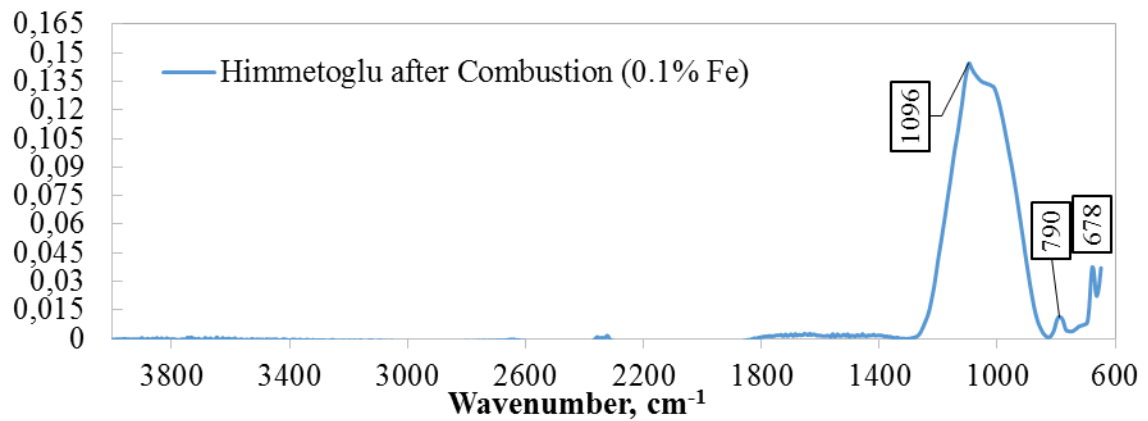


Figure B-19 FTIR spectra of Himmetoglu combustion postmortem (with iron powder)

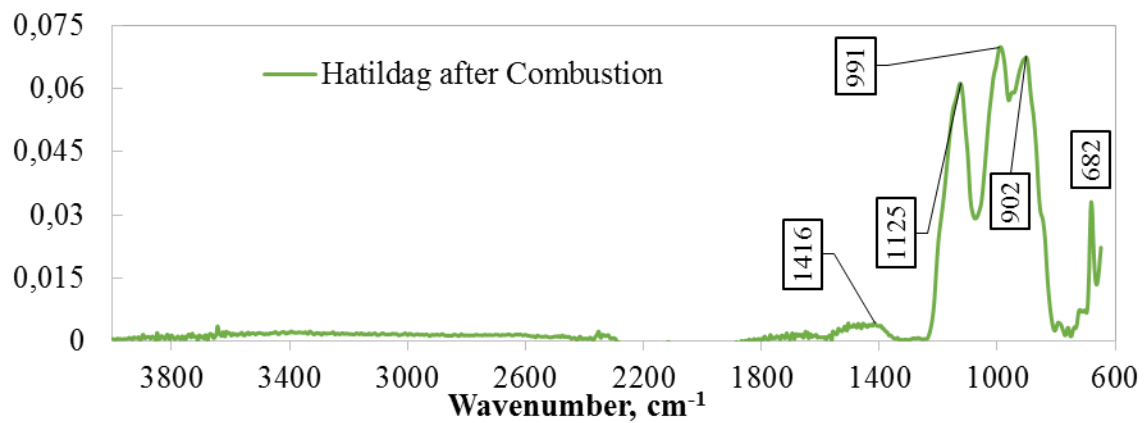


Figure B-20 FTIR spectra of Hatildag combustion postmortem

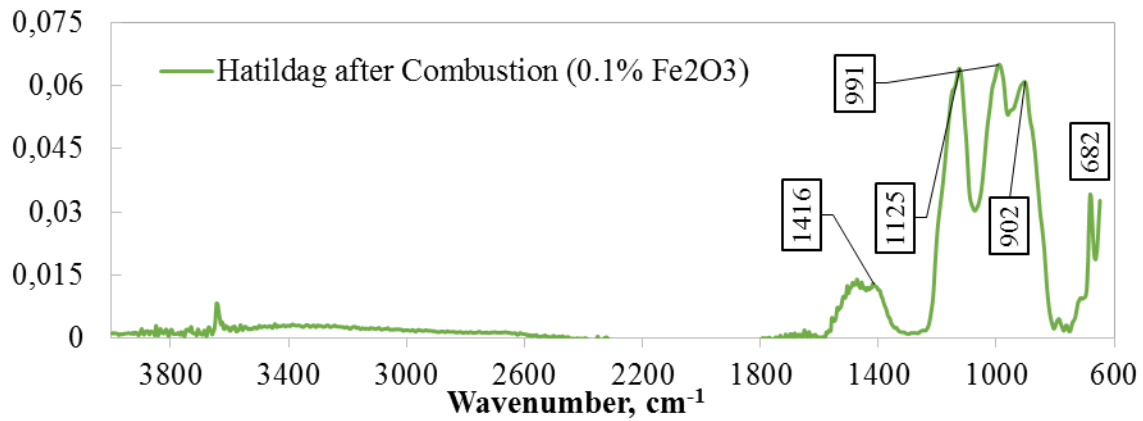


Figure B-21 FTIR spectra of Hatildag combustion postmortem (with iron powder)

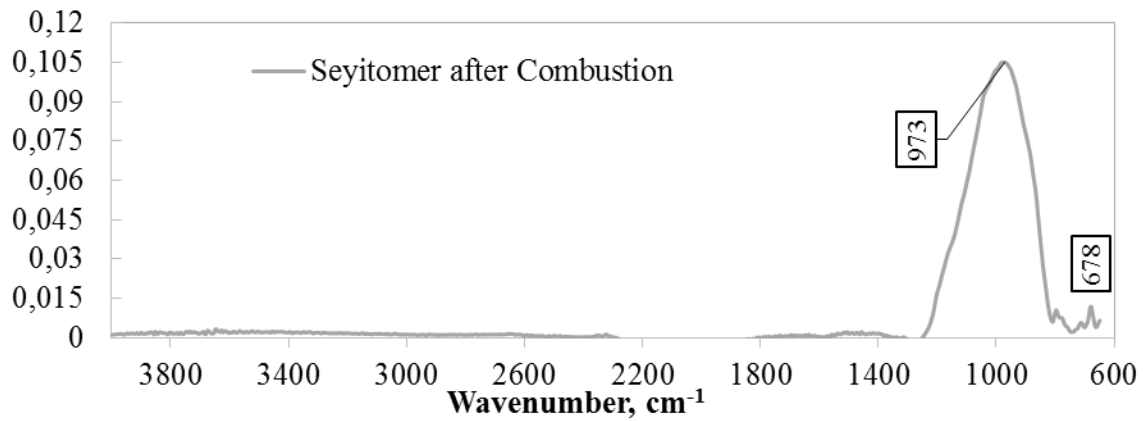


Figure B-22 FTIR spectra of Seyitomer combustion postmortem

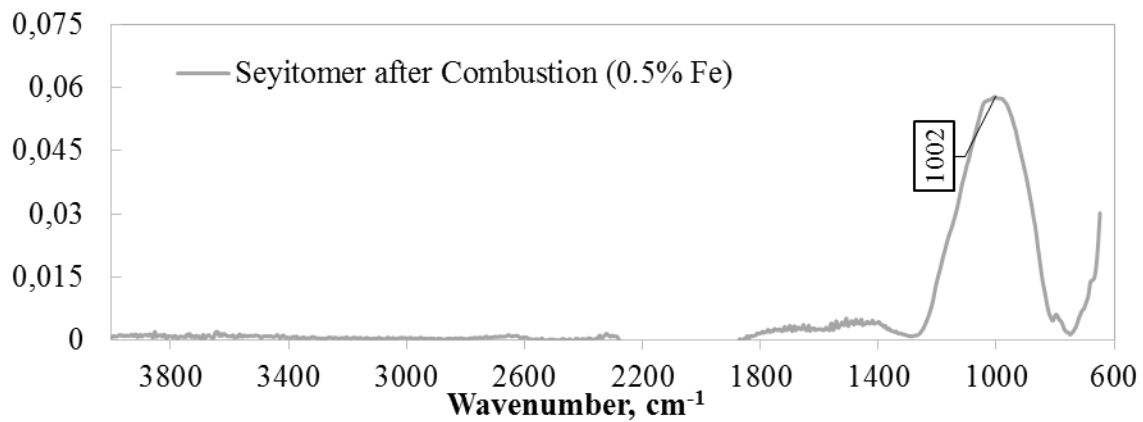


Figure B-23 FTIR spectra of Seyitomer combustion postmortem (with iron powder)

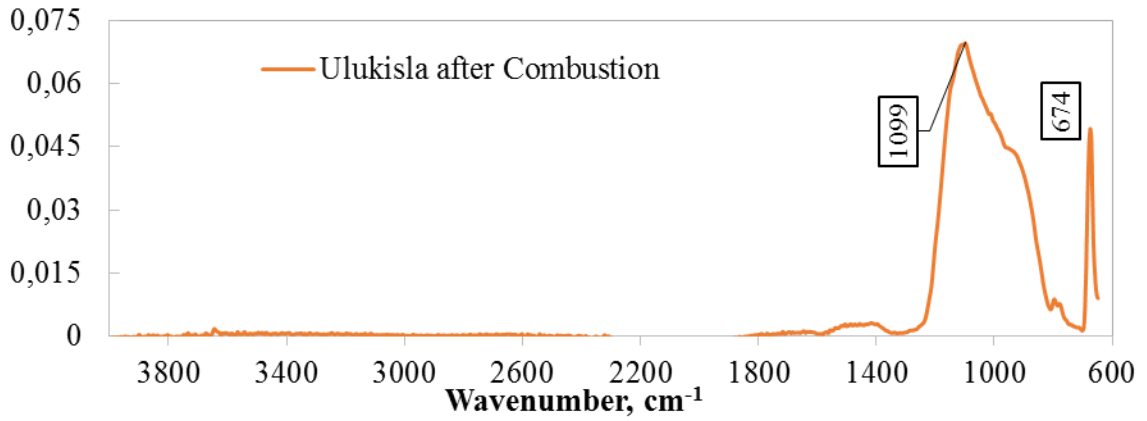


Figure B-24 FTIR spectra of Ulukisla combustion postmortem

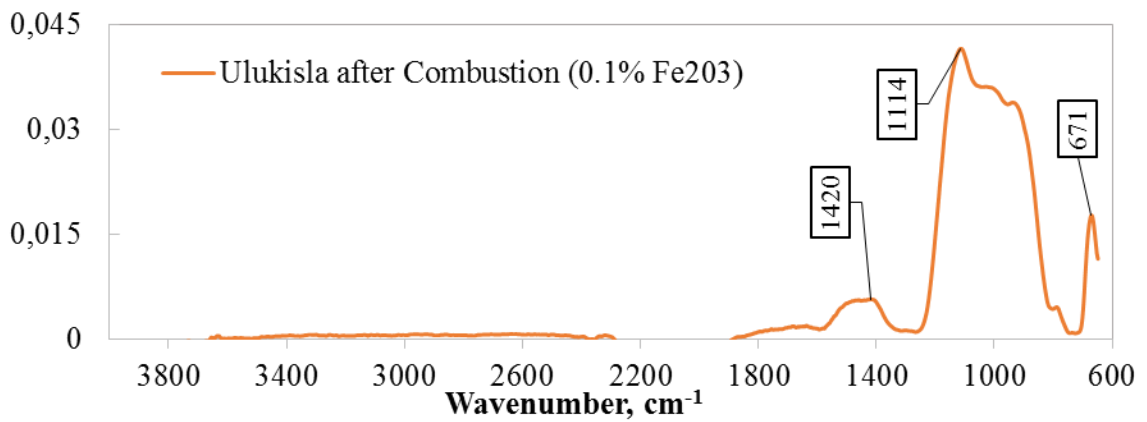


Figure B-25 FTIR spectra of Ulukisla combustion postmortem (with iron powder)

B.4 Pyrolysis Postmortems

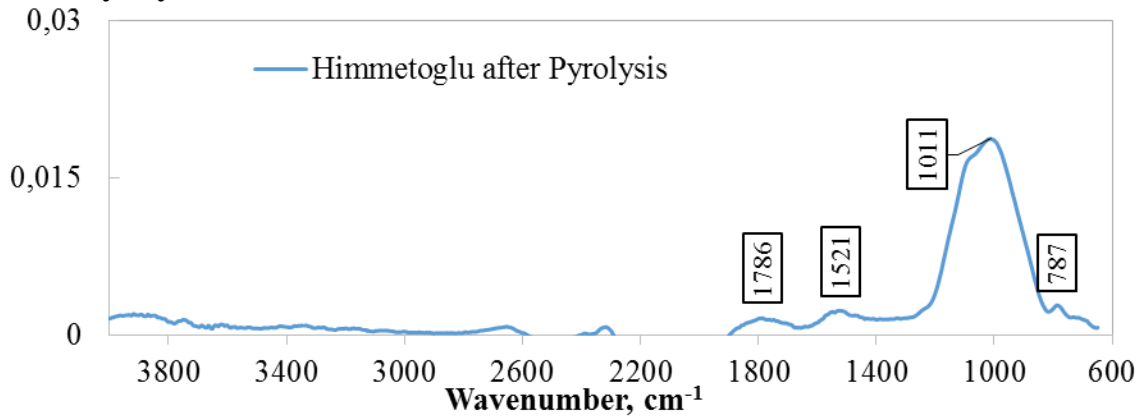


Figure B-26 FTIR spectra of Himmetoglu pyrolysis postmortem

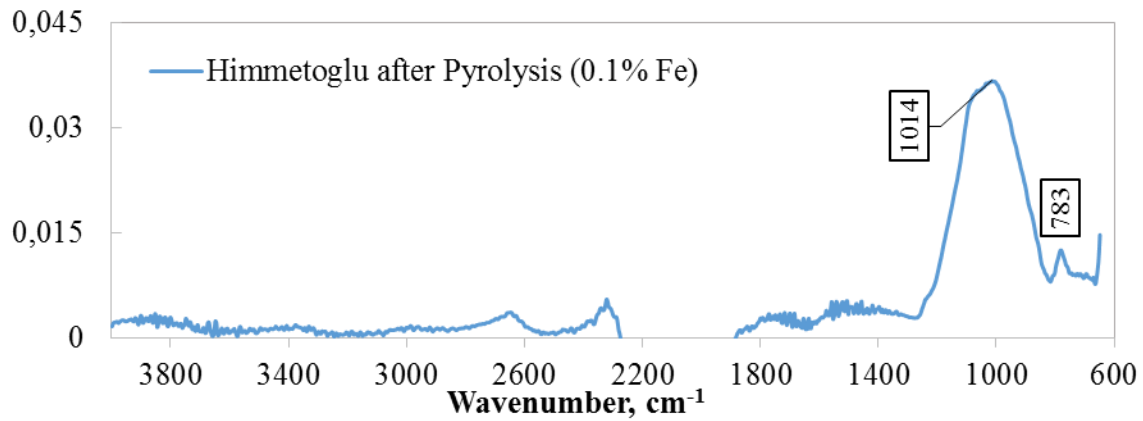


Figure B-27 FTIR spectra of Himmetoglu pyrolysis postmortem (with iron powder)

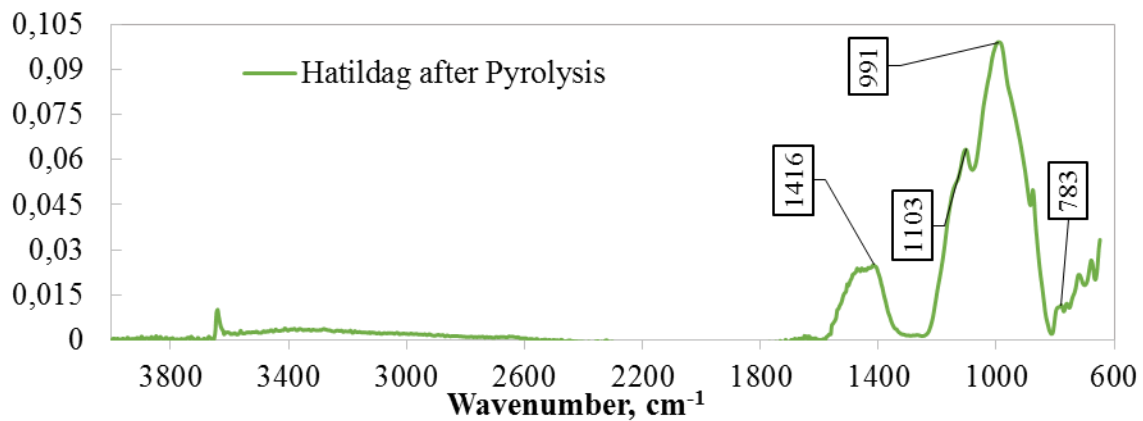


Figure B-28 FTIR spectra of Hatildag pyrolysis postmortem

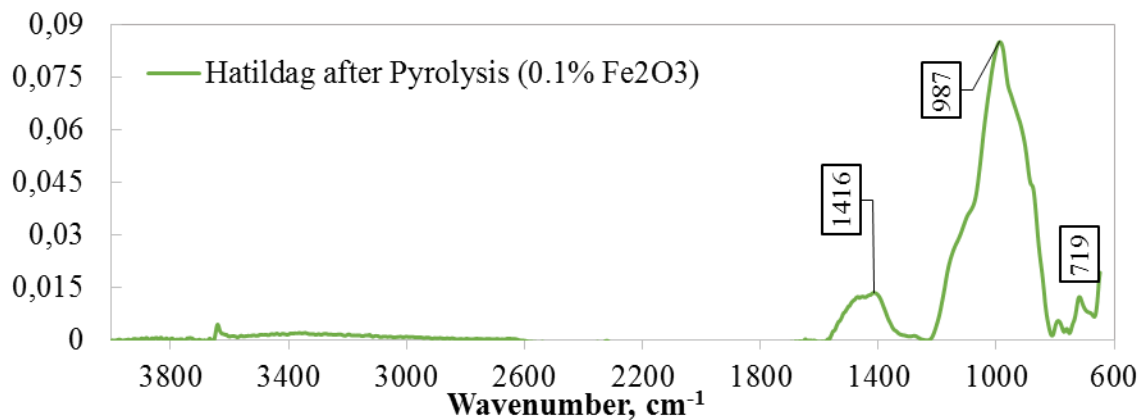


Figure B-29 FTIR spectra of Hatildag pyrolysis postmortem (with iron powder)

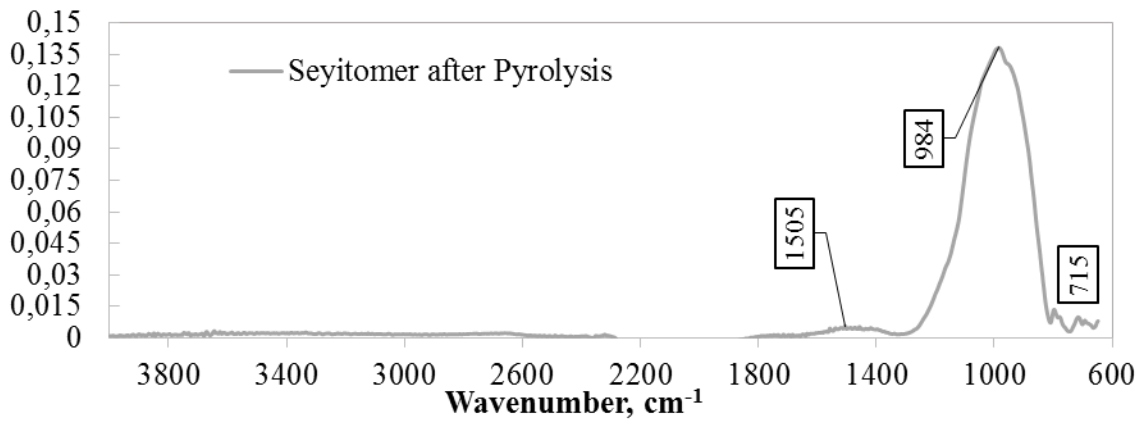


Figure B-30 FTIR spectra of Seyitomer pyrolysis postmortem

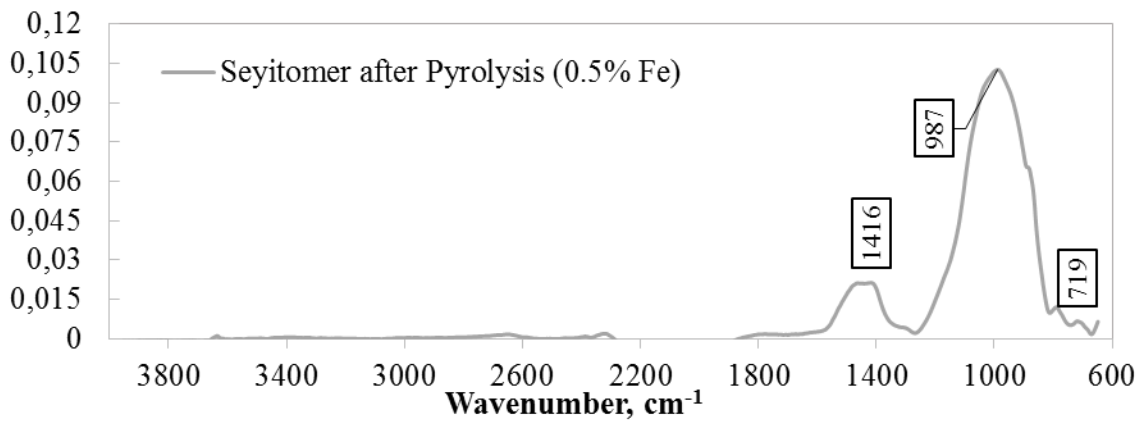


Figure B-31 FTIR spectra of Seyitomer pyrolysis postmortem (with iron powder)

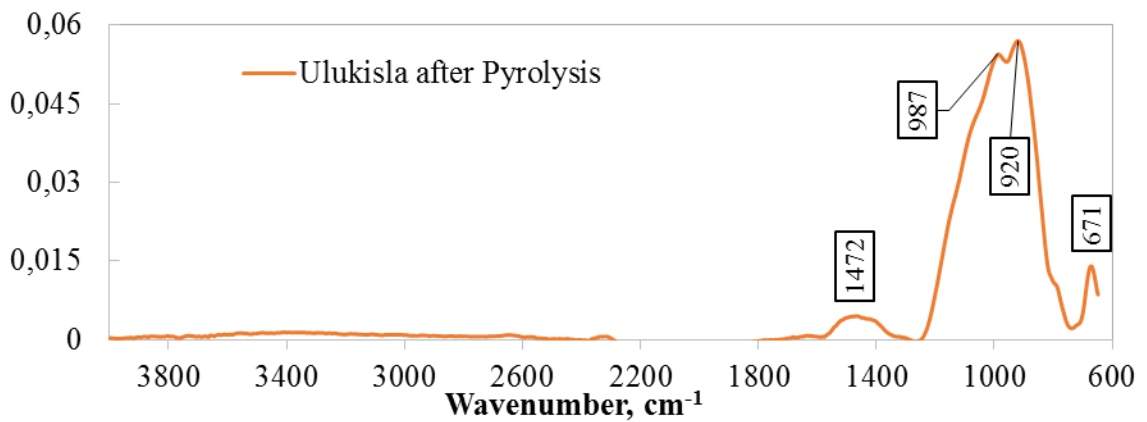


Figure B-32 FTIR spectra of Ulukisla pyrolysis postmortem

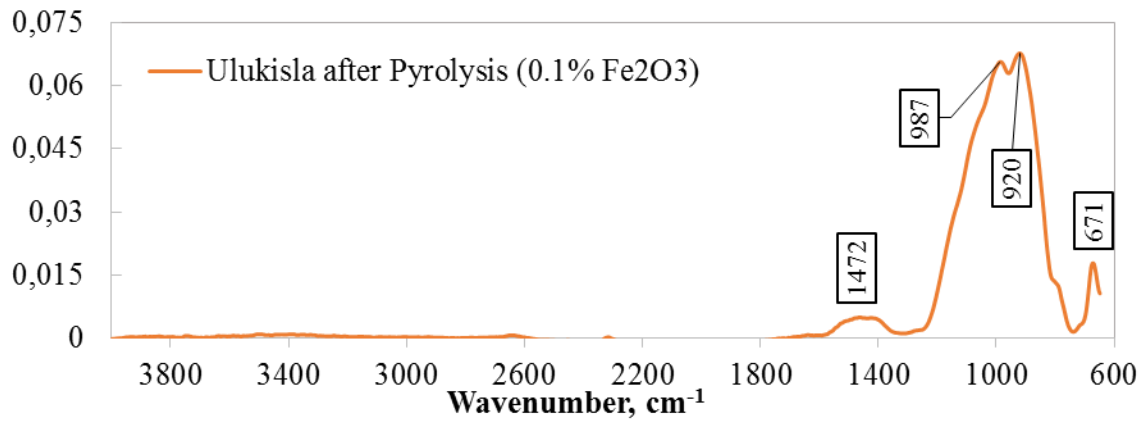


Figure B-33 FTIR spectra of Ulukisla pyrolysis postmortem (with iron powder)

B.5 Retort Simulation Postmortems

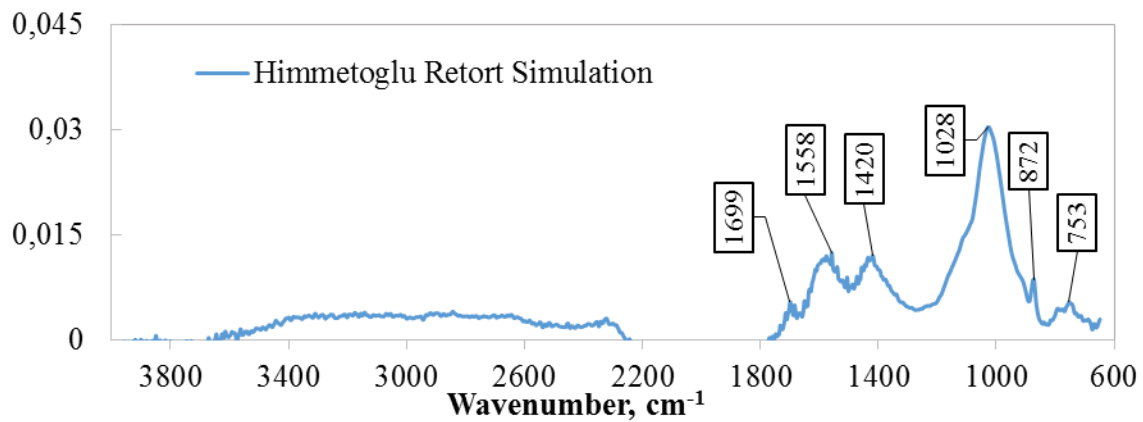


Figure B-34 FTIR spectra of Himmetoglu retort simulation postmortem

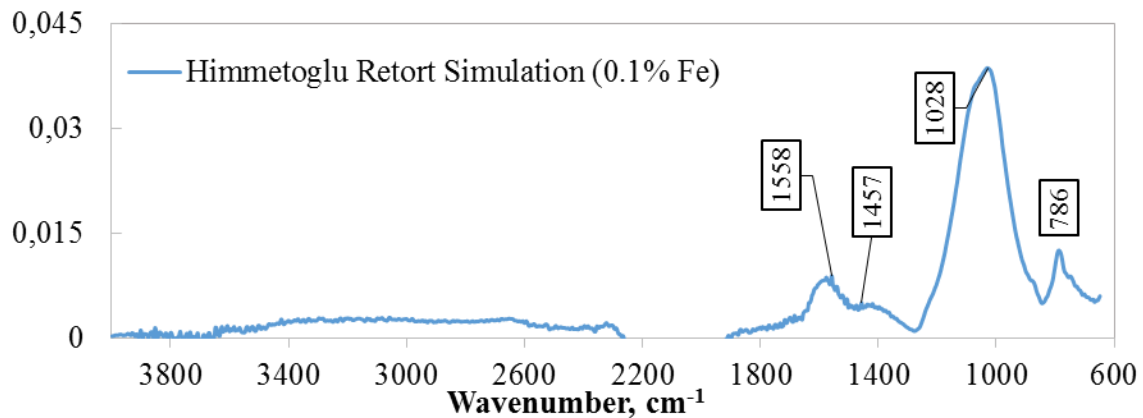


Figure B-35 FTIR spectra of Himmetoglu retort simulation postmortem (with iron powder)

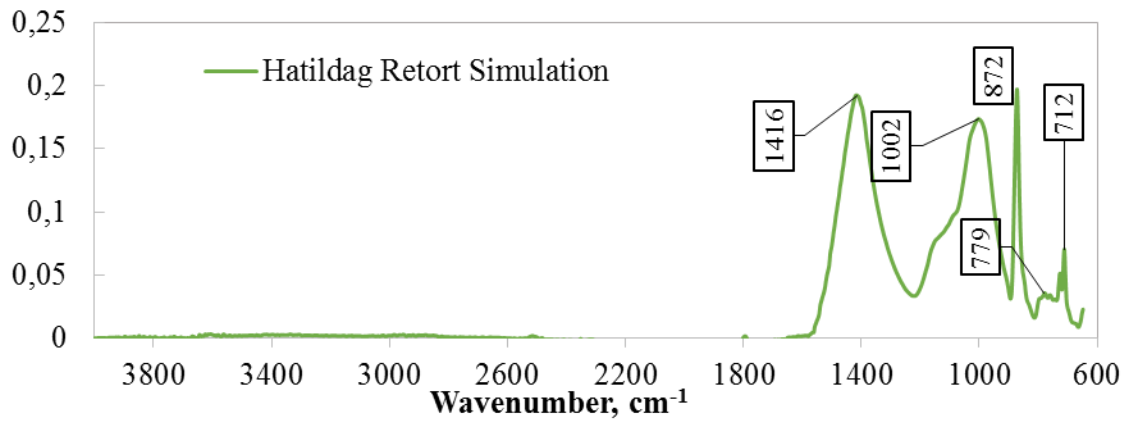


Figure B-36 FTIR spectra of Hatildag retort simulation postmortem

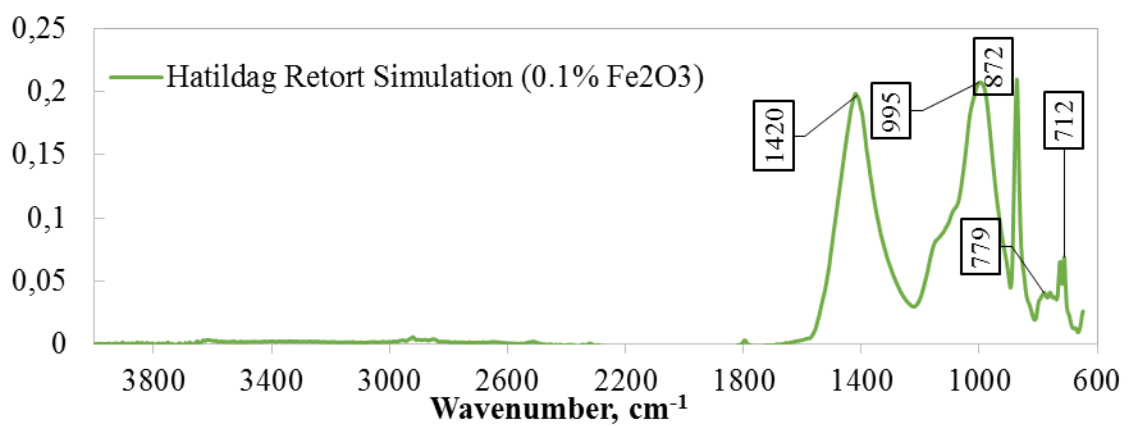


Figure B-37 FTIR spectra of Hatildag retort simulation postmortem (with iron powder)

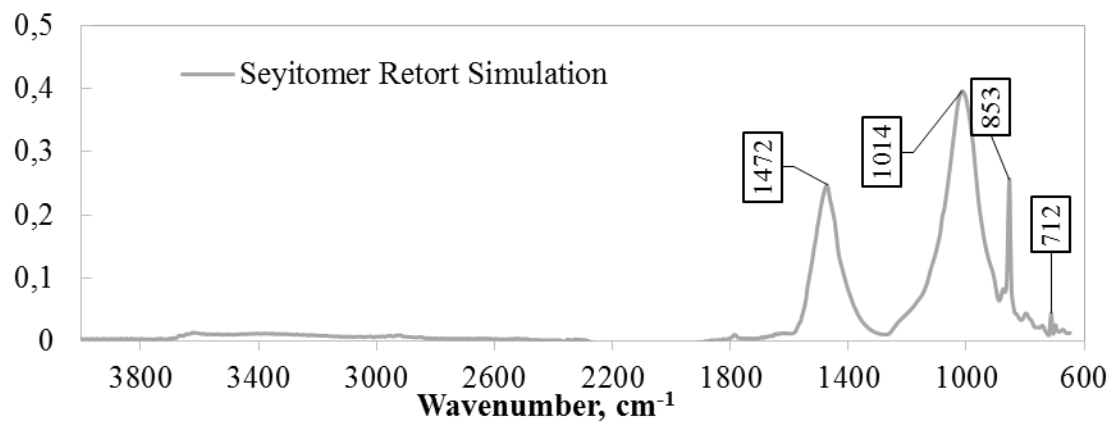


Figure B-38 FTIR spectra of Seyitomer retort simulation postmortem

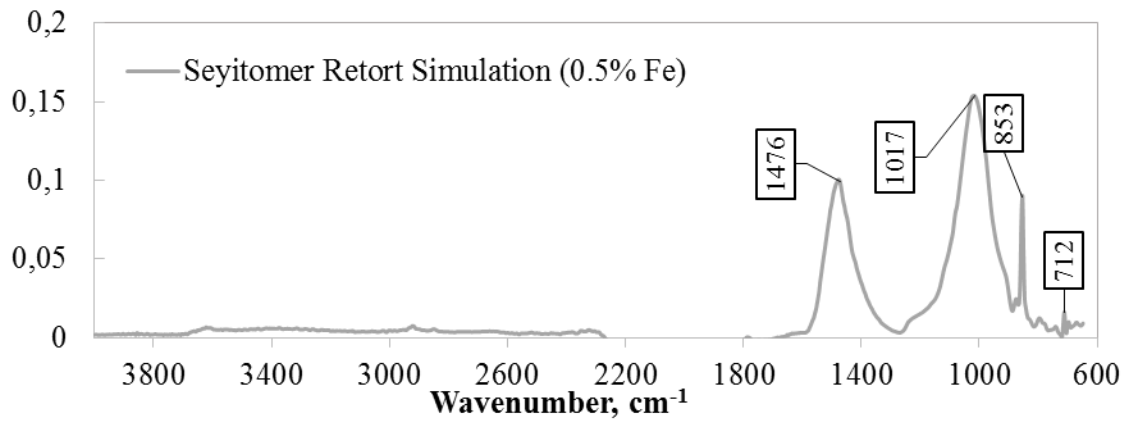


Figure B-39 FTIR spectra of Seyitomer retort simulation postmortem (with iron powder)

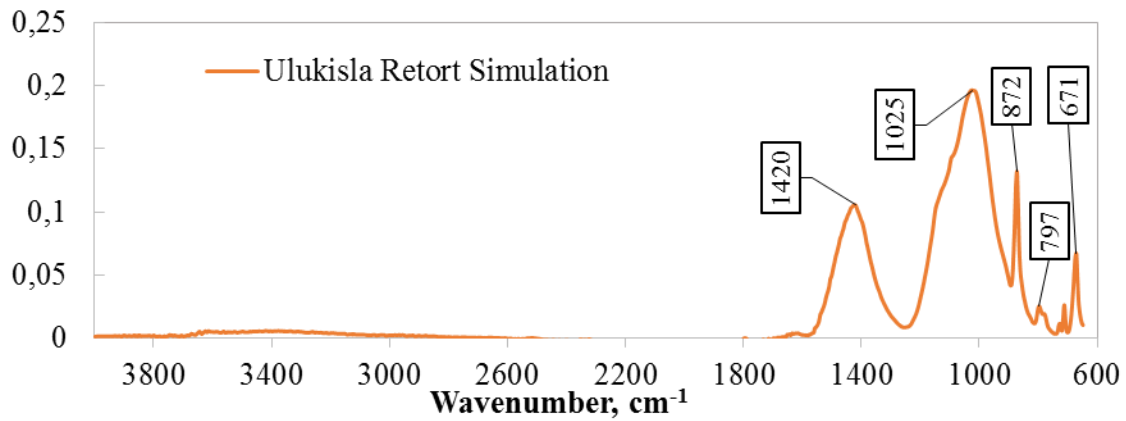


Figure B-40 FTIR spectra of Ulukisla retort simulation postmortem

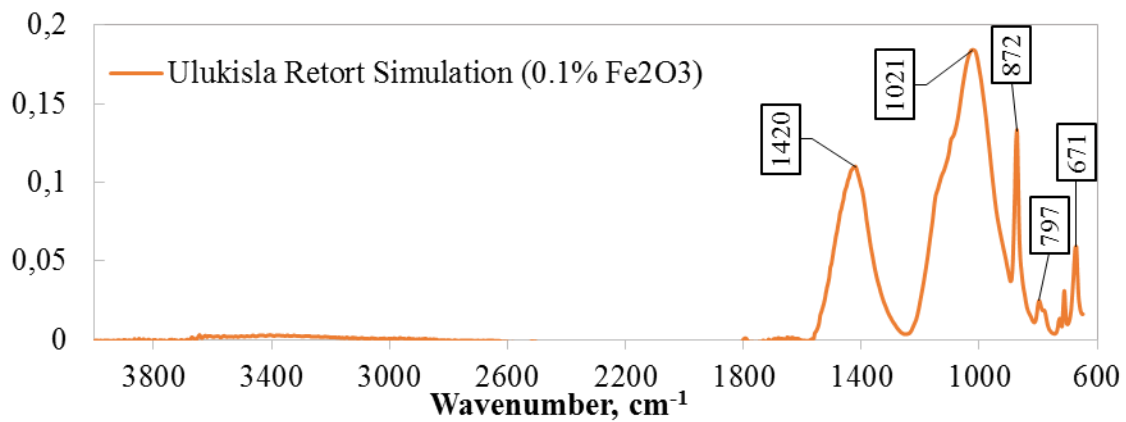


Figure B-41 FTIR spectra of Ulukisla retort simulation postmortem (with iron powder)

APPENDIX C

SCANNING ELECTRON MICROSCOPE/ ENERGY DISPERSIVE X-RAY SPECTROSCOPY

C.1 Original Samples

EDS Results

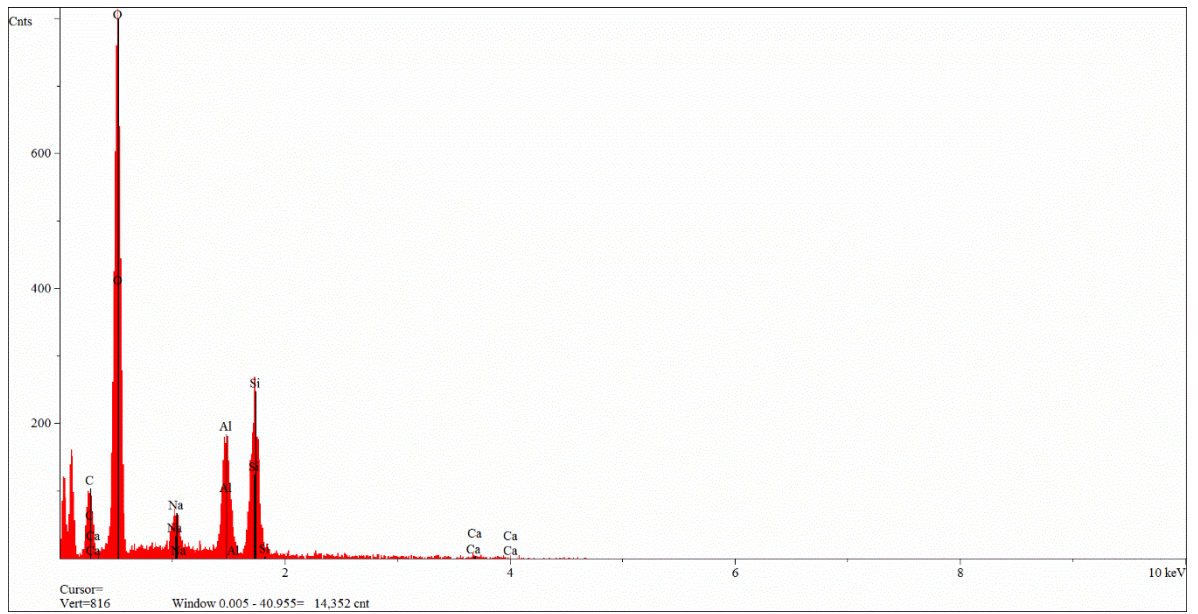


Figure C-1 EDS of albite mineral (from Himmetoglu oil shale)

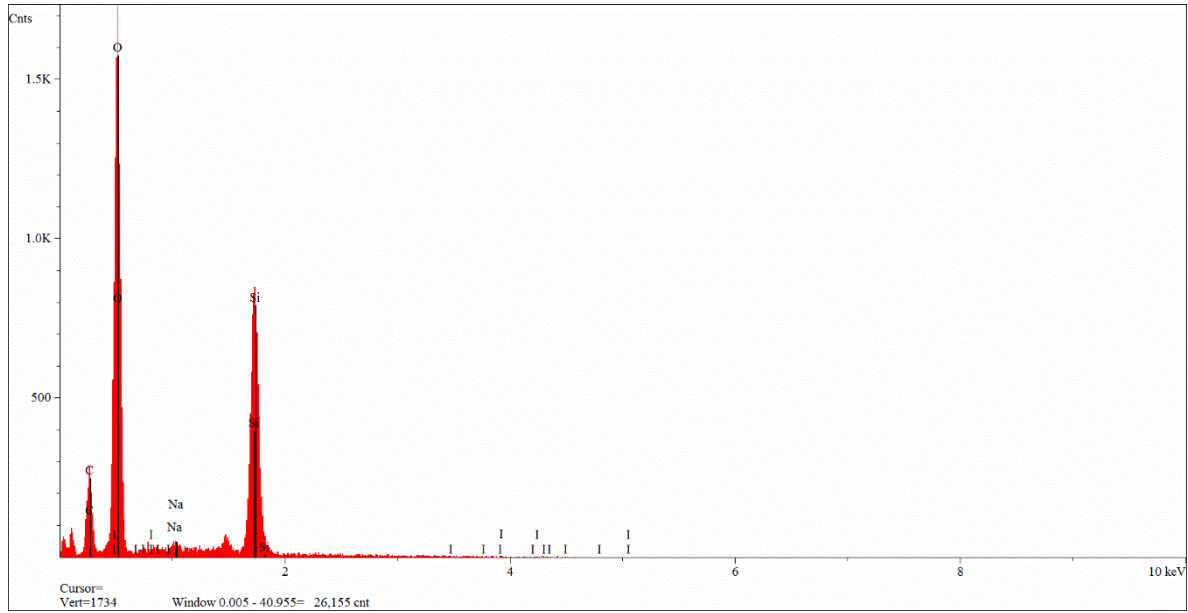


Figure C-2 EDS of (diatom) organic content (from Himmetoglu oil shale)

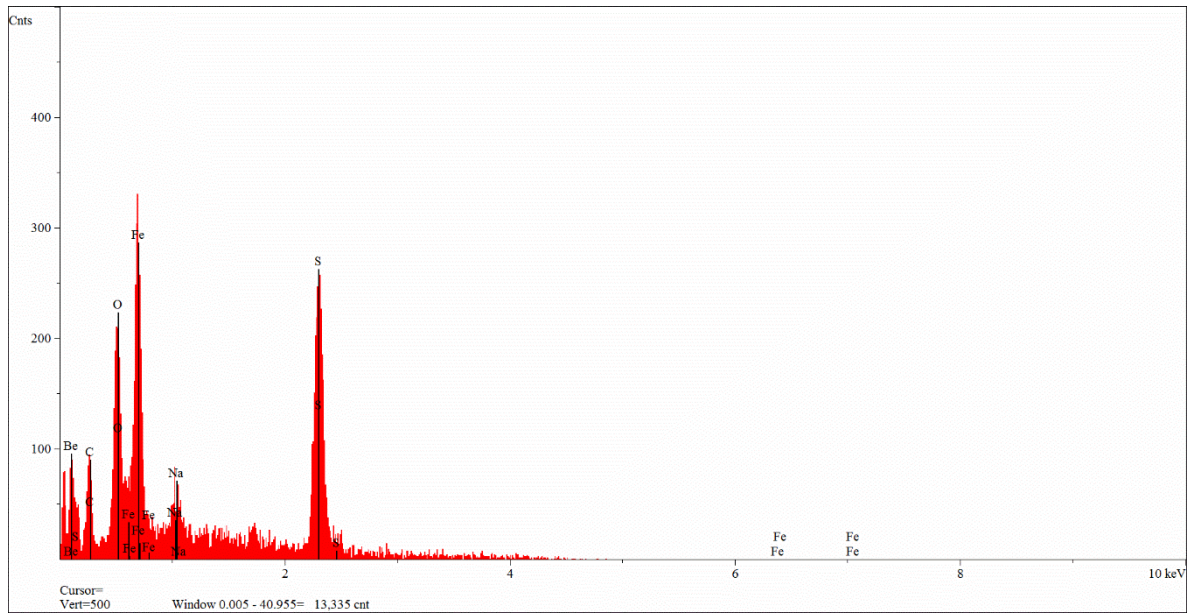


Figure C-3 EDS of pyrite mineral (from Himmetoglu oil shale)

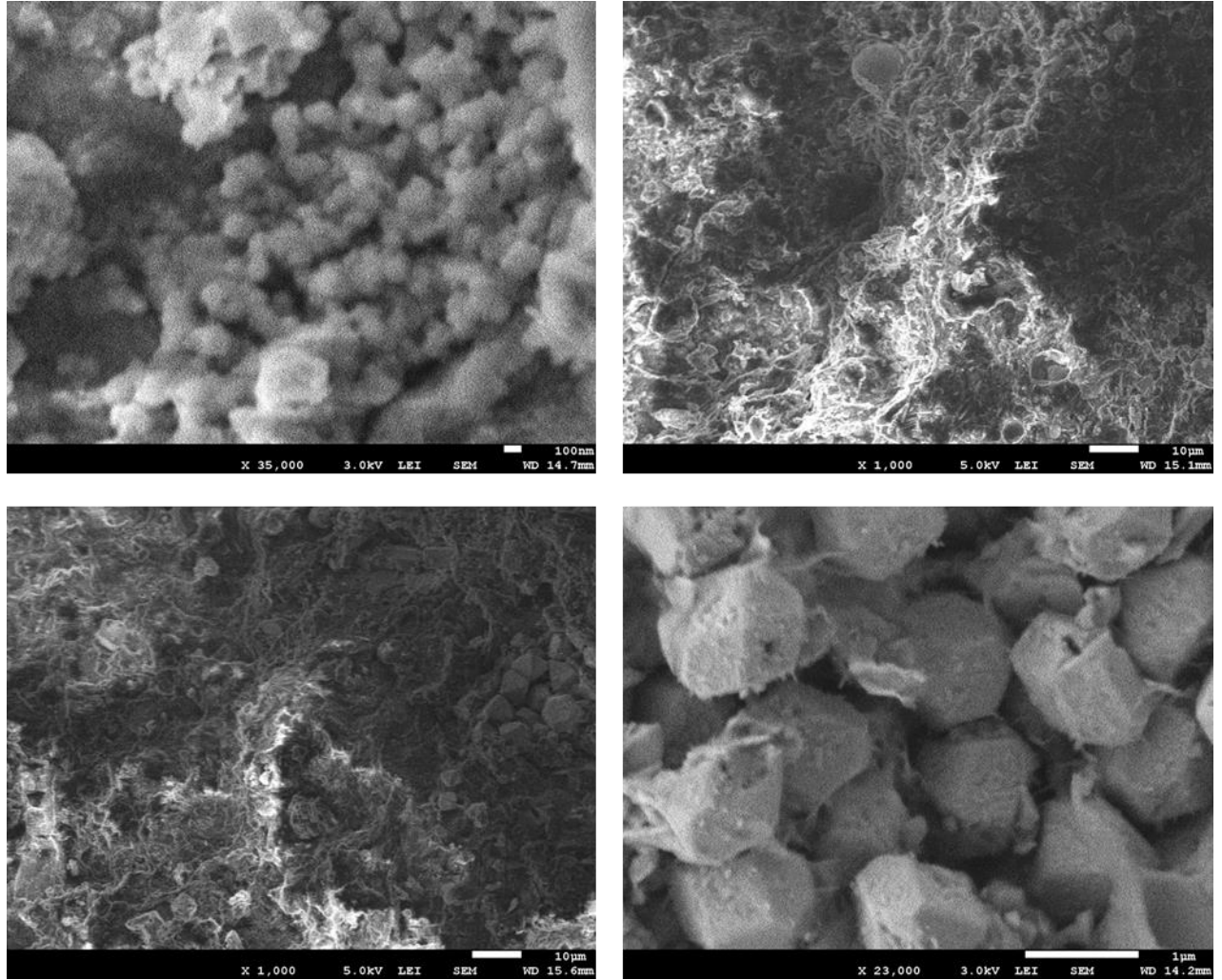


Figure C-4 SEM images of Himmetoglu oil shale

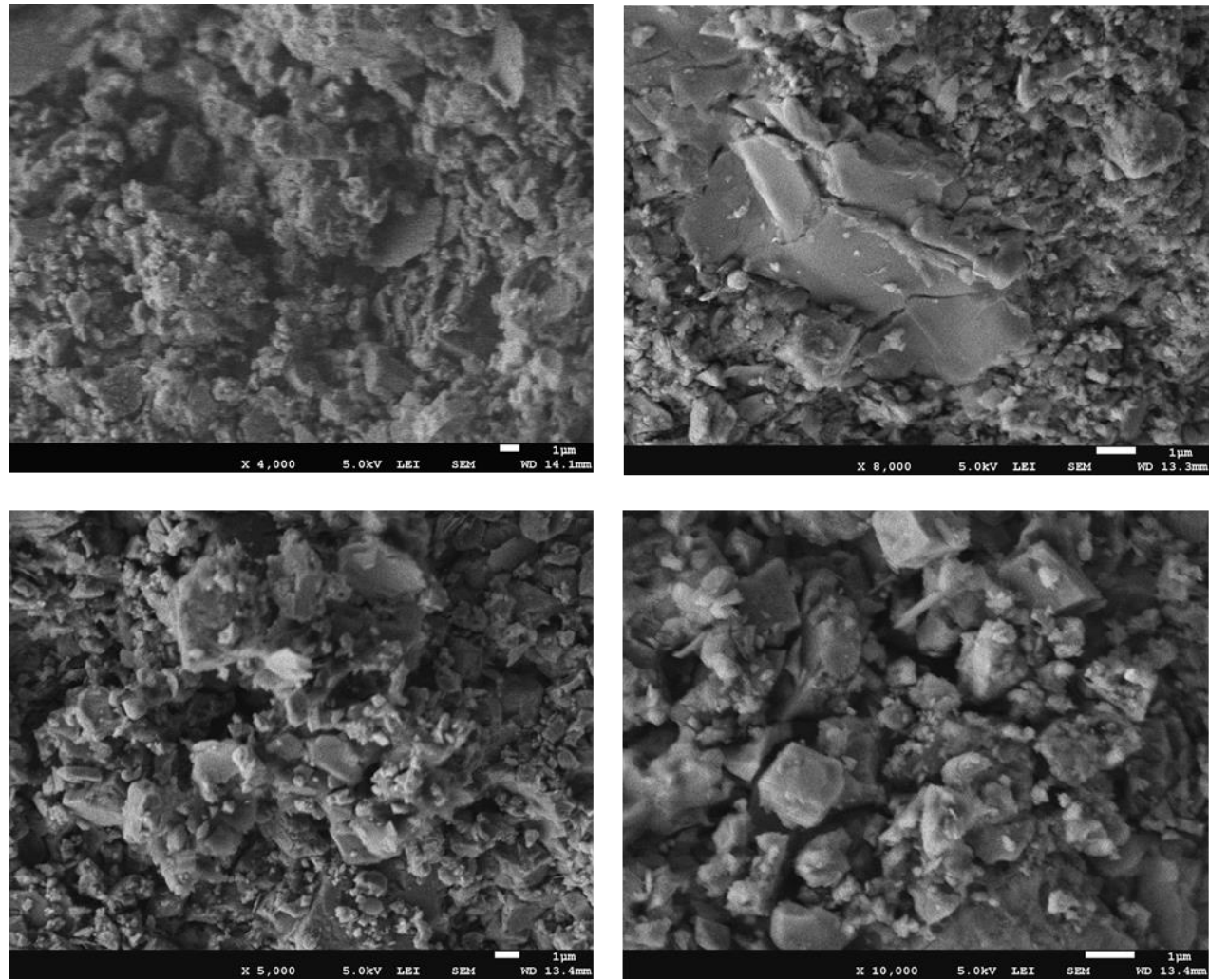


Figure C-5 SEM images of Hatildag oil shale

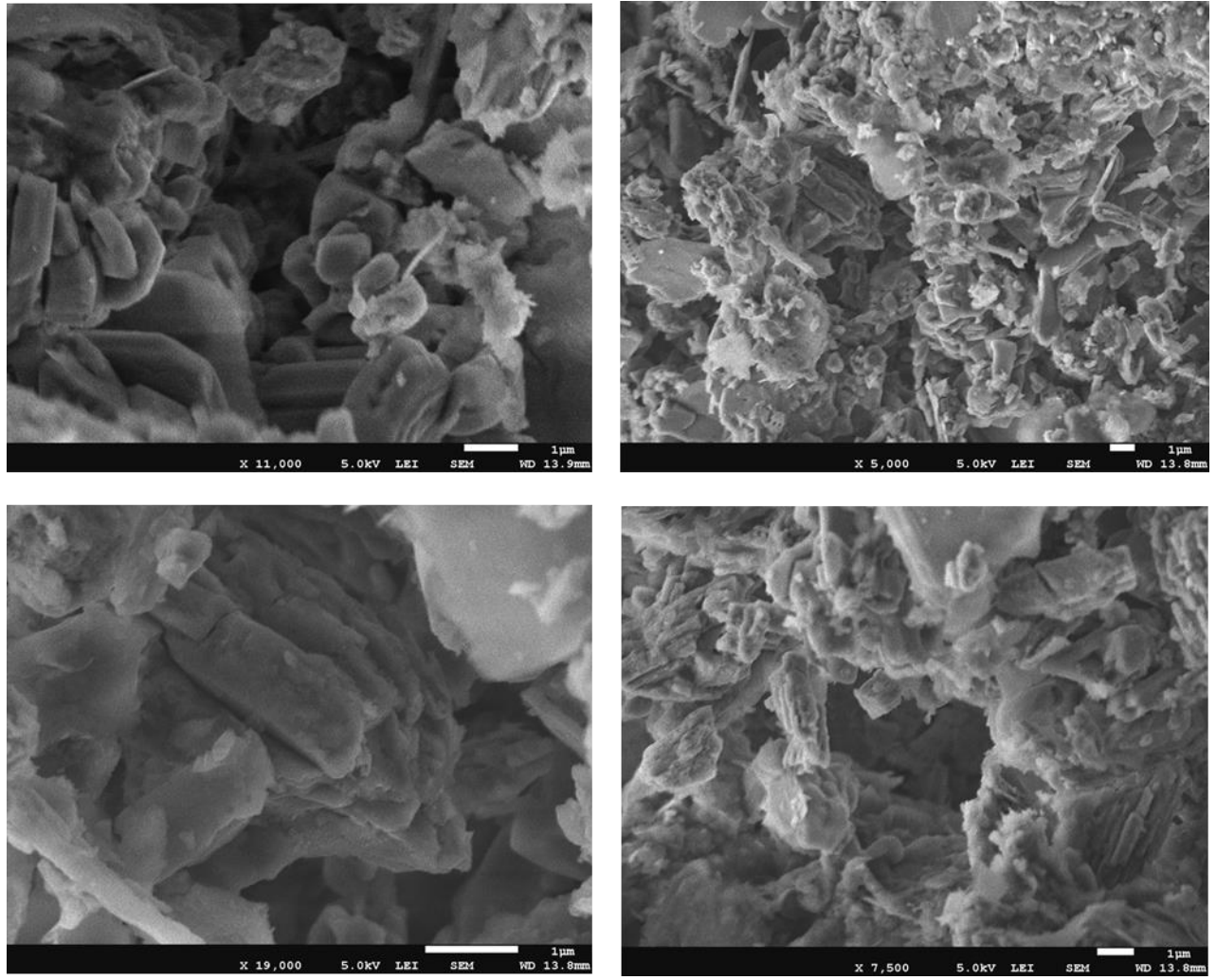


Figure C-6 SEM images of Seyitomer oil shale

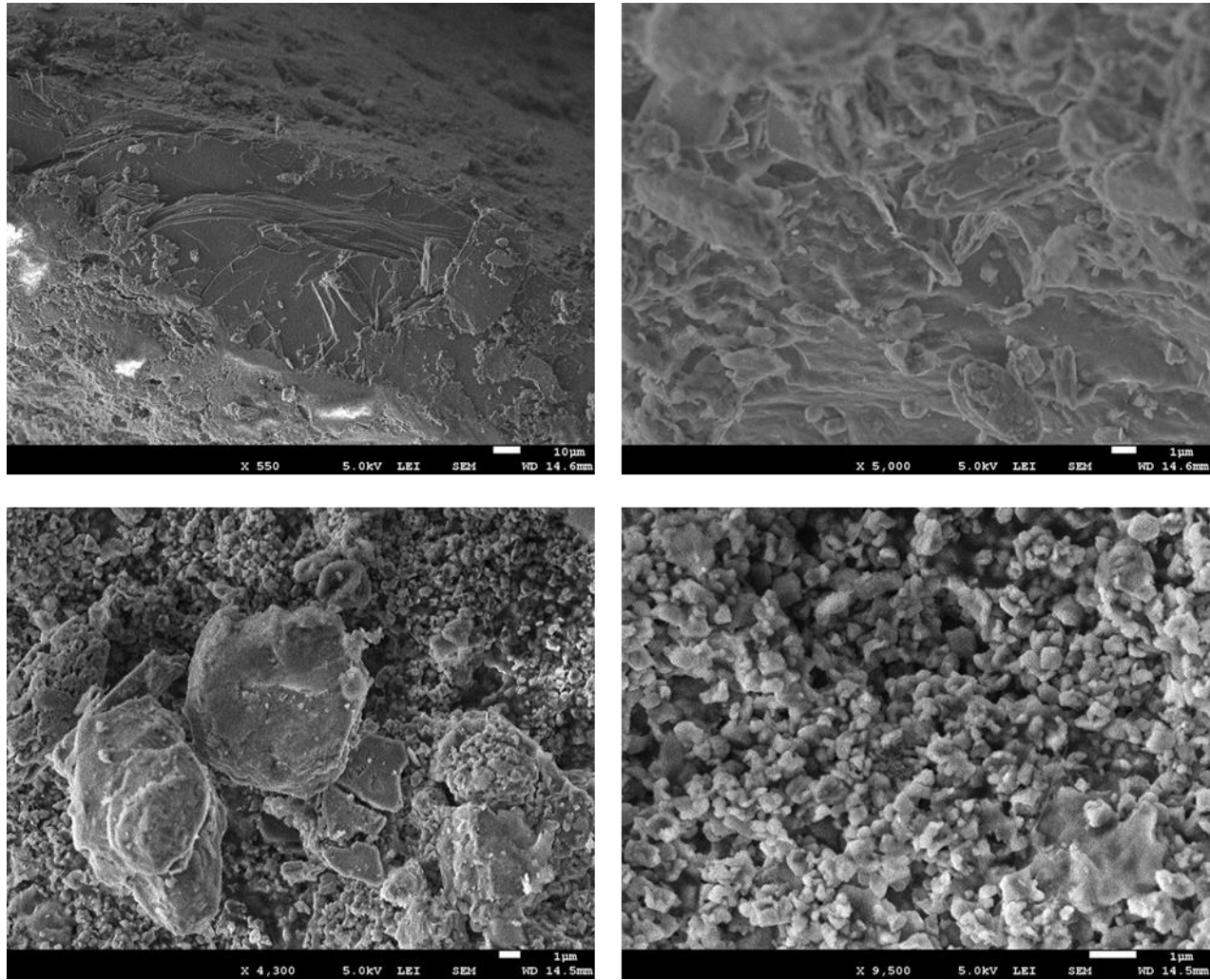


Figure C-7 SEM images of Ulukisla oil shale

C.2 Retort Postmortems

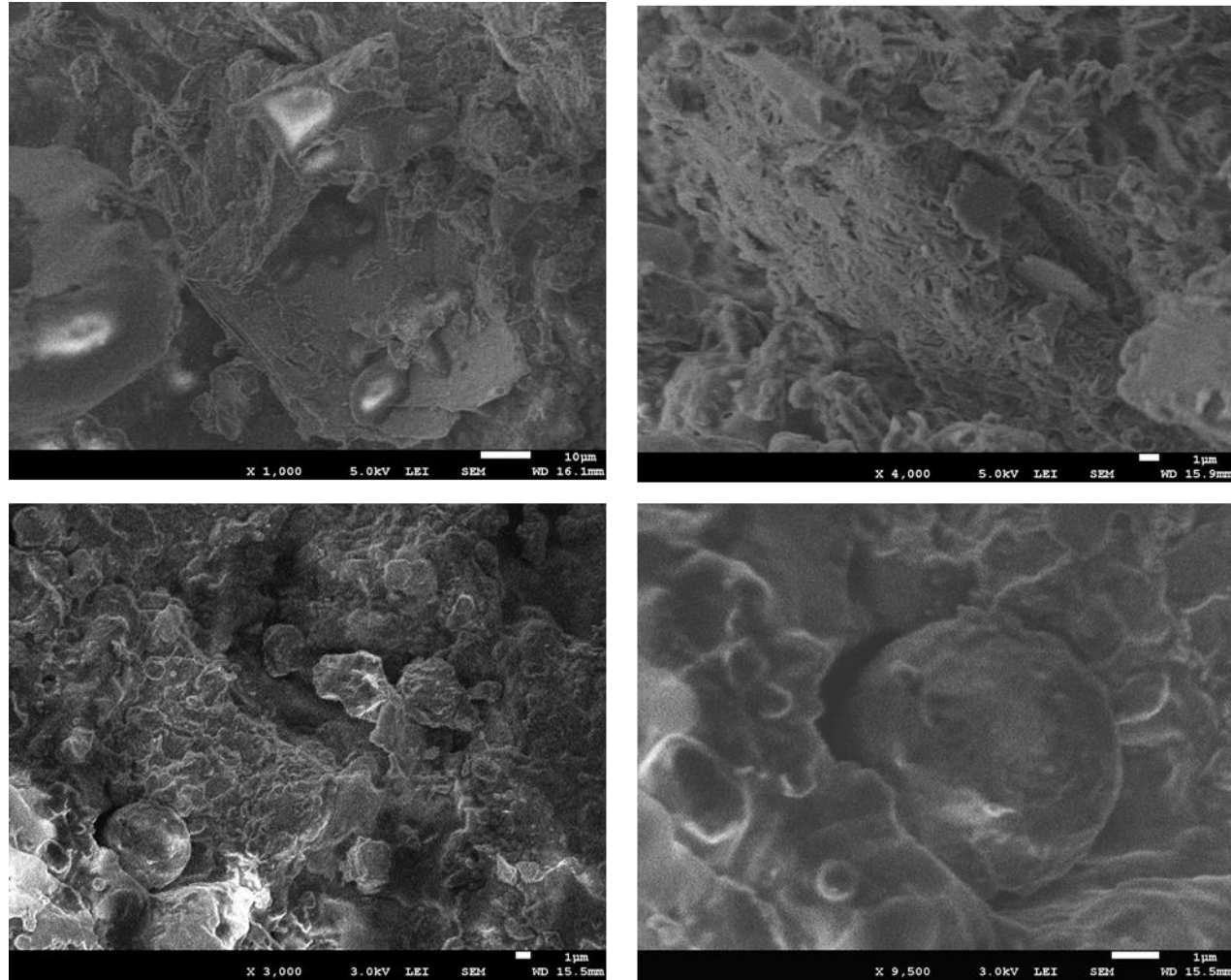


Figure C-8 SEM images of Himmetoglu retort postmortem

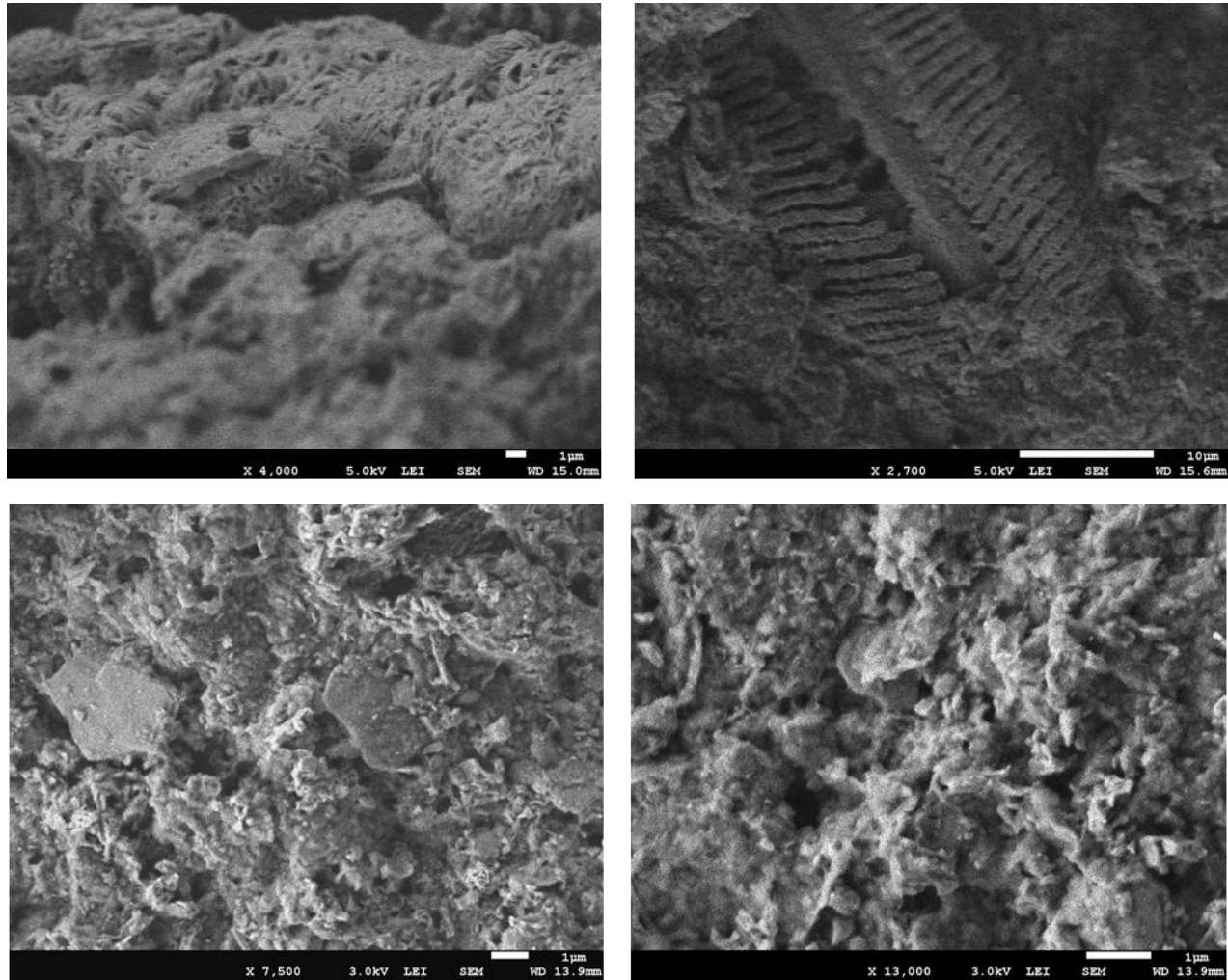


Figure C-9 SEM images of Himmetoglu retort postmortem (with iron powder)

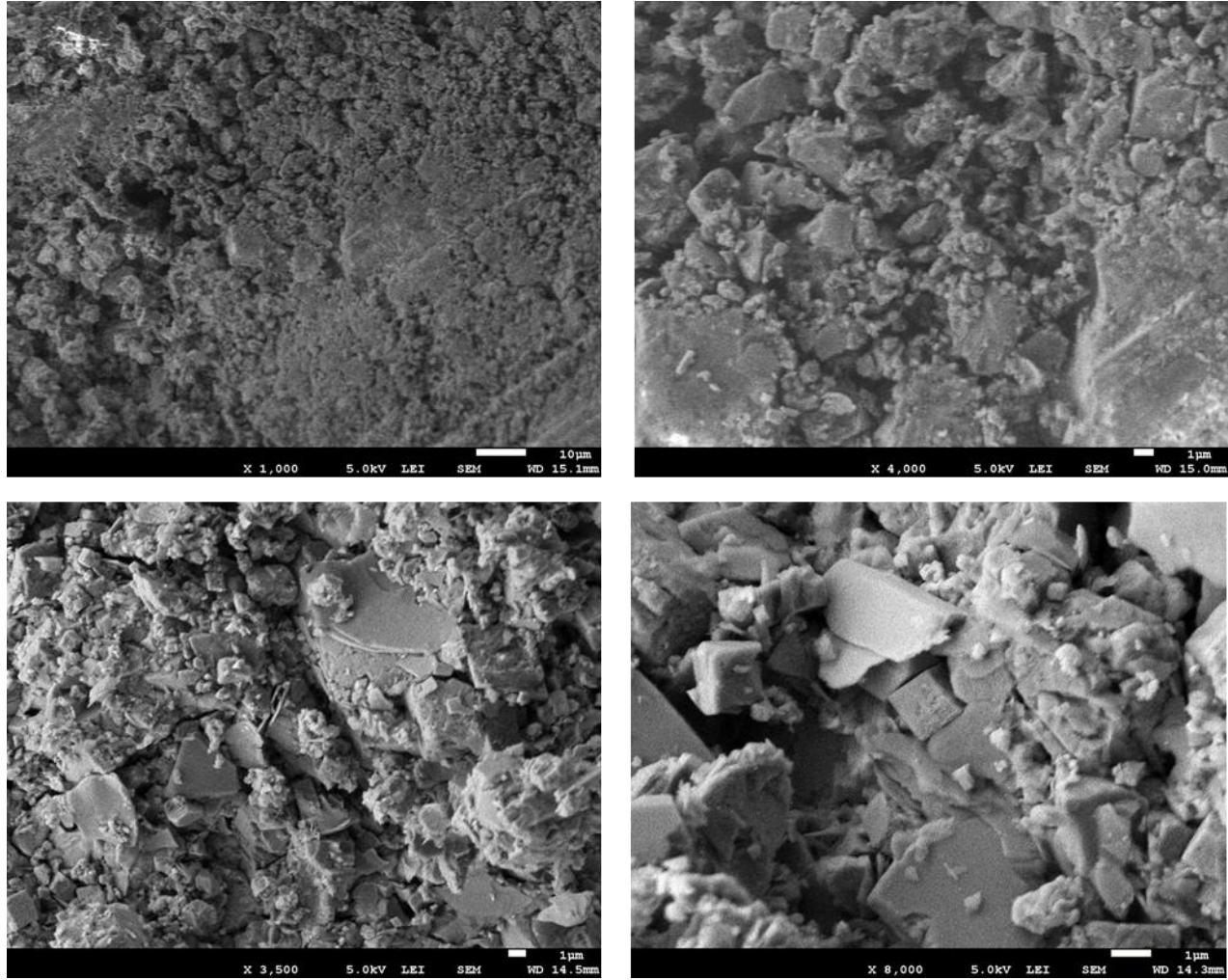


Figure C-10 SEM images of Hatildag retort postmortem

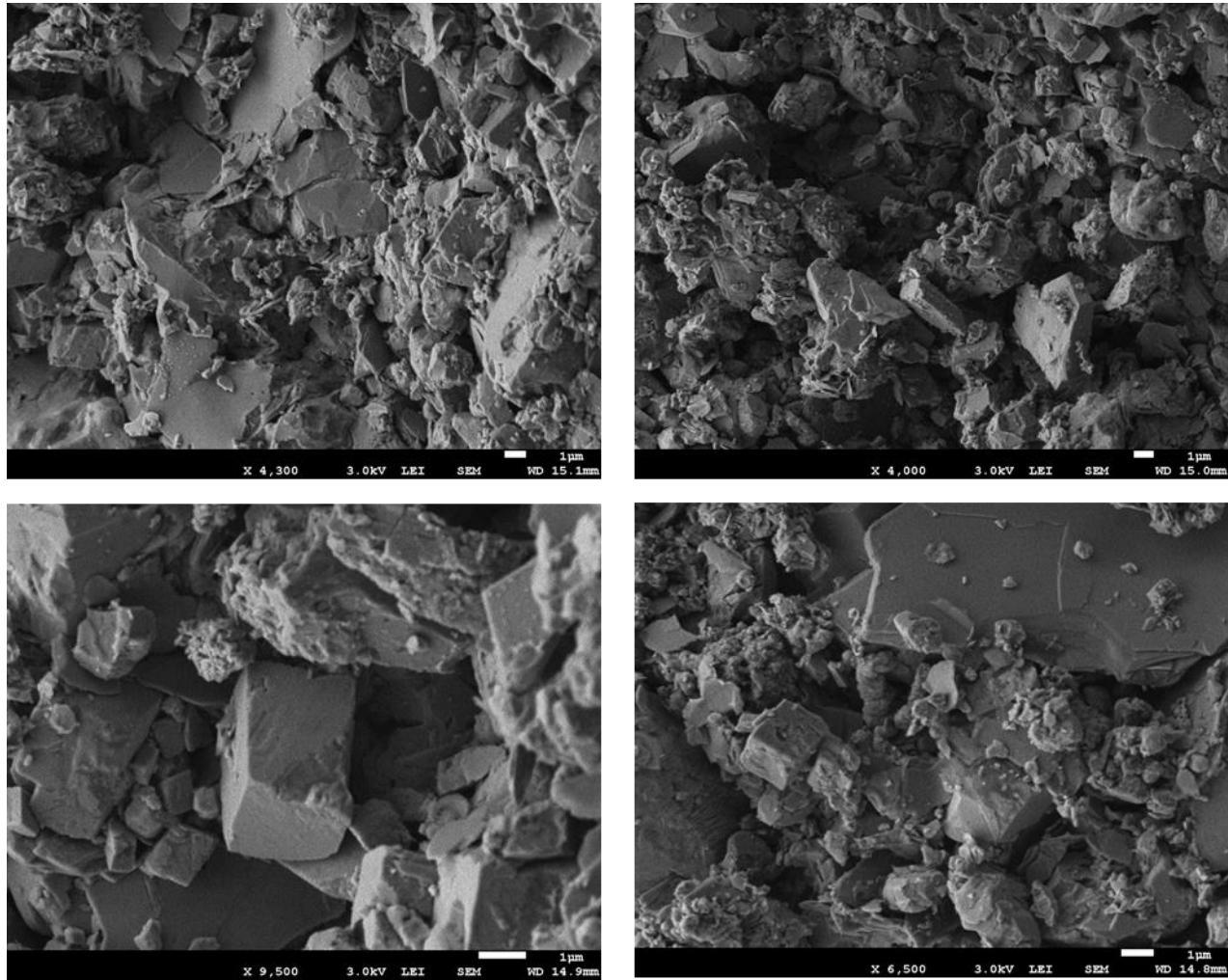


Figure C-11 SEM images of Hatildag retort postmortem (with iron powder)

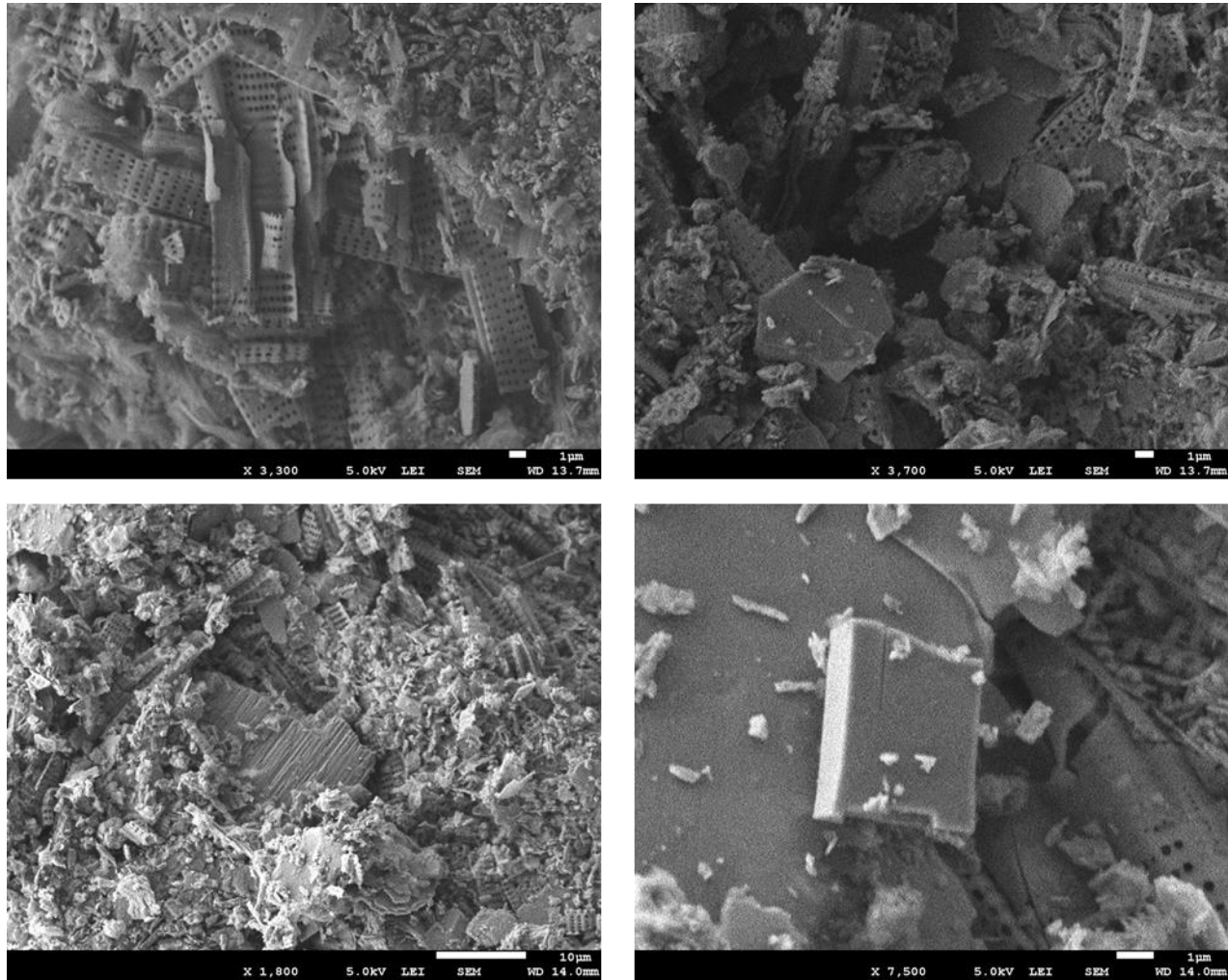


Figure C-12 SEM images of Seytomer retort postmortem

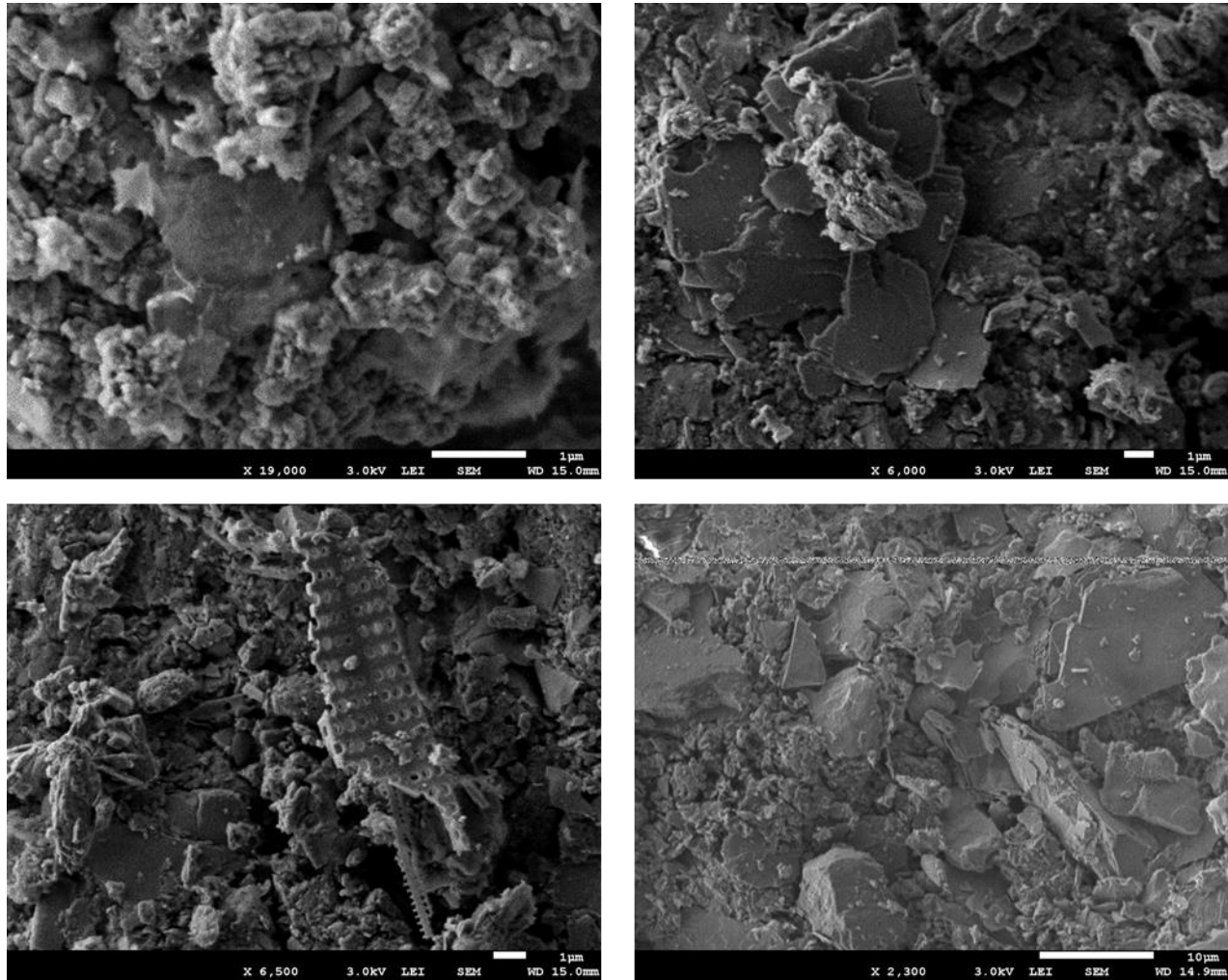


Figure C-13 SEM images of Seytomer retort postmortem (with iron powder)

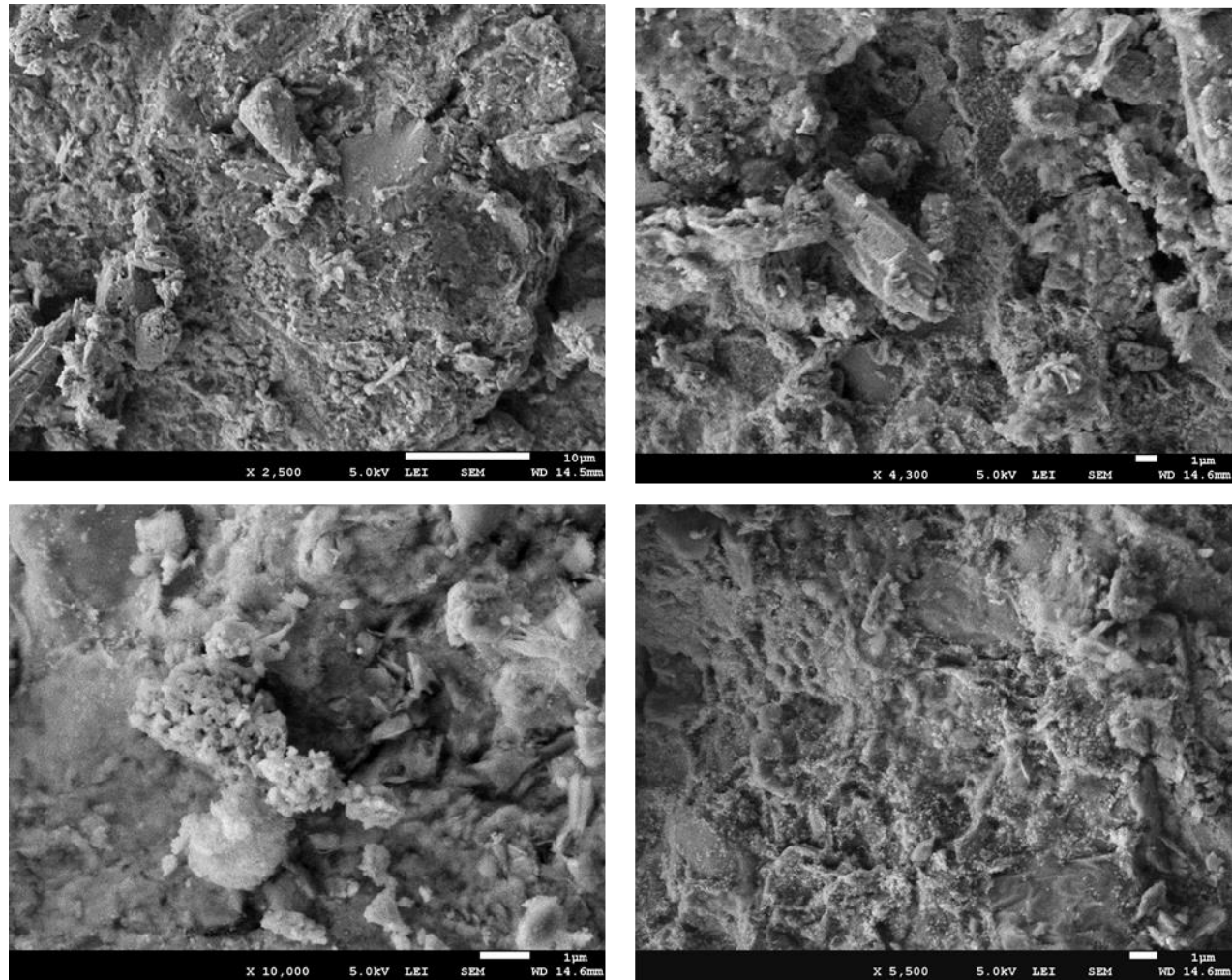


Figure C-14 SEM images of Ulukisla retort postmortem

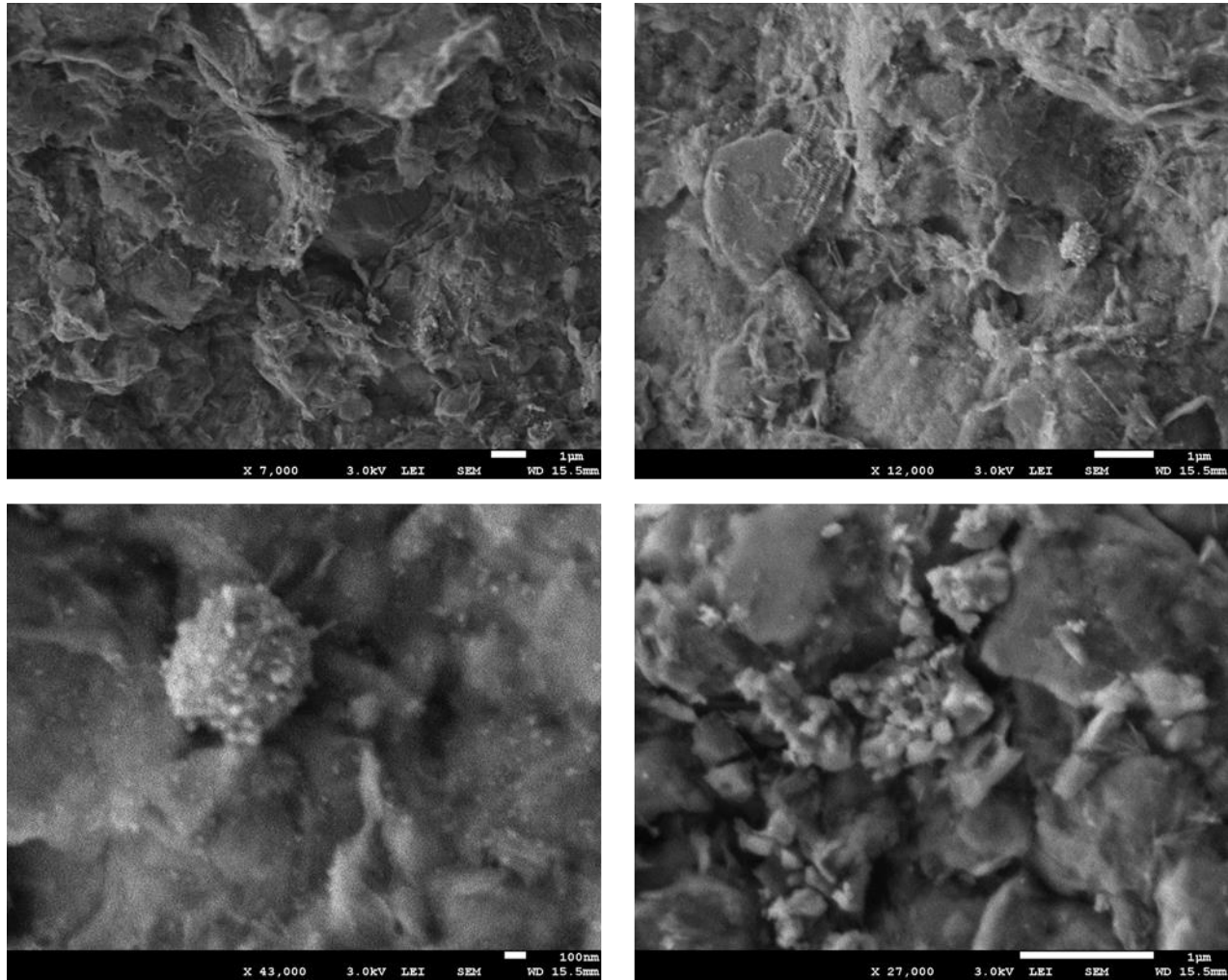


Figure C-15 SEM images of Ulukisla retort postmortem (with iron powder)

C.3 Microwave Postmortems

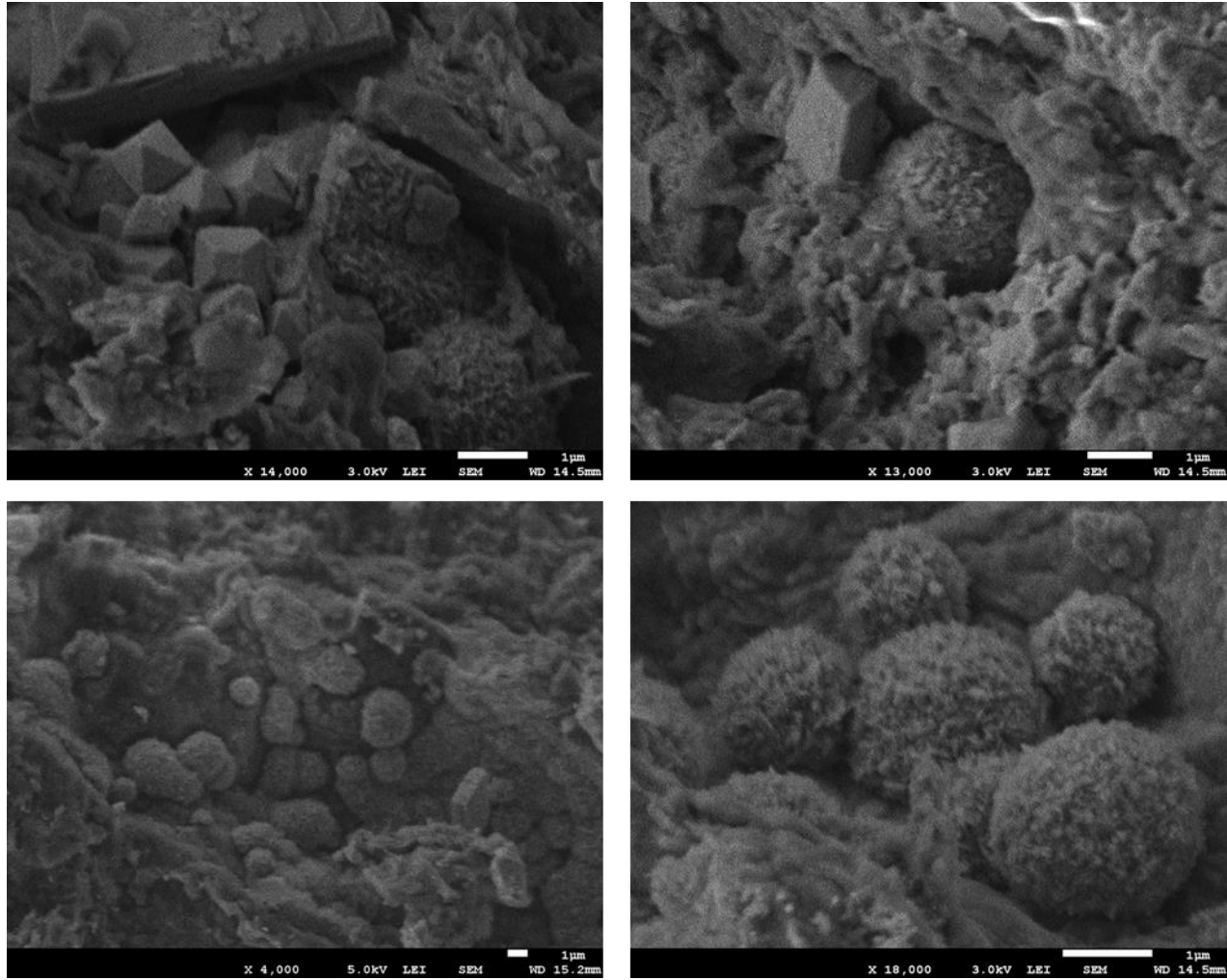


Figure C-16 SEM images of Himmetoglu microwave postmortem

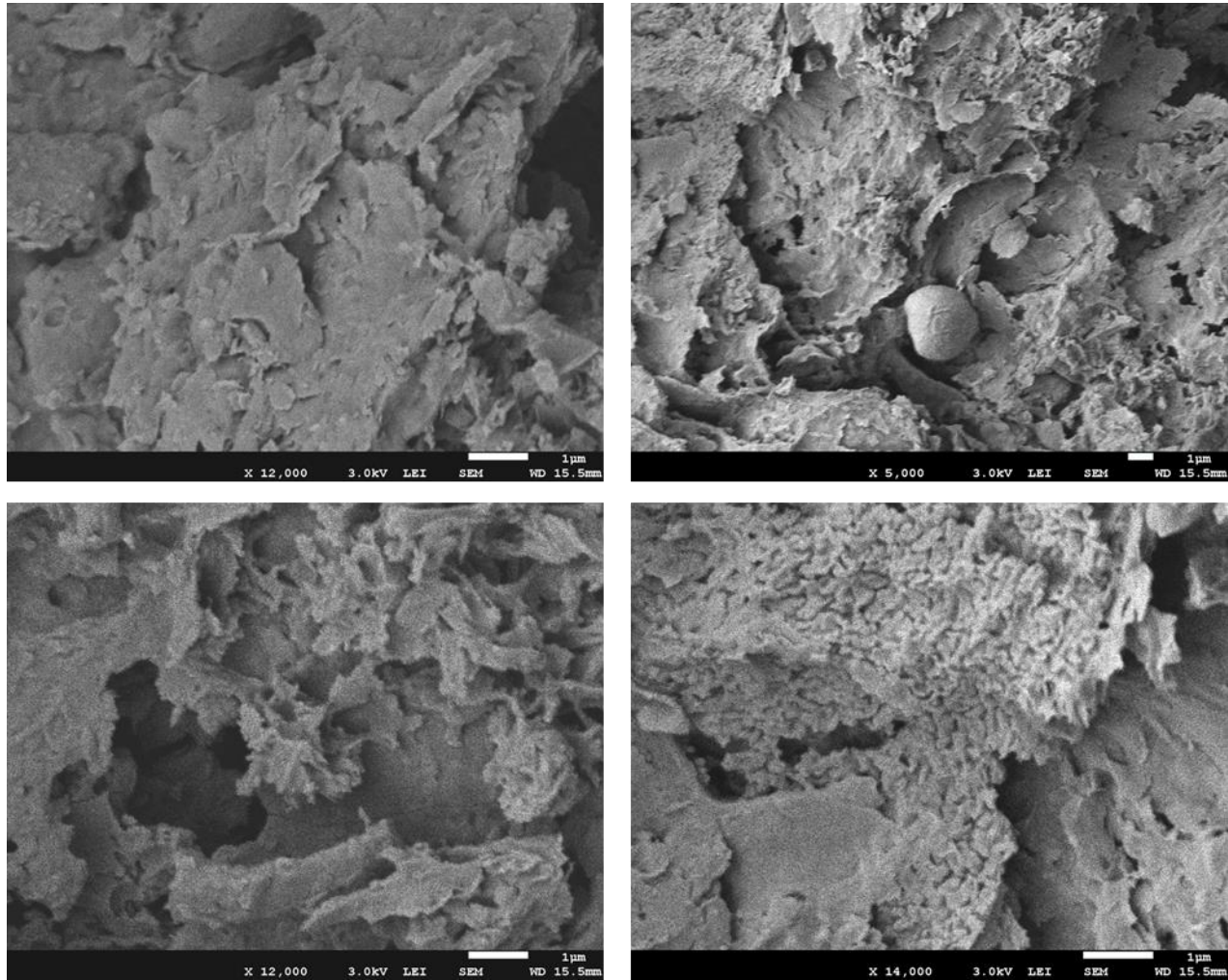


Figure C-17 SEM images of Himmetoglu microwave postmortem (with iron powder)

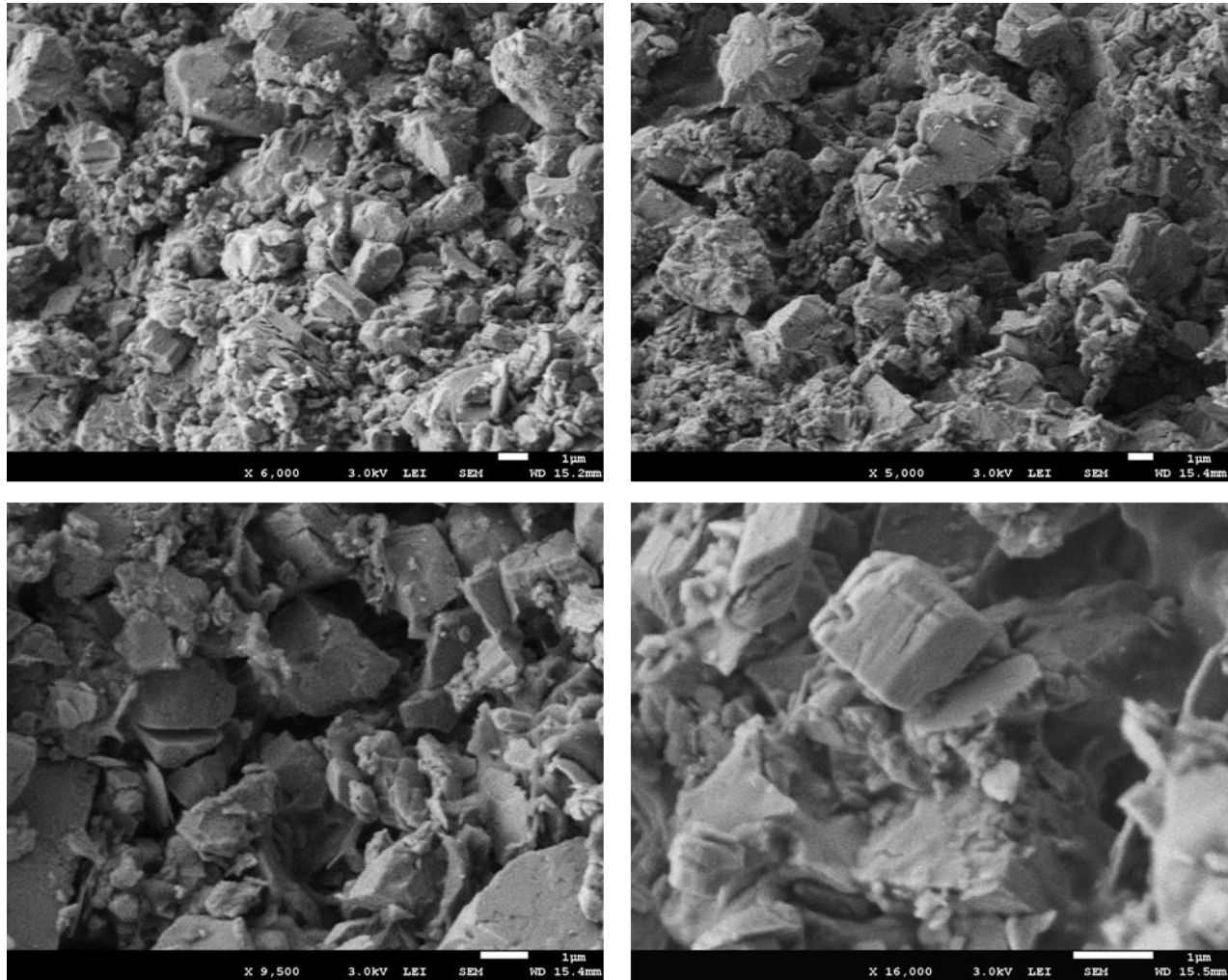


Figure C-18 SEM images of Hatildag microwave postmortem

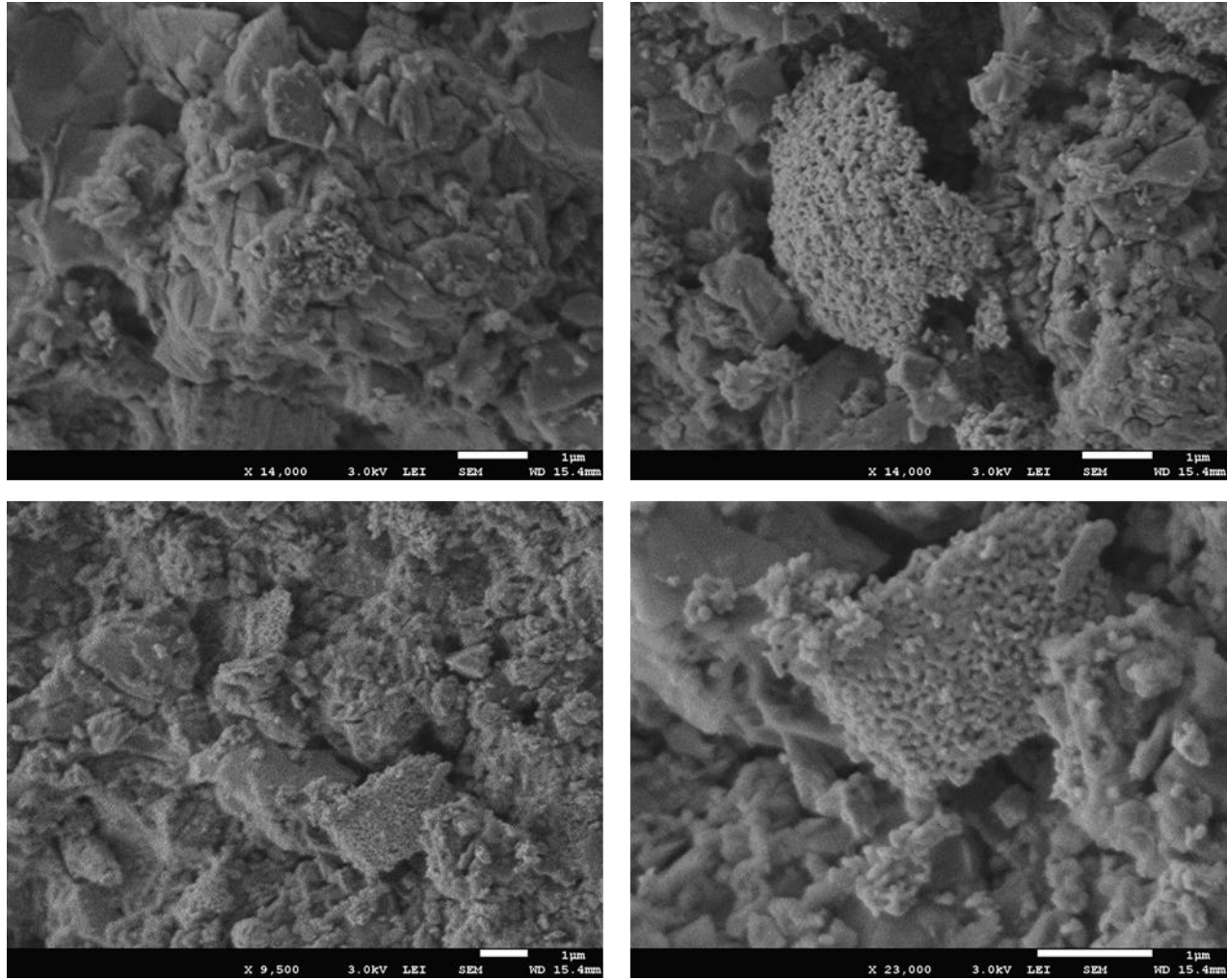


Figure C-19 SEM images of Hatildag microwave postmortem (with iron powder)

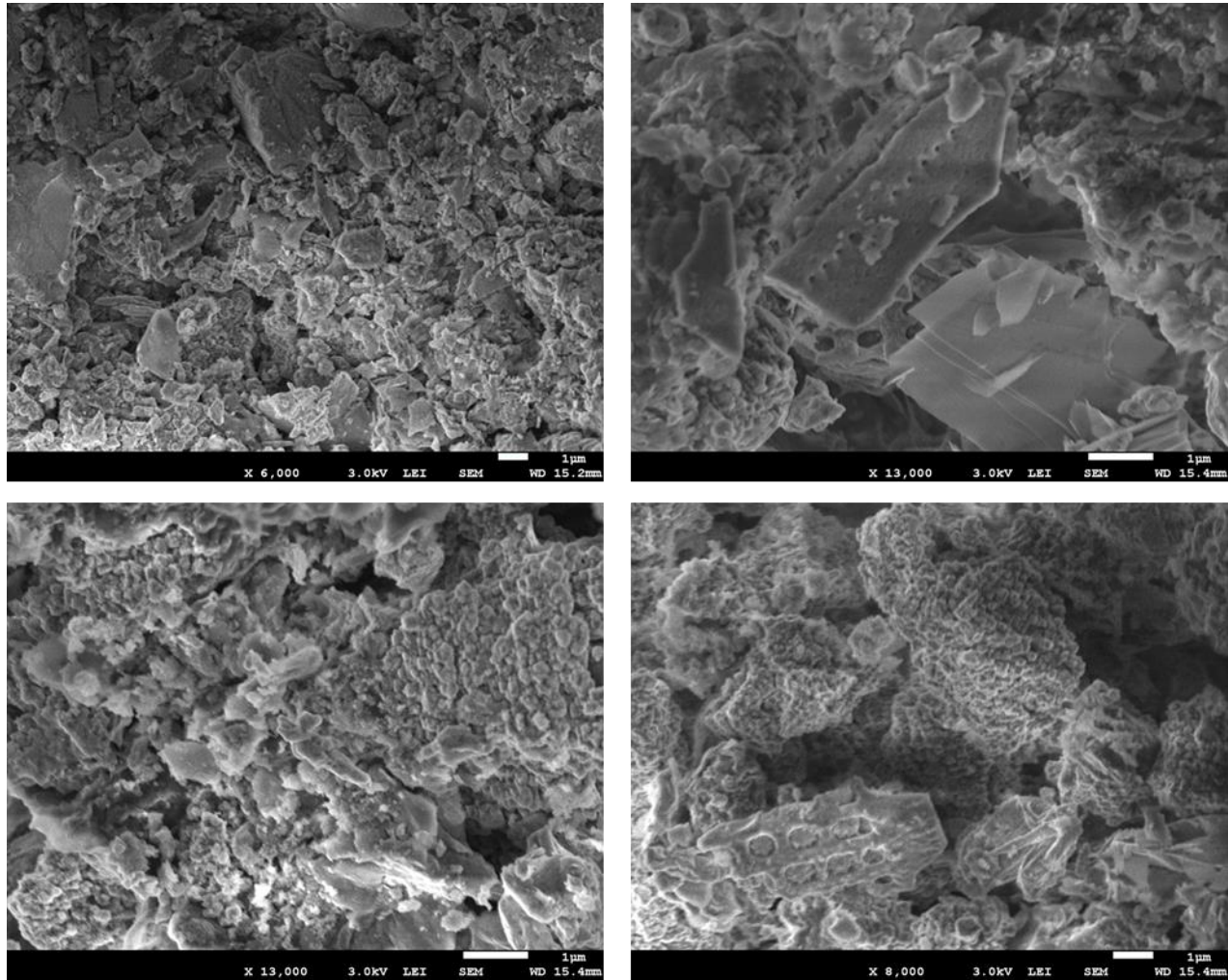


Figure C-20 SEM images of Seyitomer microwave postmortem

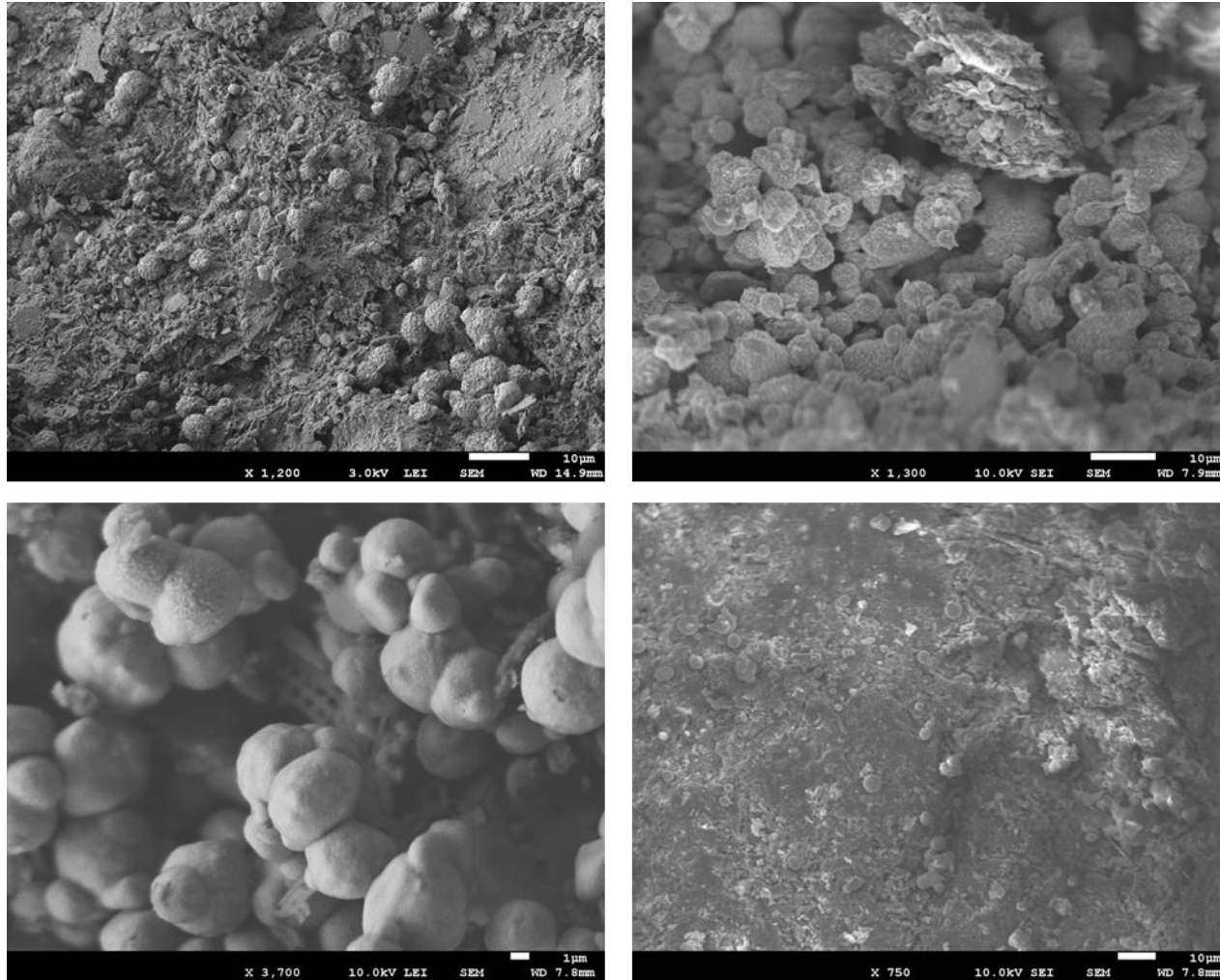


Figure C-21 SEM images of Seyitomer postmortem (with iron powder)

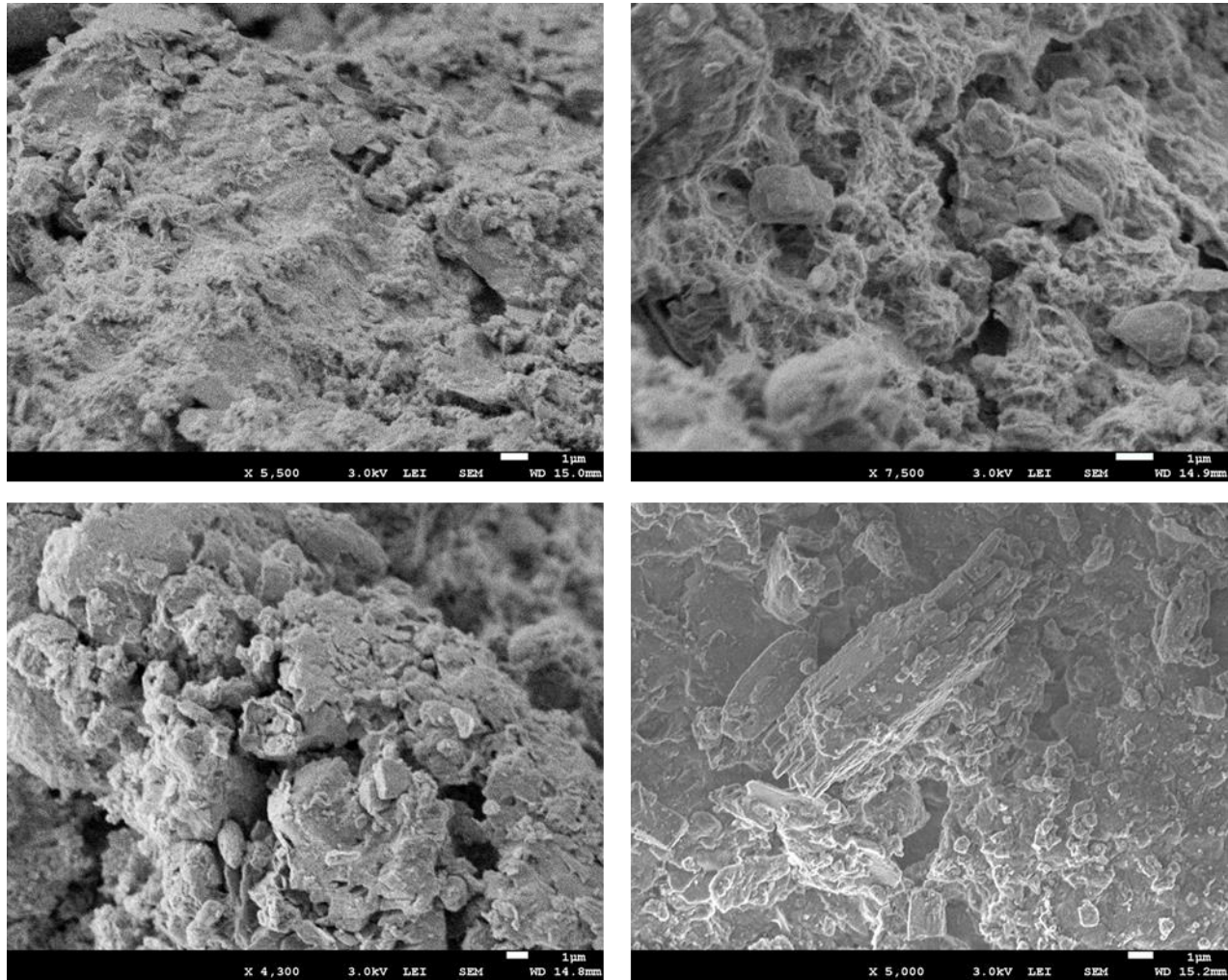


Figure C-22 SEM images of Ulukisla microwave postmortem

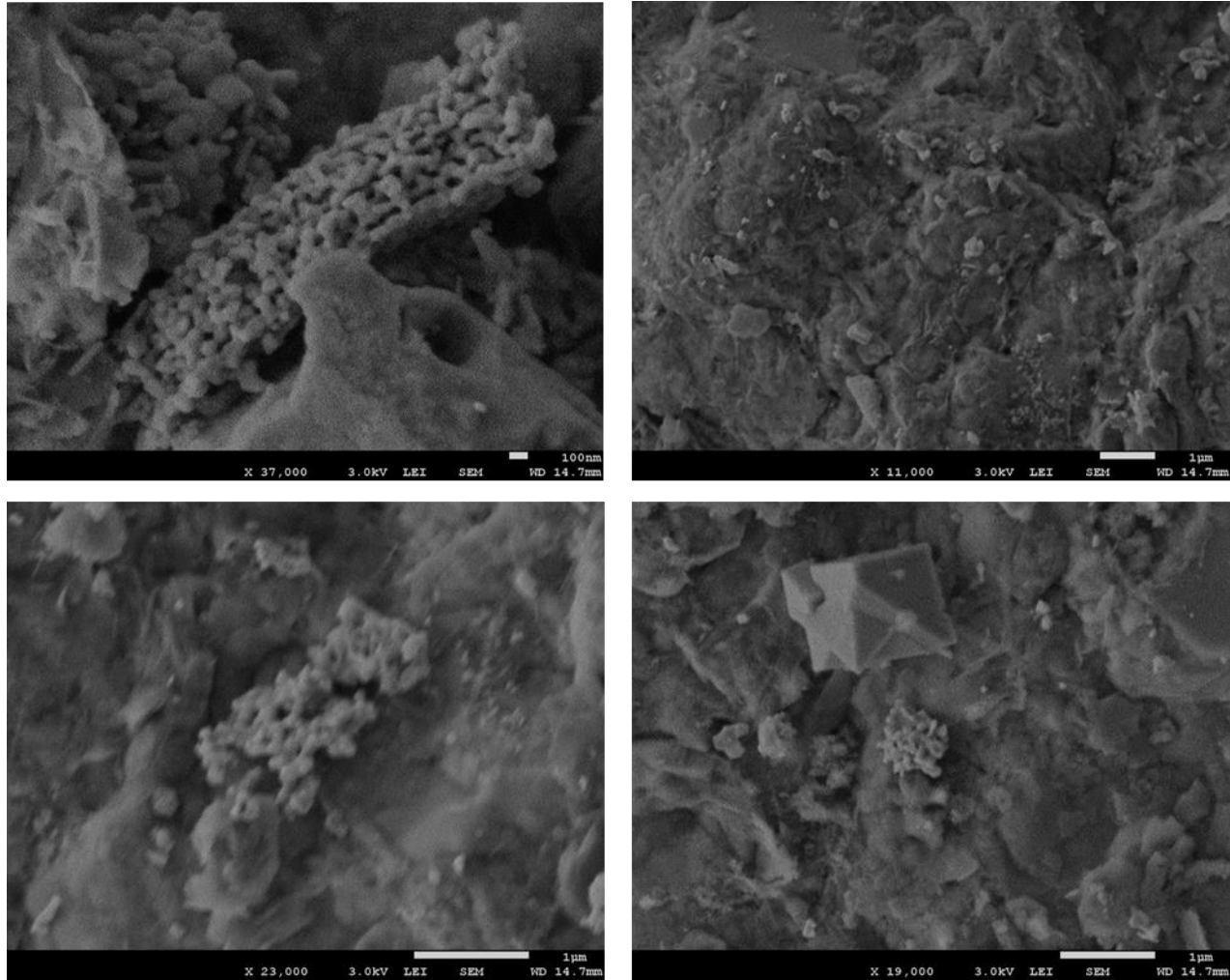


Figure C-23 SEM images of Ulukisla microwave postmortem (with iron powder)